CHITOSAN-TITANIUM DIOXIDE (Cs-TiO_2) CATALYST SYNTHESIZED ON GLASS SUBSTRATE FOR PHOTODEGRADATION

MUHAMMAD NUR IMAN BIN AMIR

INSTITUE OF GRADUATE STUDIES
UNIVERSITY OF MALAYA
KUALA LUMPUR

2016

CHITOSAN-TITANIUM DIOXIDE ($CS\text{-}TIO_2$) CATALYST SYNTHESIZED ON GLASS SUBSTRATE FOR PHOTODEGRADATION

MUHAMMAD NUR IMAN BIN AMIR

DISSERTATION SUBMITTED IN FULFILMENT OF THE REQUIREMENTS FOR THE DEGREE OF MASTER OF PHILOSOPHY

INSTITUE OF GRADUATE STUDIES
UNIVERSITY OF MALAYA
KUALA LUMPUR

2016

UNIVERSITY OF MALAYA

ORIGINAL LITERARY WORK DECLARATION

Name of Candidate: MUHAMMAD NUR IMAN BIN AMIR

Registration/Matric No: HGA140007

Name of Degree: Master of Philosophy

Title of Project Thesis ("this Work"): Chitosan-Titanium Dioxide (Cs-TiO_2) catalyst synthesized on glass substrate for photodegradation

Field of Study: Environmental Science (Catalysis)

I do solemnly and sincerely declare that:

(1) I am the sole author/writer of this Work;
(2) This Work is original;
(3) Any use of any work in which copyright exists was done by way of fair dealing and for permitted purposes and any excerpt or extract from, or reference to or reproduction of any copyright work has been disclosed expressly and sufficiently and the title of the Work and its authorship have been acknowledged in this Work;
(4) I do not have any actual knowledge nor do I ought reasonably to know that the making of this work constitutes an infringement of any copyright work;
(5) I hereby assign all and every rights in the copyright to this Work to the University of Malaya ("UM"), who henceforth shall be owner of the copyright in this Work and that any reproduction or use in any form or by any means whatsoever is prohibited without the written consent of UM having been first had and obtained;
(6) I am fully aware that if in the course of making this Work I have infringed any copyright whether intentionally or otherwise, I may be subject to legal action or any other action as may be determined by UM.

Candidate's Signature Date:

Subscribed and solemnly declared before,

Witness's Signature Date:

Name:

Designation:

ABSTRACT

Methyl orange (MO) is one of the azo compounds that is present in the wastewater mainly from the textile industry. MO is also capable of producing a secondary waste product, which might become a major pollutant towards the environment and aquatic organisms. With that in mind, research is focused to look into photodegradation methods based on the advance oxidation process by Titanium Dioxide (TiO_2) semiconductor, which offers a more effective and highly selective degradation process at minimal consumption of energy and costs. However, nanosized of TiO_2 catalyst are limited by factors such as dispersion, separation, and adsorption. In this study, Chitosan (Cs) biopolymer is incorporated into TiO_2 nanoparticles as a support and adsorption site, forming an effective photocatalyst system. It is expected that the -OH and -NH_2 functional groups of Cs would act as active sites, creating excellent interfaces that would attract MO molecules. Meanwhile, the porous structure of Cs helps adsorb the MO molecules. The stability and separation ability of the Cs-TiO_2 photocatalysts system improved as it is further immobilized on the surface of the glass substrate. TiO_2 was first synthesized using the sol-gel method ($TiO_{2(SY)}$), and its phase, particle size, morphology, band gap, and chemical structure are analyzed and compared to that of TiO_2-Commercial Degussa P25 ($TiO_{2(DP25)}$). Then, TiO_2 nanoparticles (both $TiO_{2(SY)}$ and $TiO_{2(DP25)}$) were incorporated with Cs solution before being immobilized on glass plates via the dip-coating technique. The surface interactions and the band gap of Cs-TiO_2/Glass photocatalyst was determined using techniques such as FESEM+EDS, FTIR, and UV-DR analysis, respectively. The photocatalytic activity of both photocatalysts (Cs-$TiO_{2(DP25)}$/Glass and Cs-$TiO_{2(SY)}$/Glass) was demonstrated on the simulated MO solution (10 ppm) irradiated under UV-light (6 W, λ=312 nm and 365 nm). UV-Vis analysis was conducted to analyze the influence of adsorption–photodegradation of MO using different photodegradation parameters. The results reported that the anatase phase, with a particle size of less than 50 nm and

homogenous spherical features of TiO_2, was successfully produced through the sol-gel method. The Cs-TiO_2/Glass photocatalyst exhibited excellent formation of coordinate covalent bonding between Ti-O to Si-O, Ti-O-to-NH_2, or Ti-O-to-OH groups. The photocatalytic activities of TiO_2 exhibited a promising increment with better adsorptions under different photocatalytic conditions, including the concentration and pH of MO, photocatalysts cycles and the weight ratio of the surface of the glass substrate. The optimum photodegradation recorded for the Cs-TiO_2/Glass for $TiO_{2(SY)}$ and $TiO_{2(DP25)}$ reached 80%, with 10 ppm of MO concentration, at a normal pH and 1 hour of retention time. Meanwhile, the optimum adsorption process that was recorded for that photocatalyst is expected to exceed 70%. It was concluded that the combination of the adsorption and catalytic photodegradation process from Cs-TiO_2/Glass photocatalyst has great potential for treating wastewater for other types of organic/inorganic pollutants.

ABSTRAK

Methyl orange (MO) adalah salah satu sebatian azo yang menghasilkan sisa air kumbahan daripada industri tekstil. MO menghasilkan bahan buangan sekunder yang merupakan punca isu pencemaran air yang utama terhadap alam sekitar yang dan toksik terhadap organisma akuatik. Dengan lebih teliti, para penyelidik berminat kepada kaedah pemerosotaan cahaya berdasarkan kepada proses pengoksidaan oleh Titanium Dwioksida (TiO_2) semikonduktor yang dipercayai dapat menawarkan proses pemerosotan yang lebih berkesan dan selektif dengan pengunaan tenaga dan kos yang minimum. Walau bagaimanapun, terdapat kekangan berkaitan dengan pemangkin TiO_2 yang bersaiz nano dari segi penyebarannya, pemisahannya dan penjerapannya. Dalam kajian ini, nanopartikel TiO_2 telah disokong dengan bahan bio-polimer Chitosan (Cs) sebagai tapak penjerapan. Dijangkakan bahawa, kumpulan berfungsi Cs iaitu OH dan NH_2 telah bertindak sebagai tapak aktif untuk interaksi yang lebih baik dengan molekul MO. Sementara itu, struktur berliang Cs membantu pada penjerapan molekul MO yang lebih berkesan. Kestabilan dan perpisahan keupayaan sistem ini bertambah baik kerana ia terus bergerak ke permukaan substrat kaca. Pertama sekali TiO_2 telah disintesis menggunakan kaedah sol-gel ($TiO_{2(SY)}$) mengikut analisa fasa, saiz zarah, morfologi, selar jalur dan struktur kimia dan dibandingkan dengan TiO_2-Komersial Degussa P25 ($TiO_{2(DP25)}$) sewajarnya. Kemudian, nanopartikel TiO_2 (kedua-dua $TiO_{2(SY)}$ dan $TiO_{2(DP25)}$) telah digabungkan dengan larutan Cs sebelum pegun di atas plat kaca melalui teknik penyalutan celup. Interaksi permukaan dan selar jalur untuk pemangkin cahaya Cs-TiO_2/Kaca telah dianalisia melalui analisis FESEM+EDS, FTIR dan UV-DR, masing-masing. Aktiviti pemangkinan cahaya bagi kedua-dua Cs-$TiO_{2(DP25)}$/Kaca dan Cs-$TiO_{2(SY)}$/Kaca) diuji pada simulasi pemangkinan cahaya di bawah sinaran UV cahaya (6 W, λ = 312 nm dan 365 nm) terhadap larutan MO (10 ppm). Analisa UV-Vis telah dilakukan untuk mengkaji kesan penjerapan-pemerosotaan terhadap MO dengan

menggunakan parameter pemerosotan yang berbeza. Ia menunjukkan bahawa, fasa anatase dengan saiz zarah kurang daripada 50nm telah berjaya menghasilkan TiO_2 dengan menggunakan kaedah sol-gel. Pemangkin cahaya Cs-TiO_2/Kaca menunjukkan interaksi yang baik dengan pembentukan ikatan kovalen koordinat antara Ti-O kepada Si-O, Ti-O-kepada-NH_2 atau Ti-O-kepada-OH groups. Aktiviti pemangkinan cahaya oleh TiO_2 menunjukkan peningkatan memberangsangkan dengan penjerapan yang lebih baik pada keadaan proses pemangkinan cahaya yang pelbagai termasuk kepekatan dan pH bagi larutan MO, serta kitaran dan nisbah berat pemangkin cahaya pada permukaan substrat kaca. Pemorosotan yang optimum ditunjukkan oleh kedua-dua pemangkin-cahaya Cs-TiO_2/Glass yang berbeza iaitu $TiO_{2(SY)}$ dan $TiO_{2(DP25)}$ yang telah digunakan boleh memperolehi 80% dengan penggunaan kepekatan MO iaitu 10 ppm dengan pH biasa dan 1 jam masa tahanan. Sementara itu, proses penjerapan yang optimum telah dirakamkan untuk pemangkin-cahaya tersebut dijangkakan melebihi 70%. Kesimpulannya bahawa, gabungan proses penjerapan dan pemerosotaan cahaya yang diperolehi oleh pemangkin cahaya pemangkin cahaya Cs-TiO_2/Kaca mempunyai potensi yang tinggi untuk proses rawatan sisa air yang lebih baik untuk lain-lain jenis bahan pencemar organik/bukan organik.

ACKNOWLEDGEMENTS

This thesis would not have possible without the efforts and support of people at the Nanotechnology and Catalysis Research Centre (NANOCAT) and my surrounding friends.

First of all, I would like to express my deepest gratitude to my supervisors Dr Nurhidayatullaili Muhd Julkapli and Prof Sharifah Bee Abd Hamid for their source of guidance, assistance and concern throughout my research project. Their wide knowledge and valuable comments have provided a good basis for my project and thesis. Furthermore, I would like to thank to their willingness to spend their valueless time and help in guiding me through the whole project. I deeply express my thanks to them in helping me in editing the contents and wording of this thesis.

Besides that, I would like to express a special thanks to all staffs in NANOCAT, faculty of Physic and chemistry in University Malaya (UM), respectively for their continuous guidance and assistance during all the samples preparation and testing. Most importantly, I would like to greatly acknowledge my colleagues in UM and all my dearest friends in NANOCAT. I deeply appreciated their precious ideas and support throughout the entire study.

This research was supported by a grant from the Fundamental Research Grant Scheme (FRGS), University Malaya Research Grant (UMRG) and Postgraduate Research Fund (PPP) for the sources of funding through this study. I gratefully acknowledge UM for financial supporting that helping me in this study and MyMaster scholarship from Kementerian Pendidikan Malaysia (KPM). Lastly, I would like to take this opportunity to express my deepest gratitude to my beloved parents, wife and all family members through their encouragement and support me to continue studying.

TABLE OF CONTENTS

LIST OF FIGURES

LIST OF TABLES

LIST OF SYMBOLS AND ABBREVIATIONS

Cb	:	Conduction band
Cs	:	Chitosan
e^-	:	Electron
DR	:	Diffusive Reflectance
EDS	:	Energy Dispersive Spectrometer
FTIR	:	Fourier Transform Infra-Red Analysis
FESEM	:	Field Emission Scanning Electron Microscopy
g	:	Gram
HR	:	High Resolution
h^+	:	Positive hole
hv	:	Energy (photon)
L	:	Liter
mL	:	Milliliter
MO	:	Methyl orange
ppm	:	Part per million
PVC	:	Polyvinyl Chloride
TEM	:	Transmission Electron Microscopy
TGA	:	Thermal Gravimetric Analyzer
$TiO_{2(DP25)}$	:	TiO_2 – Commercial Degussa P25
$TiO_{2(SY)}$	:	TiO_2 – Synthesis via sol-gel
UV	:	Ultraviolet
UV-Vis	:	Ultraviolet/visible
µm	:	Micrometer
Vb	:	Valence band
XRD	:	X-ray Diffraction

LIST OF EQUATIONS

CHAPTER 1: INTRODUCTION

1.1 Research background

It has been verified that many aromatic compounds derived from synthetic dyes could be successfully degraded and effectively mineralization to end products, which are CO_2, H_2O, and nutrient acids (Kijima, 2010). Various environmental applications to remove synthetic dyes in water and air have been utilized using the photocatalytic properties of Titanium Dioxide (TiO_2) nanoparticles, which is a very well-known semiconductor, used as a photocatalyst, due to the stability of its chemical structure, biocompatibility, and physical, optical, and electrical properties (Kijima, 2010). Furthermore, it was reported that dyes, metal ions, organic acids, and pesticide effectively possess the ability to adsorb Chitosan (Cs), due to its high adsorption potentials (Benavente, 2008; Zainal *et al.*, 2009). A variety of useful features of Cs make it a versatile adsorbent, which is evident in the electrostatic attraction between the $–NH_2$ functional groups and the solutes, both of which are capable of generating the adsorption of organic substrates by Cs (Benavente, 2008). The chelating groups ($–NH_2$ and –OH groups assist as coordination and reaction sites, respectively) on the Cs is attributed to the binding ability of Cs for synthetic dyes (Zainal *et al.*, 2009), while the adsorption process that is simply mediated by Cs is amongst the most successful technique that were effectively used against inorganic, organic, and heavy metal pollutants from polluted water bodies. The combined effects of Cs and TiO_2 were known as adsorption–photodegradation that are coated on a glass substrate (Cs–TiO_2/Glass), demonstrate an improvement when used to treat or pre-treat dye-containing wastewater under visible light. The immobilization of Cs-TiO_2 photocatalyst on a glass substrate also assist in the separation upon the photocatalysis process.

In this study, reactive TiO_2 (using $TiO_{2(SY)}$ and $TiO_{2(DP25)}$) was coated or incorporated into Cs on the smooth surface of the glass substrate (separately using that different TiO_2). It is expected that this would be incredibly useful in the investigation of the mixed effect

of adsorption–photodegradation, mediated by Cs–TiO_2 photocatalyst (both Cs-$TiO_{2(SY)}$ and Cs-$TiO_{2(DP25)}$ photocatalysts are known for this study). The actual photocatalytic degradation process, which makes use of TiO_2, has been shown to be extremely successful in degrading MO, which is representative of synthetic dye compounds. Furthermore, the presence of Cs was acknowledged to have a very encouraging effect on the adsorption capability of the TiO_2 nanoparticles. Therefore, it was expected that both TiO_2 and Cs respective advantages are compatible upon the glass substrate, resulting in a diverse approach in dealing with several wastewater pollutants, especially for the synthetic dyes. Glass substrates demonstrated distinctive advantage as a photocatalyst support, such as retaining transparency even after the immobilization of the photocatalyst, which allows for the penetration of light, improving its photocatalytic activities. A byproduct of this approach is that the photocatalyst will gain large surface areas. Other benefits of a glass substrate include superior adsorption properties, higher surface area, and increased surface or reduced charge recombination.

1.2 Problem statement

Environmental pollution is one of the major and most urgent problems of the modern world. Industries are the greatest polluters, with the textile industry generating high liquid effluent pollutants, due to the large quantities of water being used in fabric processing (Pereira & Alves, 2012). Dyes are an important class of synthetic organic compounds used in many industries, especially textiles. Consequently, they have become common industrial environmental pollutants during synthesis, and later during fiber dyeing (Chequer *et al.*, 2013). The textile industry is facing a challenge in the field of quality and productivity, due to a globalized market. As the highly competitive atmosphere and the ecological parameters become more stringent, the prime concern of textile manufacturers is to be aware of the quality of their products and the effect of the manufacturing process on the environmental (Pereira & Alves, 2012).

The contamination of water stream from industrial wastes containing some hazardous organic compounds, even at low concentrations, have become a global concern and subsequently, a potential health hazard. The remediation of the contaminant is challenging, due to its unique chemical and physical characteristics. To this, photocatalytic oxidation has been proposed as one of the most effective techniques to treat the hazardous and toxic organic pollutants from water, using semiconductors as photocatalysts (Faramarzpour *et al.*, 2009). This system has shown promising results, and is more environmental friendly, cost effective, and utilizes either UV-light from sunlight. Therefore, the potential of using the photocatalysis technique as an alternative to degrade harmful organic pollutants should be looked into.

Studies by Fujishima (1972) discussed the discovery of water photoelectrolysis on TiO_2 with corresponding exceptional chemical and physical properties. To date, electrochemical oxidation reaction of a Ti substrate under a specific set of environment conditions have been widely reported by many researchers. However, TiO_2 are still far from becoming a potential candidate for a photocatalytic system. Bundling problems and weak adherence, due to the multi-phase Ti substrate, remains a great concern. In addition, poor visible light absorption and the rapid recombination of charge carriers limit its applicability. Thus, realizing a high efficiency in a photocatalytic system using TiO_2 as a photocatalyst is a complex undertaking, unless several related issues are resolved.

1.3 Scope of present work

The TiO_2 was synthesized via the sol-gel method ($TiO_{2(SY)}$) and the commercialized one ($TiO_{2(DP25)}$) was then duly compared to the synthesized sample. The band gap energy, chemical bonding, and phase and structure property of TiO_2 nanoparticles (both $TiO_{2(SY)}$ and $TiO_{2(DP25)}$) were characterized using FESEM+EDS, HR-TEM, XRD, Raman and FTIR, and UV-DR analysis. Both $TiO_{2(SY)}$ and $TiO_{2(DP25)}$ nanoparticles were used as an

indicator for the preparation coated Cs on the glass substrate, called Cs-TiO_2/Glass photocatalyst. Subsequently, the photocatalyst was characterized using FESEM+EDS, FTIR, and UV-DR analysis. Later, the Cs-TiO_2/Glass photototcatalyst were tested in the UV-induced (λ=365 nm) degradation system of MO solution, and the data obtained from the UV-Vis Spectrophotometer were analyzed for its corresponding photocatalytic activity. The processes involved in the adsorption-photodegradation of MO was conducted at room temperature and pressure. The effect of certain parameters, such as the initial concentrations and pH of the MO model pollutant sample solution. Include, the cycles structure on the glass substrate, and the weight ratio used between Cs and TiO_2 to prepare these photocatalysts were also studied. In the final stage, the final sample of photocatalysts with the MO pollutant was obtained post-photocatalytic activity and analyzed for its adsorption.

1.4 Objectives

The objectives of this study are:-

1. To synthesis and study the surface, physical and morphological characteristic of anatase TiO_2 nanoparticles.
2. To fabricate via dip-coating method and characterize based on functional group analysis, morphological with elemental analysis and band gap energy of both Cs-$TiO_{2(SY)}$/Glass and Cs-$TiO_{2(DP25)}$/Glass photocatalysts.
3. To study the photocatalytic of Cs-TiO_2/Glass towards monoazo dye (MO) by the process of adsorption and photodegradation.

1.5 Organization of Thesis

This thesis has been structured into 5 respective chapters.

Chapter 1- Present a general review of the project including the problem statement, research motivation and objectives of the study.

Chapter 2- Highlight on the literature review and research background of the wastewater treatment technology, photocatalysis of synthetic dyes remediation, TiO_2 photocatalysis and Cs system, and photocatalytic of Cs-TiO_2 at different wastewater treatments conditions.

Chapter 3- Described on the synthesis of TiO_2 and its characterization followed by preparation of Cs-TiO_2/Glass photocatalyst and the application of these photocatalyst towards MO degradation.

Chapter 4- Presented and discussed on the characterization of synthesized TiO_2, properties of Cs-TiO_2 into glass substrate and photocatalytic activities of Cs-TiO_2/Glass starting with photocatalysts optimization that are cycles and weight ratio and further analysis at initial concentration and different pH medium used of model pollutant used which is MO.

Chapter 5- Summarizes the overall conclusions and recommendation for future research proposal of this study.

CHAPTER 2: LITERATURE REVIEW

2.1 Wastewater

Water pollution from domestic and industrial sectors continue to be critical towards environmental problems (H. Liu *et al.*, 2004). Therefore, an effective wastewater treatment is required to deal with the disposal of human and industrial effluents without being hazardous to human health or the environment.

The amount of wastewater generated domestically and the industry in developed countries require slightly advance treatments (Gray, 2004). One of the major sources of aquatic pollution from the toxic effluents is the result of wastewater damaging untreated received waters (Ngadi *et al.*, 2014).

2.1.1 Impact synthetic dyes waste on human life and aquatic medium

One of man-made pollutants that are toxic, carcinogenic, and mutagenic to human life are pollutants containing dyes (Harruddin *et al.*, 2015). The usage of dyes is estimated to be approximately 40% of the global population, which presents a carcinogenic effect containing bounded chlorine. The dye components become more dangerous when released into surface waters, such as rivers, seas, or reservoirs. The problems become more significant, as the synthesized dyes are mostly stable against the biological, photochemical, and degradation process.

2.1.2 Pollutant: Synthetic dyes

The azo reactive dye, which includes (–N=N–) groups, are associated with a substituted aromatic structure of sp2 hybridized C-atoms, also known as Methyl Orange (MO). The azo groups are mostly bound to benzene or naphthalene rings, aromatic heterocyclic, or enolizable aliphatic groups. MO is commonly used as an anionic monoazo dye in laboratory assays and textiles (Zainal *et al.*, 2009). Moreover, MO is difficult to remove, due to its stability against light, heat, and oxidizing agents. The

presence of ionizing groups, known as auxochromes, results in a much stronger alteration of the maximum absorption of the compound, and provides a bonding affinity. Legislations have been enacted for the discharge of MO, which consequently makes it necessary to develop several efficient technologies for the removal of MO from wastewater (H. Liu *et al.*, 2004).

2.2 Wastewater treatment: Conventional method

Generally, wastewater treatment begin with the determination of the type of wastewater and possible treatments (Stovall, 2007), followed by a combined treatment depending on the results of the former. This includes operations to remove solids, organic matter, and nutrients. Finally, the water is purified by disinfecting it using chlorine, and sometimes ozone or ultraviolet (UV) radiations. Table 2.1 presents the list of treatment technology while Table 2.2 explain about the advantage of facilities from the USEPA (1998) on the facility-specific treatment technology that is generally used for conventional wastewater treatments.

Table 2.1: List of technologies for conventional wastewater treatment

1. Equalization	**13.** Sand Filtration
2. Neutralization	**14.** Multimedia Filtration
3. Flocculation	**15.** Ultrafiltration
4. Emulsion Breaking	**16.** Carbon Adsorption
5. Gravity-Assisted Separation	**17.** Reverse Osmosis
6. Skimming	**18.** Air Stripping
7. Plate/Tube Separation	**19.** Ion Exchange
8. Dissolved Air Flotation	**20.** Biological Treatment
9. Chromium Reduction	**21.** Activated Sludge
10. Cyanide Destruction	**22.** Sequencing Batch Reactors
11. Chemical Precipitation	**23.** Vacuum Filtration
12. Filtration	**24.** Pressure Filtration

Table 2.2: Advantages of facilities for conventional wastewater treatment (USEPA, 1998)

Facilities	Advantages
Aquatic Systems	
Stabilization lagoons	Low capital cost Low operation and maintenance costs Low technical manpower requirement
Aerated lagoons	Requires relatively little land area Produces few undesirable odors
Terrestrial Systems	
Septic tanks	Can be used by individual households Easy to operate and maintain Can be built in rural areas
Constructed wetlands	Removes up to 70% of solids and bacteria Minimal capital cost Low operation and maintenance requirements and costs
Mechanical Systems	
Filtration systems	Minimal land requirements; can be used for household-scale treatment Relatively low cost Easy to operate
Vertical biological reactors	Highly efficient treatment method Requires little land area Applicable to small communities for local-scale treatment and to big cities for regional-scale treatment
Activated sludge	Highly efficient treatment method Requires little land area Applicable to small communities for local-scale treatment and to big cities for regional-scale treatment

2.2.1 Limitations on conventional wastewater treatment

There are several limitations on the conventional wastewater treatment facilities with respect to their facilities and specific and/or additional treatment systems (Table 2.3). Some of these limitations include the generally high amounts needed towards the construction, ease of operation, and elevated costs for personnel and operation systems. Natural biological systems, on the other hand, are more land-intensive, require less-skilled operators, and can produce effluents of variable qualities, depending on time of the year, variety of the plants, and the volume of wastewater loading (Ghosh, 2006). Moreover, the complexity and cost of wastewater treatment technologies increases with the quality of the effluent produced.

Table 2.3: Limitations of Conventional Wastewater Treatment Technologies

Facilities	Limitations
Aquatic Systems	
Stabilization lagoons	Uses an extensive area of land. May produce undesirable odors.
Aerated lagoons	Mechanical devices are required to aerate the basins. Effluents with a high suspended solids concentration will produces.
Terrestrial Systems	
Septic tanks	Provides a low treatment efficiency. Periodically the tanks `are compulsory to pump. The landfill has required for disposal purpose for each sludge and septage.
Constructed wetlands	Remains largely experimental. Requires periodic removal of excess plant material. Requires suitable native plants to derive the best used in areas.
Mechanical Systems	
Filtration systems	Mechanical devices are fully required.
Vertical biological reactors	Expensive. Sophisticated technology. Technically skilled manpower for operation and maintenance must be provided. Requires spare-parts-availability. Has a high energy requirement.
Activated sludge	Expensive. Disposal area for sludge (that is usually land-spread) is required. Requires full experience of manpower for operation and maintenance.
Other Systems	
Membrane bioreactor (Clara *et al.*, 2005)	The costs and requirements for operation and maintenance, as well as power consumption, are expensive.
Adsorption	Required a specialized and expensive distillation (or extraction) for product recovery. Adsorbent progressively is deteriorating in capacity as the number of cycles increases. Relatively high capital cost. Requires high steam to desorb high-molecular-weight hydrocarbons. Hazardous waste may obtain from spent adsorbent, and some contaminants may cause harmful to the environment.
Coagulation-flocculation	pH adjustment is required before or after treatment. Temperature sensitive. Requires high content of dosage. Produce certain amount of Physico-chemical sludge in the higher amount. The operational costs are slightly expensive.
Column separation (Jung *et al.*, 2009)	Some substances in water potentially contaminated the column. To gain in low effluent the column need to be regularly cleaned. It is designed to remove certain metals only. Must consider high operating cost to run and process the water treatment effectively.

2.3 Wastewater treatment: Photocatalysis system

Heterogeneous catalysis is one of the most common environmental clean-up techniques used in wastewater treatment. Most of the photodegradation processes are used for municipal wastewater, cosmetics and pharmaceutical wastewaters, gray water and paper mill wastewater (Lazar *et al.*, 2012). The photocatalysis process is regarded as an eco-friendly approach, mainly because it lacks chemical inputs or outputs, with no sludge residue being generated (Bagheri, Muhd Julkapli, *et al.*, 2015). Simultaneously, a similar technique is also capable of treating wastewater contaminated by the textile industry and organic/synthetic dyes.

Nanosized photocatalyst are touted for many potential applications in purifying polluted water. The photocatalysis oxidation process is a potential replacement for physical and biological techniques, as it can be carried out under ambient conditions employing atmospheric oxygen as its oxidant, resulting in the total mineralization of the contaminants to CO2, mineral acids, or water.

2.3.1 Photocatalysis system: Introduction and principle

Recently, photocatalysis are attracting increased interest because of its chemical stability, recyclability, low costs, and non-toxic processing routes (Bagheri, Hir, *et al.*, 2015; Bagheri, Muhd Julkapli, *et al.*, 2015; Muhd Julkapli *et al.*, 2014). Photocatalysis is a catalytic reaction (oxidation/reduction) that produces a catalyst via the absorption of either UV light or visible irradiation. The process is initiated with the appropriate positioning of the valence band (VB) and conduction band (CB) of semiconductors materials (Lazar *et al.*, 2012).

A sensitized photoreaction is representative of a photocatalysis system; where the light (photo) adsorbed by the catalyst takes place through energy transfer via the formation of an activated state of the reactant of interest, which is more easily oxidized than their

corresponding ground state, or electron transfer by acting either as an electron acceptor or donor (Castellote & Bengtsson, 2011). In order to encounter an oxidizer/acceptor molecule and a reducer/donor molecule for photocatalysis, the photoelectron and photohole have to reach the surface simultaneously.

The combination between the relevant processes of interest, with high efficiency solar energy conversion, can generate increased activity that would be ideal for photocatalytic semiconductors. Moreover, the semiconductor should be non-toxic, biologically and chemically inert, and stable over long periods, easily processable and readily available (Leary & Westwood, 2011). Indeed, an even more advanced photocatalytic treatment technique provides substantial environmental remediation prospects, including water decontamination and purification, deodorization of air, and others (Bagheri, Hir, *et al.*, 2015; Bagheri *et al.*, 2012). During the photocatalyst process, the semiconductor material absorbs the introduced light and promotes the electron from the VB to the CB. Once they reach excitation, the produced electron- hole pair induces the redox reaction, which will photocatalytically degrade organic contaminants (Bagheri, Mohd Hir, *et al.*, 2015; Bagheri, Muhd Julkapli, *et al.*, 2015; Bagheri *et al.*, 2012; Muhd Julkapli *et al.*, 2014).

One of the drawbacks of using the photocatalysis system is the presence of organic materials within the system (X. Chen *et al.*, 2015; Pu *et al.*, 2015; J. WANG *et al.*, 2015). Exces- sive suspended material loading results in light scattering, which reduces the photocatalytic performance of the process (Muhd Julkapli *et al.*, 2014; Pu *et al.*, 2015). Therefore, the integration of the photocatalysis procedure with a physicochemical treatment process, which includes adsorption and coagulation as its pretreatment stages, is regarded as nec- essary for an effective industrial process (H.-Y. Jiang *et al.*, 2015). The integration of adsorption and photocatalytic treatment mitigates many problems

associated with the wastewater industry. This hybrid process can address the limitations of each method when operated separately, which enhances the total removal efficiency of the entire process (Danwittayakul *et al.*, 2015; Villa *et al.*, 2015; Yuxiang Zhu *et al.*, 2015).

2.4 TiO_2 photocatalysis system

In 1972, Fujishima and Honda discovered photocatalytic water splitting on a TiO2 electrode under ultraviolet light (Bagheri *et al.*, 2014; Hashimoto *et al.*, 2005; McCullagh *et al.*, 2007). After that, several promising environmental and energy applications have emerged from this observation, including photovoltaics, photocatalysis, the sensor, and photochromic (Bagheri *et al.*, 2014). TiO_2, which is the most tested semiconductor to date, is a promising photocatalyst because of its appropriate electronic band structure, chemical inertness, photostability, and commercial availability (Table 2.4). The effective utilization of clean, safe, and plentiful solar energy through TiO_2 photocatalysis represents promising solutions to the serious environmental challenges and energy crisis (Bagheri *et al.*, 2014; S. G. Kumar & Devi, 2011).

Table 2.4: Advantages and disadvantages of different types of TiO2 nanoparticles as a photocatalyst

Type of TiO2 semiconductor	Advantages	Disadvantages
Granular TiO2 (Hosseini *et al.*, 2007)	• Large surface area. • Broadband gap. • More active sites. • High photocatalytic activity. • Promising photoelectrochemical properties. • Good gas sensitivity.	• Hard to recycle and re-utilize in water. • Can cause the secondary pollution of water.

Continued on next page

Mesoporous TiO2 (G. Liu *et al.*, 2008)	• Can be utilized as a catalyst support, ceramic membrane top cycle, and adsorbent. • Promoting the diffusion of the reactants and products; facilitating access to the reactive sites on the surface of the photocatalyst.	• Low separation efficiency of photogenerated electron-hole pairs.
Aerogels TiO2 (Popa *et al.*, 2009)	• Higher surface area. • Tailored pore size distribution.	• Low crystallinity. • Electron-hole recombination rate.

TiO_2-based photocatalysts has been touted as a potential treatment for full-scale degradation of organic compounds in wastewaters (Linsebigler *et al.*, 1995). TiO_2 is regarded as a stable photocatalyst, due to its wide band gap (3.0 and 3.2 eV), dependence on phase transformation, and only active in the UV region, which is less than 10% of the overall solar intensity (Linsebigler *et al.*, 1995).

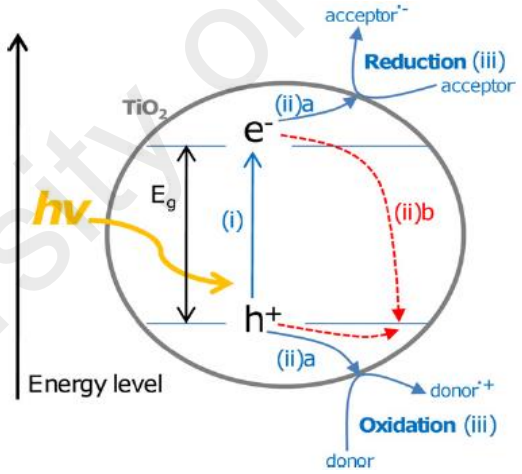

Figure 2.1: Main processes in semiconductor photocatalysis. (i) Photon absorption and electron–hole pair generation. (ii) Charge separation and migration; (ii) a to surface reaction sites (ii) b to recombination sites. (iii) Surface chemical reaction at active sites. Adapted from "Carbonaceous nanomaterials for the enhancement of TiO_2 photocatalysis," by Leary and Westwood (2011). Copyright 2010 by the Elsevier Ltd

The principle of photocatalysis is illustrated in Figure 2.1. These two primary reactions, known as oxidation and reduction, occur simultaneously from photogenerated holes and electrons, respectively. From Figure 2.1, the process of creating electron–hole pairs initiated the absorption of photons. The energy of the incident light must be higher than the energy difference between the VB and CB if an electron is to be promoted from

the former to the latter (Leary & Westwood, 2011). The exposure of TiO2 nanoparticles to UV light through an energy that complements or surpasses its band gap energy (anatase >3.2 eV; rutile >3.0 eV) results in an electron excitation from the VB into the CB, leaving behind a positive hole (S. G. Kumar & Devi, 2011; Tachikawa *et al.*, 2011). Photogenerated charge carriers are exploited in a different process at the particles' surface, whereby the holes migrate to the particles' surface, inducing charge transfer to the adsorbed molecules (Daimon & Nosaka, 2007; Lukes *et al.*, 2005).

This makes a TiO_2 photocatalytic system useful and advantageous in improving wastewater effluents. The degradation process using a photocatalytic system will help achieve standards of pollution control and prevent environmental pollution on surface water and soil. This technology is commercialized for industrial applications, due to its low operation temperature, low cost, and significantly low energy consumption, based on the comparison detailed in Table 2.4.

Table 2.5: The attributes between TiO_2 photocatalyst (photocatalysis process) as compared to conventional wastewater treatment (J. Kumar & Bansal, 2013)

The attributes	**Photocatalysis process using TiO_2 photocatalysts**	**Conventional wastewater treatment**
Efficiency	The photocatalytic activity are stable and sustainable. Low energy UV light is used for photocatalyst activation and even solar light can be used. Suitability towards visible or near UV light. High conversion efficiency and high quantum yield. Good adsorption in solar spectrum.	Require disinfection process to remove pathogens. Require high consumption of energy for the treatment process.
Cost effectiveness	Economically it is comparable with activated carbon adsorption method for intermediate and large capacities. Low cost. No consumption of expensive and hazardous oxidizing chemicals (H_2O_2 and O_3).	Slightly expensive for operating cost include maintenance. Consume a large amount and expensive hazardous chemical for treatment process.

Continued on next page

Other	Green technology process because degradation products (i.e; CO_2, H_2O) are environmentally harmless. Can be react with wide range of substrate and high adaptability to various environment. Almost all organic pollutants can be mineralized. Complete mineralization of the majority of organic pollutant can be achieved.	Wastewater treatment facilities containing organic compounds fall within this 3 given categories:- - Non-destructive procedures. - Biological destructive. - Oxidative destructive processes. The most common treatment to remove the contaminants of wastewater is adsorption process and produce sludge as the end-products after treatment.

2.4.1 TiO_2 photocatalysis system: Synthesis method and properties

There are a variety of methods and issues related to the process of fabricating a TiO_2 photocatalysis system. The most common method that has seen wide usage in ceramic engineering and materials science is the sol-gel process. It involves a wet-chemical technique, known as the chemical solution deposition. This approach has seen wide usage in the fabrication of TiO_2 photocatalysts systems (Tseng *et al.*, 2010).

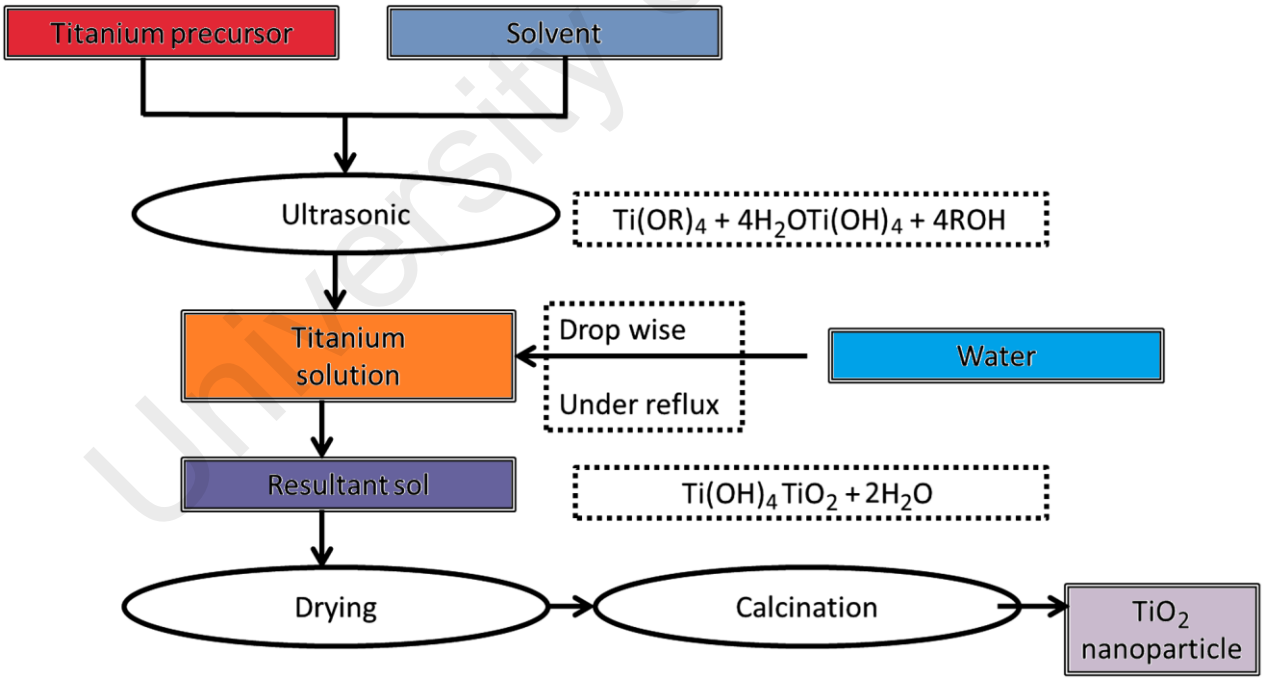

Figure 2.2: TiO_2 sol-gel method process

Figure 2.2 illustrates the preparation of TiO_2 with the sol-gel method by using Titaniumtetraisopropoxide (TTIP) precursor for an integrated network. The sol-gel technique relies on inorganic polymerization reactions, which includes four main steps:

hydrolysis, polycondensation, drying, and thermal decomposition (Figure 2.2). The precursors of the metal or non-metal alkoxide hydrolysis take place with alcohol or water. On top of alcohol and water, a base or an acid such as Acetic acid also helps precursor hydrolysis (Chekin *et al.*, 2013; Su *et al.*, 2004; M. Zhang *et al.*, 2001). While, solvent was subsequently removed postcondensation, leaving behind a gel. Calcination at higher temperatures is required to decompose the organic precursor (M. Zhang *et al.*, 2001). The size of the sol-gel particles is based on the solution composition, temperature, and pH which have their own advantages and disadvantages that have been listed from Table 2.5. Controlling these parameters allows us to tune the size of the TiO2 particles (Yongfa Zhu *et al.*, 2000).

Table 2.6: Advantages and disadvantages of sol-gel method in production of TiO_2 nanoparticles

Advantages	Disadvantages
• Sol preparation in the ambient temperature of and the processing of gel. • Product homogeneity. • Low temperature of sintering. • Ease of making multicomponent materials. • Good control over powder particle size. • Controllable particle shape and size distribution.	• Expensive. • Slow reaction. • Not suitable for bulk production. • Separation limitation.

In addition, a thermal treatment, or a firing process at the last stage, is also necessary to prompt further polycondensation and enhance the mechanical properties and structural stability via final sintering, densification, and grain growth (Byranvanda *et al.*). However, the sol-gel technique has some drawback, such as the raw materials currently used are expensive, time consuming, and existence of a large number of pores in the gel during the drying process. (that has been mentioned in Table 2.6)

2.4.2 TiO_2 photocatalysis system: Applications

Due to its promising photocatalytic activities, TiO_2 nanoparticles have been used in antiseptic and antibacterial compositions, degrading organic contaminants and germs, and as a UV-resistant material used in the paper industry for improving the opacity of paper. Indeed, TiO_2 nanoparticles is also used as photocatalysis for water splitting to generate hydrogen, for degrading environmental pollutants in aqueous contamination and for wastewater treatment, carbon dioxide remediation, self-cleaning activity, and air purification (Fujishima *et al.*, 2007; Leary & Westwood, 2011).

Oudenhoven *et al.* (2004) discussed several important properties that are related to photocatalyst used for water splitting. The properties that are initially determined are the bandgap of the photocatalyst itself, which should fall between 2.43 eV and 3.2 eV. Both VB and CB should be lower than the oxygen oxidation potential and higher than the hydrogen reduction potential, respectively. Assistance from some sort of co-catalyst for hydrogen generation is necessary. It can initiate the photocatalyst reaction to split water in the protons and hydroxyl (-OH) anions. The generation of water from molecular oxygen and hydrogen are reduced due to the transport of the electrons to the surface.

2.4.3 TiO_2 photocatalysis system: Limitations

There are some limitations that are inherent in nanosized TiO_2 when it's used as a photocatalyst. The first is its involvement in the efficiency of particular catalytic materials, and second, the suitable illumination time that will result in an effective reaction is difficult to determine. Third, the surface area of the catalyst must be improved to maximize the mass transfer reaction. Therefore, the donor and acceptor molecules must reach the catalysts' surface prior to recombination (Riley, Borja, Williams, Gill, & Plawsky). TiO_2 nanoparticles were easily suspended in water, clog filter membranes, and

penetrate filter materials. Practically, there are economic costs to filtering out the slurry inside the water post-treatment.

In general, catalytic ozonation and photocatalytic oxidation are processed in a suspension of sub-micrometer-sized particles. Thus, there is a strong necessity for an extra separation stage to get rid of the photocatalyst from treated water, which contains a key disadvantage of water treating applications.

2.4.3.1 Separation process

Although several semiconductors have proven to be ideal candidates for the treatment of water pollution, the efficient separation and recycling of this fine-powdered photocatalyst is still a scientific problem when applied in practice (Sclafani et al. 1990, Sato et al. 2004). Moreover, it is still very difficult to separate and recycle these nanoscaled photocatalysts because of their small size. Thus, a facile and effective approach to recover suspended semiconductor particles is greatly desirable.

2.4.3.2 Selectivity

Because the selectivity of most photocatalyst semiconductors are not conducive to take away highly toxic contaminants with the existence of other contaminants (Shengwei et al. 2010).

2.4.3.3 Dispersion

Another significant problem related to photocatalytic efficiency is a limitation on the dispersion of the photocatalyst throughout the solution. This consequently limits the interaction between the photocatalyst and the targeted pollutant (Sahar and Masoud Salavati, 2015).

2.5 TiO_2 support photocatalysis system

Generally, the incorporation of support material in TiO_2 result in superior photocatalysis and purification systems. Support material is required to overcome, or at least minimize, the inherent drawbacks that are the direct result of the physical properties of supported photocatalysts. The support materials for the TiO_2 semiconductor are used in many applications and are related to photocatalytic systems are groundwater denitrification and the photocatalytic oxidation of water pollutants. Usually, semiconductor supports are classified by their chemical nature, which can either be organic or inorganic supports. These series of support materials play an important role in immobilizing active catalysts, increase the surface area of the catalytic material, decrease sintering and improve hydrophobicity, thermal, hydrolytic, and the chemical stability of the catalytic material. The common materials used to support TiO_2 are glass, carbon fibers, and woven fiber cloths (Ibhadon & Fitzpatrick, 2013). Table 2.5 shows the photocatalytic activity of a variety of TiO_2 with support materials towards different pollutants. From Table 2.5, most of the supported TiO_2 photocatalyst, with its chosen material, performs well and show high levels of photodegradation towards the selected pollutants.

Table 2.7: List of TiO_2 with support material in photocatalysis system to stimulate photodegradation process towards different pollutants

TiO_2 photocatalysis system	**Pollutants (concentration)**	**Light illumination**	**Photodegradation (%)**	**References**
Different pollutants				
Activated carbon–TiO_2	Acid Red 88 (14 ppm)	UV-Light	95%	Gao *et al.* (2011)
Au–TiO_2	Acetaldehyde (20 ppm)	Visible Light	94%	C. Pan and Dong (2011)
Activated carbon composite material–TiO_2	Tartrazine (8 ppm)	UV-Light	➢ 80%	Andriantsiferana *et al.* (2014)
TiO_2–Kao composites	Acid red G & 4-nitrophenol	UV-Light	➢ 90%	X. Zhang *et al.* (2011)

Continued on next page

	(15 ppm)			
Gaseous pollutant				
TiO_2–ZrO_2	Phenol (15 ppm)	Visible Light	90%	Kambur *et al.* (2012)
Ag–TiO_2 thin film	Benzene, toluene, ethylbenzene and xylene (10 ppm)	UV-Light	79, 82, 86 and 88%	Peerakiatkhajorn (2013)
Methylene blue pollutant				
Polyterthiophene derivatives–TiO_2 nanocomposites	Methylene blue (20 ppm)	UV-Light	90.5%	Jamal *et al.* (2014)
Carbon–TiO_2 hybrid aerogel	Methylene blue (10 ppm)	Visible Light	100%	Shao *et al.* (2013)
ZnO–TiO_2 hybrid	Methylene blue (8 ppm)	UV-Light	99.9%	Cheng *et al.* (2014)
Graphene–TiO_2 nanowire	Methylene blue (10 ppm)	UV-Light	➢ 90%	X. Pan *et al.* (2013)
TiO_2–graphene–carbon composite nanofibers	Methylene blue (15 ppm)	UV-Light	➢ 90%	C. H. Kim *et al.* (2012)
SiO_2–TiO_2 thin film	Methylene blue (5 ppm)	Visible Light	81%	Klankaw *et al.* (2012)
Rhodamine B pollutant				
BiOBr–TiO_2	Rhodamine B (5 ppm)	UV-Light	92% and 100%	Wei *et al.* (2013)
Reduced Graphene Oxide–TiO_2	Rhodamine B (10 ppm)	UV-Light	98.8%	Sher Shah et al. (2012)
Activated carbon–TiO_2	Rhodamine B (10 ppm)	Visible Light	98%	Asiltürk et al. (2012)
Polymer–TiO_2 hybrid nanoparticles	Rhodamine B (12 ppm)	UV-Light	95%	Xiao *et al.* (2013)
Activated carbon fiber–TiO_2	Rhodamine B (20 ppm)	UV-Light	67.6%	Meng *et al.* (2014)

2.5.1 Cs-TiO_2 support photocatalysis system: Principle and advantages

Chitosan (Cs) is the deacetylated derivative of chitin, and it is a linear polymer of [α(1→4)-linked 2-amino-2-deoxy-β-D-glucopyranose]. Cs is simple, while the amino group (-NH_2) in chitosan replaces the chitin acetamide groups (-$NHCOCH_3$) at C-2 positions and the disaccharide repeating unit of chitosan ($C_{12}H_{22}O_8N_2$), representing

idealized structures (Dutta *et al.*, 2004). These features include its abundance, hydrophilicity, anti-bacterial property, biodegradability, non-toxicity, and biocompability. Using Cs as a support material for TiO_2 photocatalysis requires some modification due to its thermal stability. It was reported that Cs effectively adsorbs dyes, metal ions, organic acids, and pesticide, due to its high adsorption potentials. Varieties of useful features of Cs make it a versatile adsorbent, where the photocatalytic process of the TiO_2 support with Cs is detailed in Figure 2.3.

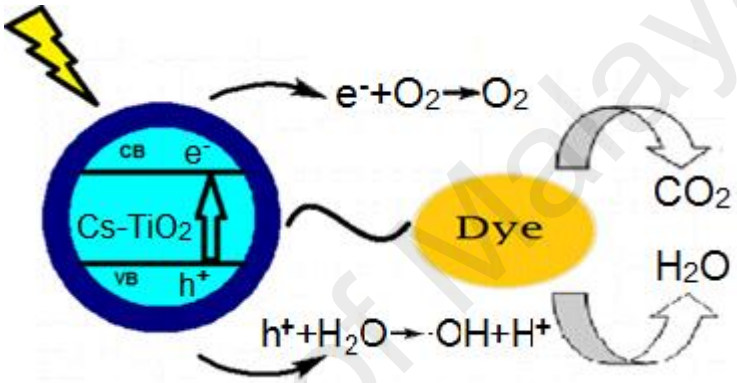

Figure 2.3: Photocatalytic activity of Cs-TiO_2 photocatalyst to dye/MO degradation

Supporting nanosized photocatalysts on the Cs can effectively prevent nanoparticles from agglomerating during nucleation and growth. Indeed, it is also used to overcome the difficulty in separation and the recovery of nanosized powder materials. The role of Cs is another important factor that helps immobilize the active catalyst, specifically TiO_2, which can increase the surface area of catalytic material, decrease sintering, and improve hydrophobicity, thermal, hydrolytic, and the chemical stability of the catalytic material (Ibhadon & Fitzpatrick, 2013).

2.5.2 Cs-TiO_2 support photocatalysis system: Synthesis method and properties

The sol-gel technique is frequently used to synthesize TiO_2 photocatalyst based on the high-temperature calcination of nanocrystalline particles. High-temperature annealing (>400°C) can remove organic additives, which can further promote chemical interconnection among the particles in establishing their electrical connection. Figure 2.4

shows that this approach is defined as the ex-situ synthesis of nanocomposites (Guo *et al.*, 2014).

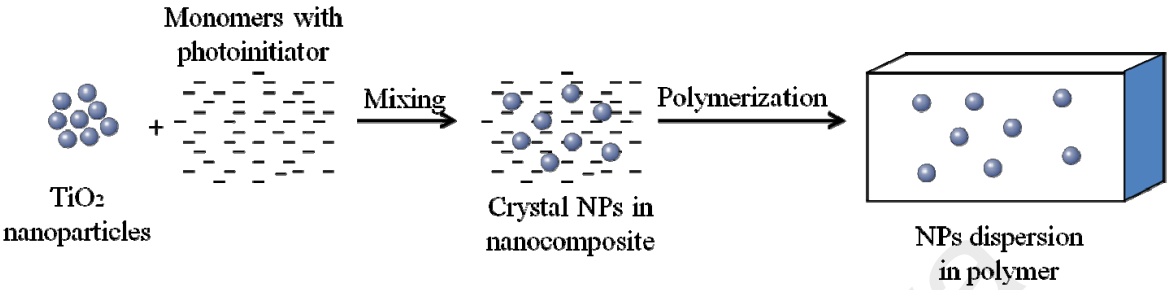

Figure 2.4: Ex situ synthesis schemes for the preparation of nanocomposites. Adapted from "Comparison of in situ and ex situ Methods for Synthesis of Two-Photon Polymerization Polymer Nanocomposites," by Guo *et al.* (2014). Copyright 2014 by the authors

The ex-situ synthesis method is more suitable for large-scale industrial applications compared to the in-situ method. The key concern for this approach is based on the preparation of the nanoparticles, which increase in size to form a homogenized solution in the polymer and obtain long-term stability against aggregation. Thus, the sonication method is applicable for dispersing any nanoparticles in the polymer and the creation of an excellent formation (Guo *et al.*, 2014).

2.5.3 Cs-TiO_2 support photocatalysis system: Limitations

Cs has poor solubility at a pH of more than 6.5, while it is soluble in acidic conditions. This can be explained by the solution containing free -NH_2 groups on its polymeric chains, which are capable of protonation, resulting in a positive charge. The -NH_2 group in Cs has a pKa value of ~6.5, which leads to a protonation in acidic-to-neutral solution, with a charge density that is dependent on pH and the %DA-value. This is confirmed by confirming that within an acidic medium, the -NH_2 group on Cs is protonated, thus dissociating the hydrogen bond between Cs and TiO_2 (Wongkupasert, 2008). Moreover, the high temperature calcination does not permit the use of biomaterials, because the high temperature destroys the active structure of the thermally-sensitive substrates.

2.5.4 Cs-TiO_2 support photocatalysis system: Applications

There are several convenient interdisciplinary applications for the Cs-TiO_2 used in polluted wastewater, usually containing multiple hazardous materials (K.-S. Huang *et al.*, 2014). The most common practice is to have a photocatalytic system that include Cs-TiO_2 as its photocatalyst to treat wastewater. Table 2.6 show the Cs-TiO_2 photocatalytic system that resulted in a high percentage of photodegradation and adsorption.

Table 2.8: List of TiO_2 support with Cs that used for the photocatalysis system

TiO_2 photocatalysis system	**Pollutants (concentration)**	**Light illumination**	**Photodegradation (%)**	**References**
TiO_2-Cs nanocomposites	MO (14 ppm)	UV-Light	90%	Fajriati *et al.* (2014)
TiO_2impregnated Cs beads	Toxic dyes (12 ppm)	Visible Light	~63.1%	Farzana and Meenakshi (2013b)
TiO_2 immobilized on chitosan-based hydrogel	C.I. Acid Orange 7 (15 ppm)	UV-Light	90%	Marković *et al.* (2015)
Cs-TiO_2 composite	Toxic dyes (8 ppm)	Visible Light	~93.51%	Farzana and Meenakshi (2013a)
TiO_2/Chitosan immobilized on a glass plate	Phenol (20 ppm)	UV-Light	90%	Nawi *et al.* (2011)

This increase is due to the compound of Cs [β–(1–4)–2–amino–2–deoxy–D–glucose], which has been hydrolyzed to a derivative of chitin containing high amounts of $–NH_2$ and -OH functional groups. In fact, both $–NH_2$ and –OH groups on Cs chains could assist coordination and reaction sites. The electrostatic attraction formed between the $–NH_2$ functional groups and the solutes can generate the adsorption of organic substrates by Cs, whereas the chelating groups (the $–NH_2$ and –OH groups) on the Cs can be attributed to the binding ability of that Cs for synthetic dyes. Both $–NH_2$ and –OH groups on Cs chains

can serve as coordination and reaction sites. The adsorption of organic substrates by Cs happens via the electrostatic attraction formed between the $–NH_2$ functional groups and the solutes.

2.6 TiO_2 immobilized substrate

There are various routes on the immobilization process of different substrates onto a TiO_2 photocatalyst. The deposition method of the prepared solution by the sol-gel process was applied towards substrates such as glass, silica gel, metal, ceramics, polymer, thin films, fibres, zeolite, alumina clays, activated carbon, cellulose, reactor walls, and others (Schäffer, 2012). The main objective in having support materials for a photocatalytic system is to avoid the post-separation difficulties associated with the powder form of the TiO_2 catalyst (Lazar *et al.*, 2012). It is effective for precipitating high reaction rates from the thin film or glass substrate, which could prevent scattering and enhanced transmittance of light, as opposed to its powdered counterpart (Subha & Jayaraj, 2014). The removal process, assisted by a photocatalytic system of the selected model pollutants, use different types of immobilized substrate, and is shown in Table 2.7.

Table 2.9: List of TiO_2 immobilized substrate system that used for the photocatalysis system

TiO_2 photocatalysis system	**Pollutants (concentration)**	**Light illumination**	**Photocatalytic performance (%)**	**References**
TiO_2 and Ag immobilized on corona pretreated polypropylene non-woven fabric	C.I. Acid Orange 7 (10 ppm)	UV-Light	➢ 60%	Marković *et al.* (2015)
TiO_2 Immobilized on Manihot Carbon	Indigo Carmine (8 ppm)	UV-Light	100%	Antonio-Cisneros *et al.* (2015)
TiO_2 immobilized on cotton as template	Phenol (14 ppm)	Visible Light	92%	J. WANG *et al.* (2015)
N-doped TiO_2 immobilized on glass spheres	Methylene Blue (MB) and Eriocrome Black-T (EBT) (10 ppm)	UV-Light	52% (for MB) & 41% (for EBT)	Vaiano *et al.* (2015)
TiO_2 films deposited by cathodic arc (CA films) on glass substrates	Cr(VI) (8 ppm)	UV-Light	100%	Kleiman *et al.* (2011)
TiO_2 immobilized on a mesh-type substrate	Gaseous Formaldehyde and Benzene (6 ppm)	UV-Light	~99%	Chang and Seo (2014)
TiO_2 immobilized on ITO substrate (TiO_2/ITO)	organic pollutant (BB26) (10 ppm)	UV-Light	➢ 90%	C. Kim *et al.* (2009)

2.6.1 TiO_2 immobilized glass substrate photocatalysis system: Principle and advantages

The glass substrate is suitable as a catalyst support, due to its transparency to UV light in photocatalytic applications. This can consequently provide a large surface area and improve the photocatalytic performance of TiO_2. The main advantage of a glass substrate is the transparency of the system, even post-immobilization. This allows for the penetration of light, and resulted in the improvement of the photocatalytic activities.

There are also several other advantages, including higher surface area, superior adsorption properties, and increased surface -OH groups or reduced charge recombination in the process of photocatalysis, all of which are made possible by immobilized systems (Lazar *et al.*, 2012).

2.6.2 TiO_2 immobilized glass substrate photocatalysis system: Synthesis method and properties

There are various techniques that can be used immobilize TiO_2 thin film on inorganic/organic substrate, including chemical vapor deposition, chemical spray pyrolysis, electrodeposition, and sol–gel method (Sonawane *et al.*, 2003).

Sol-gel analysis is a prominent process that can be used for multiple dip-coating of glass substrate immobilization. The immersion of a glass substrate into a solution containing hydrolyzable metal compounds results in the formation of metal oxide coating on the glass substrate. This is followed by the formation of gels on the surface of the glass substrate after withdrawing it at a designated rate into an atmosphere of known humidity and density. The final step involved heating the substrate to about 450° C to remove any remaining solvents (Spagnoli, 1992).

Sol-gel is a widely used process to design both hydrophobic and hydrophilic coatings for the selective compounds into a material or a substrate. During the process, a precursor material is polymerized and further hydrolyzed to obtain a colloidal sol. Next, the sol is deposited on the substrate, and solid films on a glass substrate, for example, is obtained via heating. The sol-gel process is used to obtain ultrafine or spherical-shaped powders, thin film coatings, fibrous, porous or dense materials, and extremely porous aerogel materials. The prepared sol can be applied on the substrate by spray, dip and spin-coating methods (S. Wang, 2014).

In dip-coating, the glass substrate is dipped into the tank or glass beaker containing the colloidal sol. The final coating thickness is determined mainly by the deposition speed and solution's viscosity. According to the previous study by S. Wang (2014), there are several factors that need to be taken into account when dip coating, such as the functionalization of the initial substrate surface, immersion time, withdrawal speed, number of cycles dipped, solution composition, concentration and temperature, number of solutions in each dipping sequence, and environment humidity, all of which influence the final cycle of coating. Dip coating can be used to coat on complex structures as well (S. Wang, 2014).

2.6.3 TiO_2 immobilized glass substrate photocatalysis system: Limitations

Several study investigated the immobilization techniques that are simple do not need any expensive equipment. The production of immobilized TiO_2 catalysts is regarded as a low cost technique. Most of the TiO_2 immobilized glass substrate was used to treat wastewater, which consequently improved the photocatalytic activity. Coating the TiO_2 catalysts resulted in excellent photocatalytic activities and mechanical stabilities with efficient long-term stabilities (Doll & Frimmel, 2004; Schäffer, 2012).

However, the coated photocatalysts on the substrate or film/thin film are lower in surface areas compared to its powdered counterpart. The study is related to the photocatalytic activity, showing that the performance of the films is outperformed by its powdered counterpart (Aziz & Sopyan, 2009). The study by Gan *et al.* (2008) proved that the immobilization of TiO_2 in thin film form would result in surface area constraints, which consequently reduce TiO_2's photocatalytic performance.

2.7 Cs-TiO_2 immobilized glass substrate: Theory & Hypothesis

It was expected that the advantages of both TiO_2 and Cs (that was depicted from Figure 2.5) could be combined on a glass substrate. This consequently offers a diverse approach, and involves the removal of the MO dye pollutant via the adsorption and photodegradation with photocatalysts.

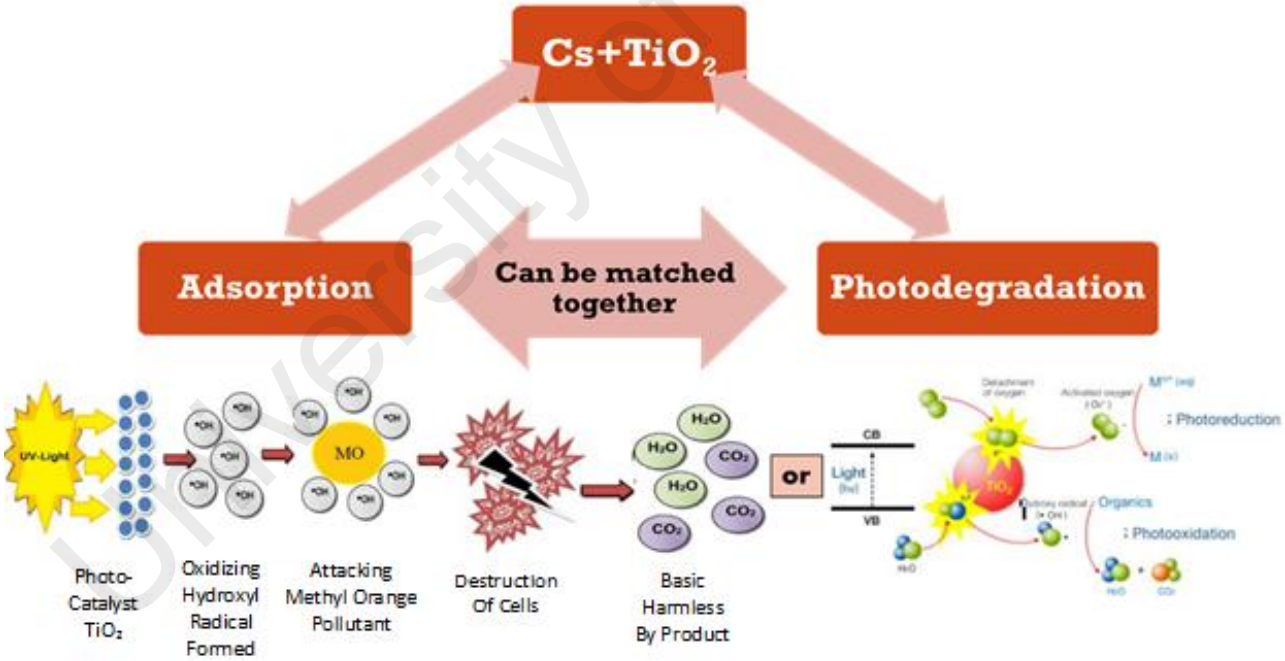

Figure 2.5: Mechanism of Cs together with TiO_2

Furthermore, the function of TiO_2 and Cs are described in (Zainal *et al.*, 2009). In short, the Cs-TiO_2 combination immobilized on a glass substrate gain some advantages, such as high oxidation/reduction potential during the photodegradation process. In the MO solution, the surface hydroxyl groups scavenge the positive holes for a very reactive

oxidization of hydroxyl radicals (•OH), which can promote the degradation process and subsequently lead to the total mineralization of the organic substrate. In the meantime, the use of the commercial Cs is known to restrict the movement from the base of the medium used, resulting in a very encouraging influence on the adsorption capability towards both TiO_2 on the glass substrate, and it also can be used to adsorb the pollutant compound (MO).

2.8 Photocatalytic activities: Effect on photocatalytic conditions

The applicability of combining Cs and TiO_2 to form photocatalysts is indeed promising for the effective adsorption and photodegradation treatment of dye-containing effluents. Therefore, in laboratory conditions, the various pH and the concentration of experimental wastewater model pollutant compound were observed. Furthermore, the consideration of the operational conditions in the treatment process, which involved the photocatalytic treatment process, would affect the performance of the photocatalytic degradation systems.

2.8.1 pH of wastewater medium

Wastewater containing various contaminants, especially dyes, discharges at different pHs. Generally, the pH that is suitable for water discharge, specifically in Malaysia, is pH 6.0-9.0, as stated in the Environmental Quality (Industrial Effluent) Regulations 2009. Therefore, it is important to study the role of the pH on the degradation of specific pollutants. It was reported that the pH of the medium significantly influence the catalysts' particles, the size of catalyst aggregates, and the positions of conductance and valence bands, which consequently affect the final performance of the photocatalysis.

Indeed, the performance of TiO_2 photocatalysis may differ in different types of pH medium, due to the amphoteric behavior of the metal oxides. Furthermore, the pH can influence the surface charge properties of metal oxides during the photocatalytic process.

Thus, reactions could take place on the surface of metal oxides via different mechanism at different pH values. This can be explained by the fact that the surfaces of most metal oxides are negatively and positively charged, as conditional upon the fluctuations of pH values. In order to widen the range of pH values, MO molecules save their respective negative charges. Therefore, the ability of MO to adsorb on the surfaces of metal oxides is increased once the solution's pH is acidic (Pakmehr et al., 2014).

2.8.2 Concentration of pollutants

Semiconductor is related to the use of the pollutants' increasing initial concentrations. Subsequently, it may significantly influence the photocatalytic activities, due to the fact that it becomes the path length of the photons entering the solution decreases, while the reverse is observed when the number of photon absorption is increased by the catalyst at lower concentrations (Bhalerao *et al.*, 2013). Table 2.8 illustrates the different concentrations of MO used in the photodegradation process, which results in the reduction to the photodegradation activity at higher amounts of MO by variety of photocatalysts.

Table 2.10: List of different photocatalysts used for the photodegradation process with different MO concentrations (effect of initial concentrations)

Photocatalysts	MO concentration (ppm)	Light illumination	Photocatalytic performance (%)	References
Fe-doped TiO_2 films	1	UV-Light	77.6	Y. Zhang and Li (2013)
	5		72.2	
	10		34.4	
TiO2/activated carbon	18	UV-Light	96.6% (required 25 min. irradiation time)	X. Wang *et al.* (2009)
	37		More than 90% (required 40 min. irradiation time)	
	58		More than 90% (required 60 min. irradiation time)	
	76		Less than 90% (required more than 60 min. irradiation time)	
	97		Less than 90% (required more than 60 min. irradiation time)	
α-Fe_2O_3-supported Hy zeolite	10	UV-Light	100	Jaafar *et al.* (2012)
	30		80	
	50		40	
	70		20	
	100		Less than 10%	

The increased concentration of the MO saturated the active sites of the catalyst surface with organic species, thus reducing light penetration and subsequent hydroxyl radical formation. Studies by X. Wang *et al.* (2009) shows that greater irradiation time are required to complete the photodegradation process with increasing initial concentrations of MO.

2.8.3 Cycles of photocatalyst on glass substrate

Semiconductors catalysts such as TiO_2, CaF, MgO, SiC, Ti, ITO and others are used as heterogeneous buffer cycles by the researchers (Talebian *et al.*, 2013). The photodegradation process of some organic pollutants need exact dosage of that photocatalysts use. The presence of sufficient active sites on photocatalysts surface, optimal dosage of photocatalysts, and high total active surface area are the factors that influence performance of photocatalyst towards initial solute concentration, which can be analyzed on the basis of optimum catalyst loading. Simultaneously, it will decrease the photoactivated volume of suspension together with penetration of UV light caused by higher of photocatalysts dosage which increase turbidity of the suspension. Therefore, light scattering can caused aggregation as well as reduced irradiation field due to the higher photocatalysts dosage (Bhalerao *et al.*, 2013).

CHAPTER 3: MATERIALS AND METHODOLOGY

3.1 Introduction

This chapter highlights the 5 different stages of the work; from sample preparation to photocatalytic activities analyses. At the first stage (**Stage 1**), the preparation of single catalyst of the TiO_2 (the used of specific commercial and synthesis TiO_2 samples separately for the whole experimentation) using a TTIP precursor was synthesized via the sol-gel method (it's also known as $TiO_{2(SY)}$). Prior to the calcination process, the as-synthesized TiO_2 nanoparticles sample was analyzed using the Thermal Gravimetric Analyzer (TGA) to determine the exact temperature and the required time for the overall calcination process (based on previous studied). Furthermore, the $TiO_{2(SY)}$ and $TiO_{2(DP25)}$ photocatalysts were characterized using Fourier transform infrared spectroscopy (FTIR), X-ray Diffraction (XRD), Raman spectroscopy, High-resolution transmission electron microscopy (HR-TEM), FEG-Emission Scanning Electron Microscopy (FESEM) + Energy Dispersive Spectrometer (EDS), and UV-Vis Diffuse Reflectance Spectroscopy (UV-DR). In the second stage (**Stage 2**), both $TiO_{2(SY)}$ and $TiO_{2(DP25)}$ were incorporated into a Cs matrix which are prepared separately, to produce Cs-TiO_2 hybrid catalyst solution via ex-situ preparation using the dip-coating method. Furthermore, the prepared TiO_2 and Cs solution was coated on a glass substrate (**Stage 3**), resulting in Cs-$TiO_{2(DP25)}$/Glass and Cs-$TiO_{2(SY)}$/Glass photocatalysts. The next stage (**Stage 4**), that involve all prepared samples of Cs-TiO_2/Glass photocatalyst being analyzed using the FE-Emission Scanning Electron Microscopy (FESEM) + Energy Dispersive Spectrometer (EDS), Fourier transform infrared spectroscopy (FTIR), and UV-Vis Diffuse Reflectance Spectroscopy (UV-DR) analyses. The final stage (**Stage 5**), involve the preparation of the photocatalyst samples under a photocatalytic reactor, while the adsorption-photodegradation process was conducted in the presence of UV-light lamp to degrade the simulated organic pollutants and determine the corresponding optimum

working condition and photocatalytic activity. The adsorption and photodegradation activities of Cs-TiO_2/Glass photocatalyst were further analyzed using FTIR.

3.2 Materials/Chemicals

The raw materials and chemicals required in this work to synthesizing TiO_2 are Titanium isopropoxide (purity, 97%), $Ti[OCH(CH_3)_2]_4$ and Acetic acid (purity, 99%), CH_3CO_2H, all of which were procured from Sigma-Aldrich. While, Sodium chloride, NaCl, which was purchased from Merck that contribute in dissolving the Cs. The commercial Cs (medium molecular weight) and MO was obtained from Sigma-Aldrich. De-ionized water was used to prepare all the standard solutions. Glass substrate is used as a source in dip-coating technique to produce Cs-TiO_2/Glass photocatalysts. The general information and some properties of raw materials and chemicals used for this study are detailed in Table 3.1.

Table 3.1: List of raw materials and chemicals used to fabricate TiO_2 nanoparticles and Cs-TiO_2/Glass photocatalysts as well as model pollutant MO used for photocatalytic activity

Materials	Functions	Manufacturer	Other information
Titanium(IV) isopropoxide	TiO_2 synthesis precursor	Sigma-Aldrich	Chemical formula: $Ti[OCH(CH_3)_2]_4$ Purity: 97% Infrared spectrum: Conforms to Structure Specific Gravity: 0.950 - 0.960 @ 25/25 ºC Titanium: 27.5 - 28.3 % as TiO2 Chloride (Cl): <= 65 ppm Freezing point: 17.5 - 19.5 °C - At Time of Manufacturing Color Test: <= 25 APHA - At Time of Manufacturing
Titaniun(IV) Oxide - TiO_2 Degussa-P25	Commercial product	Sigma-Aldrich	Chemical formula: TiO_2 Appearance (Color): White Appearance (Form): Powder Surface Area: 35 - 65 m2/g pH: 3.5 - 4.5 HCl Content: <= 0.30 % Loss on Drying

Continued on next page

			Purity: >=99.5% Based On Trace Metals Analysis Trace Metal Analysis: < 5000.0 ppm
Acetic acid	Hydrolysis process to synthesize photocatalyst	Sigma-Aldrich	Chemical formula: CH_3CO_2H Purity (GC): >=99.0% Appearance (Clarity): Clear Appearance (Color): Colorless Appearance (Form): Liquid
Sodium chloride	Adjusting agent for chitosan formation	Merck	Chemical formula: NaCl Molar Mass: 58.44 g/mol Grade: ACS,ISO,Reag. Ph Eur Solubility: 358 g/l (20 °C)
Cs	Support material	Sigma-Aldrich	Chemical formula: 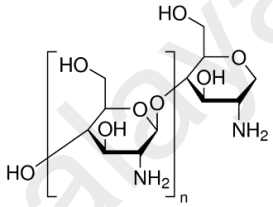 Appearance: Off White to Beige and Faint Brown to Light Brown (color). Powder and/or Chips (form. Deacetylation: 75-85 % Viscosity: 200-800 cps
Glass Microscope Slide	Substrate	Heathrow Scientific	Dimension: 25mmx75mm Thicknes: 1.2mm - Ground edges and corners for safe handling - Washed, rinsed, and dried dust-free for immediate uses
MO	Model pollutant	Sigma-Aldrich	Chemical formula: $C_{14}H_{14}N_3NaO_3S$ Molecular Weight: 327.33 g/mol

3.3 Experimental Methods

3.3.1 Stage 1: Synthesis of TiO_2 catalyst by sol-gel method

Titanium isopropoxide (TTIP), acetic acid glacial, and deionized water were used to synthesize TiO_2 via the sol-gel method. Initially, a TTIP (2.8 ml; 97%) solution was mixed in concentrated/pure acid acetic acid glacial (6ml; >90%). After that, TTIP was titrated slowly into the acetic acid glacial solution. Next, DI water (36 ml) was slowly added under vigorous stirring at an ambient temperature and mixing/rate of 350 - 500 rpm for 5 hours.

Once a clear solution was obtained (sol – transparent solution), the mixture was stirred for another hour at 80°C. To keep the reaction temperature constant, the beaker was covered with an aluminum foil and a thermometer was placed near the surface of the mixture. The solution was subsequently converted to a gel mixture at a reaction temperature of 60°C. The continuation of the reaction will eventually result in a white suspension, which was subsequently dried overnight (12 hours 80 °C) until it is amorphous (to obtained smallest crystal size structure from drying process), resulting in dried TiO_2 nanoparticles (yellowish color). Next, the TiO_2 nanoparticles was manually grounded using an agate mortar. TiO_2 powder (0.70 g) was calcined for 5 hours at 500°C, and directly stored in a controlled humidity and temperature conditions.

3.3.2 Stage 2: Synthesis of Cs-TiO_2 catalyst via ex situ preparation

The general procedure of preparing Cs-TiO_2 catalyst solution, known as ex-situ preparation, is illustrated in Figure 3.1.

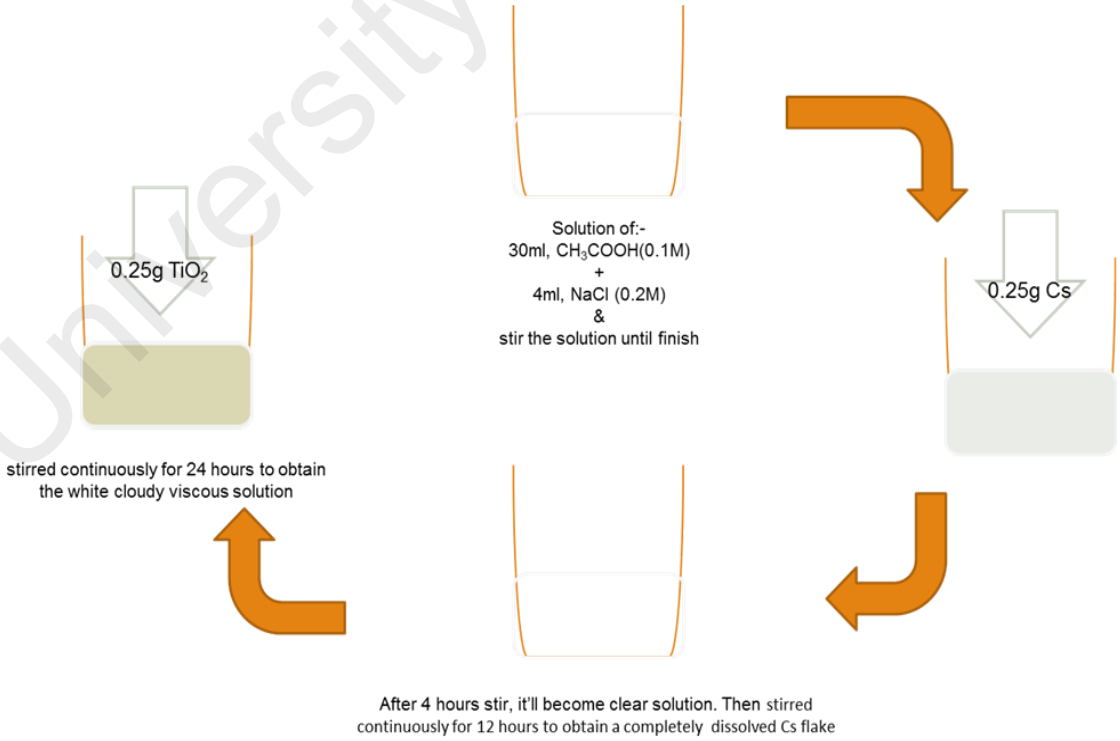

Figure 3.1: Schematic diagram on preparation of Cs-TiO_2 solution

Cs flakes (0.25 g) was dissolved in a premixed solution of acetic acid (CH_3COOH) (30ml; 0.1M) and sodium chloride (NaCl) (4ml; 0.2M). The viscous solution was stirred continuously for 12 hours to completely dissolve the Cs flakes. Then, TiO_2 powder (0.25 g) was added into the transparent viscous Cs solution. Subsequently, more CH_3COOH (5ml; 0.1M) was added directly into the solution. The slurry was stirred continuously for 24 hours to obtain the white cloudy viscous solution. The mixing process helped to vary the weight ratio of the Cs-TiO_2 solution. The Cs-TiO_2 solution was prepared at 2:1, 2:2, 2:3, and 2:4, corresponding to Cs:TiO_2, which was repeated after the finalization of the cycles (optimum condition) of the Cs-TiO_2/Glass photocatalyst.

3.3.3 Stage 3: Coating of TiO_2 and Cs solution with glass substrate (Cs-TiO_2/Glass photocatalysts)

Glass substrate (25×75 mm) was used to retain and fix the prepared Cs–TiO_2 photocatalyst, as detailed in Figure 3.2. Initially, the glass substrate was thoroughly cleaned and dried prior to being deposited into the prepared solution.

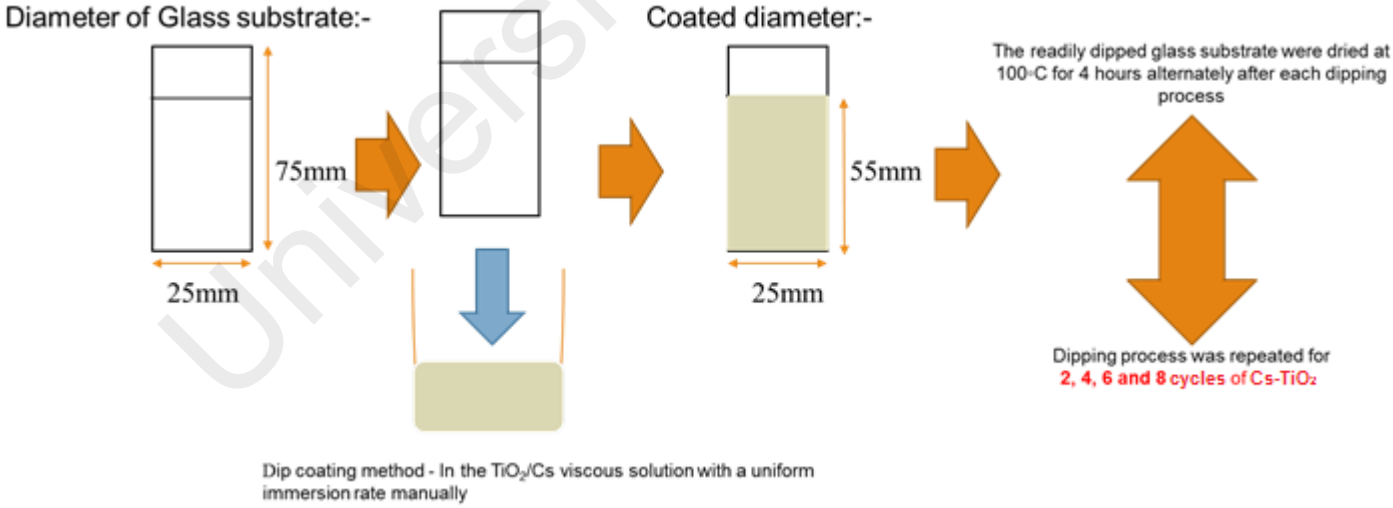

Figure 3.2: Schematic diagram on preparation of Cs-TiO_2/Glass catalyst via the dip coating method

The whole glass substrate was manually dipped in the Cs-TiO_2 viscous solution at a uniform immersion rate, resulting in a coated diameter of (25×55 mm). The readily dipped glass substrate was dried at 100°C for 4 hours alternately after each dipping process. The

glass substrate itself helps vary the amount (weight ratio) or cycles of Cs-TiO_2 that was coated on glass substrate. The dipping process was repeated for 2, 4, 6, and 8 cycles of Cs-TiO_2 photocatalyst on the glass substrate. Herein, the TiO_2 with Cs samples were called Cs-TiO_2/Glass photocatalyst. The photocatalyst of Cs-TiO_2 formed on the glass substrate will be responsible for adsorption and photodegradation reactions. Otherwise, it was stored in the dark to avoid pre-activation by visible light or sunlight (UV-light).

3.3.4 Stage 4: Characterization of the Cs-TiO_2/Glass catalyst

The characteristics of the Cs-TiO_2/Glass photocatalyst were analyzed for its binding abilities and homogeneity. The binding ability of TiO_2 nanoparticles for both $TiO_{2(SY)}$ and $TiO_{2(DP25)}$ were characterized using the TGA (for as-synthesized TiO_2), XRD, Raman, FTIR, HR-TEM, FESEM+EDS, and UV-DR. The prepared TiO_2 and Cs on the glass substrate, called Cs-$TiO_{2(DP25)}$/Glass and Cs-$TiO_{2(SY)}$/Glass, was characterized using FTIR, FESEM+EDS, and UV-DR.

3.3.4.1 Thermal Gravimetric Analyzer (TGA)

TGA is a technique that measures the change in the weight of the sample when it is heated, cooled, or held at constant temperature(s). In this study, the calcination temperature for the as-synthesised TiO_2 was examined using the TGA method. The samples (4 mg – 5 mg) were examined using the TGA (Mettler Toledo, TGA/SDTA-851^e) by placing it into a 100-µl open alumina crucible. The experimental temperature was set from the ambient to 800 ^oC, at a heating rate of 10 $^oC\ min^{-1}$ under nitrogen gas at a flow rate of 50 ml min^{-1}. It was then cooled to room temperature. This technique was used to identify the composition ratio of as-synthesized TiO_2 to ensure that pure TiO_2 nanoparticles sample is obtained prior to proceeding into calcination.

3.3.4.1 X-ray diffraction (XRD)

XRD is one of the non-destructive test methods for characterizing crystalline materials. The crystallite phase of TiO_2 nanoparticles sample was determined by using Cu Kα radiation (XRD, λ= 1.5406 Å, Bruker AXS)

D8 Advance diffractometer). It provides information on structures, phase, preferred orientations, and other structural parameters, such as average grain size, crystallinity, and strain and crystal defects. The sample (1 g) was weighed and placed into the sample holder. Prior to beginning the test, the step size was set at 0.02º, at a 0.02º/s scanning rate between 2º - 80º diffraction angle (2θ). From the results, the crystallite size can be determined using the Scherrer equation (Equation 3.1). The X'Pert Highscore Plus V 3.0.4 program interpreted the phase composition and all correlated information pertaining to TiO_2.

$$\tau = \frac{K\lambda}{\beta cos\theta} \quad \text{..... (Equation 3.1)}$$

where:-

τ = mean size of the crystalline domains;

K = a dimensionless shape factor, with a value close to unity. It has a typical value about 0.9 but varies with the actual shape of crystallite;

λ = X-ray wavelength;

β = line broadening at half the maximum intensity (FWHM);

θ = the Bragg angle.

3.3.4.2 Raman spectroscopy

Raman Spectroscopy (Renishaw in Via Reflux with high performance CCD camera and LEILA microscope) was used in this study. It is one of the spectroscopic techniques

used to study the vibrational, rotational, and other low frequency transitions in molecules. It was used to determine the substance (phase) from the characteristic spectral patterns, and quantitatively or semi-quantitatively, the amount of substance in TiO_2 nanoparticles sample with high lateral resolution. The sample (0.05 g) was placed into the sample holder and subsequently inserted into the Raman spectroscope. Sample degradation and fluorescence might occur during testing. It is significantly impact upon highly sensitive materials of TiO_2 nanoparticles. Hence, 1 % of 0.2 mV laser power at a 180 s exposure time was selected to analyze TiO_2. The argon gas laser (514 nm) was selected in this work, due to its 1800 mm^{-1} spectral resolution being sufficient to plot excellent spectra. Focusing the laser beam via ×50 objective lens helps collect the scattered radiation, and the laser spot on the sample was approximately 0.836 μm at 514 nm excitation.

3.3.4.3 Fourier Transform Infrared Spectroscopy (FTIR)

The FTIR spectrum (Perkin-Elmer 100 spectrophotometer) provide the molecular absorption and transmission (specific frequency of energy), which is useful in analyzing the samples of photocatalysts (TiO_2 nanoparticles, Cs-TiO_2/Glass photocatalyst, including Cs-TiO_2 with MO on the glass substrate after the completion of the photocatalytic process) functional group, while others are attached to the molecule's functional group, with it linking the photocatalysts. The sample holder was cleaned using acetone before the samples were placed on it. 0.3 mg of photocatalyst was mixed with 4 mg of KBr, and molded to form a pellet. The pellet was placed in the FTIR sample holder, and bombarded with IR radiation. Some of the IR radiation was absorbed by sample, while others passed through via transmission. The resolution of the FTIR was set to 4 cm^{-1}, with 16 scans in the wavelength range 400 cm^{-1} to 4000 cm^{-1}. The FTIR spectrum was collected, with its peaks labeled.

3.3.4.4 UV-Vis Diffuse Reflectance Spectroscopy (UV-DR)

UV-Vis Diffuse Reflectance analysis was conducted to determine the band gap energy and absorption edge of the TiO_2 nanoparticles and the prepared photocatalysts of Cs-TiO_2/Glass. The absorbance data of the samples were obtained from the optical spectra, recorded using UV-DR Spectrophotometer Model UV-3101PC Shimadzu, with wavelengths between 200–800 nm. The energy gap (eV) was determined by extrapolating the sharply rising portions of the plots towards the hν-axis (Tauc plot), while the band gap energy was calculated by applying the Kubelka-Munk function [F(R)], as shown in Equations 3.2 and 3.3 (Murphy, 2007; Yoong *et al.*, 2009):-

$$[F(R) \cdot h\nu]^{1/2} = K (h\nu - E_g) \quad \text{..... (Equation 3.2)}$$

where:- R = absolute reflectance of the sample cycle;

hν = photons energy;

K = a constant characteristic of the semiconductor material;

E_g = band gap energy.

and,

$$h\nu = hC / \lambda \quad \text{..... (Equation 3.3)}$$

where:- h = Planks constant (6.626×10^{-34} Joules or 4.136×10^{-15} eVs);

C = Light speed (3.0×10^{8} ms^{-1} or 3.0×10^{17} nms^{-1});

λ = Cut-off wavelengths (nm).

3.3.4.5 High Resolution Transmission Electron Microscope (HR-TEM)

HR-TEM analysis was conducted using the JEM-2100F instrument at an accelerating voltage of 200 kV. It has become a major support in the list of characterization techniques for materials scientists, due to its capability in generating image and diffraction information from the samples. Furthermore, the specified sample which is TiO_2 nanoparticles could be characterized via radiation produced by beams of accelerated electrons. It offers high magnification of up to 1.6 times, allowing us to observe extremely small and tiny lattice-fringe spacing. Prior to the HR-TEM characterization, the TiO_2 nanoparticles sample was prepared by titrating the dispersed that samples on 300 mesh copper grids. The samples were prepared and left overnight to dry. The samples were then placed into the HR-TEM sample holder prior to being inserted into the HR-TEM. Images of TiO_2 nanoparticles sample was selected and taken at 50,000, 100,000, and 500,000 × magnification. The size and lattice-fringe spacing was measured using image-J. The particle size distribution was plotted after 20 particles of TiO_2 nanoparticles sample was measured, and the lattice-fringe spacing was used to support the results from XRD analysis.

3.3.4.6 Field Emission Scanning Electron Microscopy (FESEM) + Energy Dispersive Spectrometer (EDS)

The morphology of both TiO_2 nanoparticles and Cs-TiO_2/Glass photocatalyst were investigated using Scanning Electron Microscope (JSM-7500F Jeol). First, the samples of Cs-TiO_2/Glass were sprayed with Platinum (Pt) prior to loading into the instrumentation sample stage. After that, the prepared samples were then mounted on the sample holder using double-sided electrically conducting carbon adhesive tapes to prevent surface charge on the specimens when exposed to the electron beam. The fracture surfaces of the photocatalyst sample on the glass substrate were sputtered with Pt prior to morphological observation to prevent charging during imaging. However, for TiO_2

nanoparticles sample is not necessary undergo Pt step and just proceed to next step. The SEM micrographs were obtained under conventional secondary electron imaging conditions at an acceleration voltage of 5 kV.

The elemental analysis of the TiO_2 nanoparticles and coated Cs-TiO_2/Glass photocatalyst were determined using EDS, equipped in the FESEM. EDS is an analytical technique used for elemental analysis or chemical characterization. The energy of the beam is typically in the range of 10 to 20 keV. The accumulation of the energy counts (intensity) creates a spectrum, representing the chemical analysis of the sample. The higher a peak is in the EDS spectrum, the more concentrated the element present in the sample. This allows us to obtain the weight + atomic percentages. In order to confirm the presence of the Watt content located at the bottom of the prepared photocatalysts, the cross-section of the EDS analysis was conducted. The area scan of the EDS analysis was conducted by taking the weight + atomic percentages from single spots along the prepared photocatalysts.

3.3.5 Stage 5: Photocatalytic activity of catalyst

The working solution, with MO concentration of 10 ppm, was placed into a Pyrex reactor. Then, the sample of MO solution was stirred with a magnetic bar for 10 minutes to obtain a uniform concentration of the samples. After that, the Cs-TiO_2/Glass was added into the sample. Irradiation was conducted using a UV-light lamp (6 W, $\lambda = 365$ nm) as its energy source. The apparatus set up is shown in Figure 3.3.

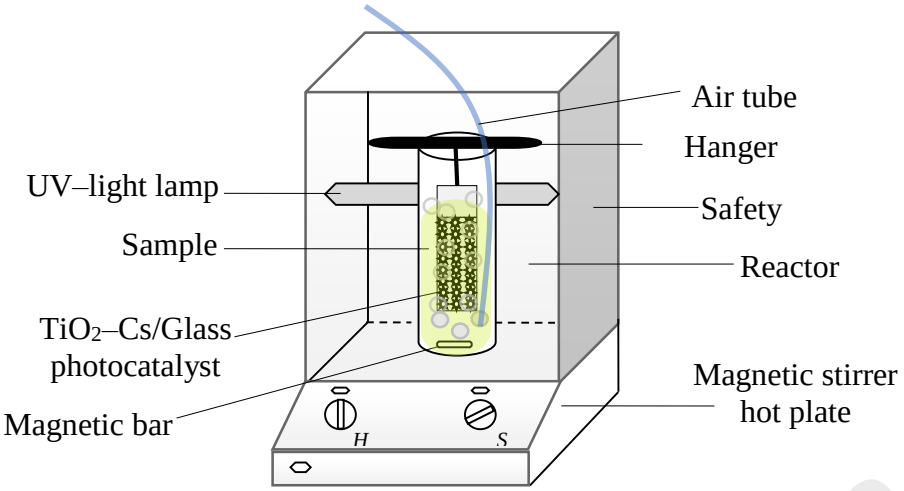

Figure 3.3: The apparatus set up for photodegradation process

For the first 15 minutes, the sample was allowed to adsorb on the surface of the photocatalyst to attain adsorption-desorption equilibrium in dark conditions. The MO sample was taken after finish the process. After that, the sample was irradiated with a UV-light lamp for the next hour. A sample of MO solution was taken at 10, 20, 30, 40, 50, and 60 minutes.

The photocatalytic activity of Cs-TiO_2/Glass systems was evaluated by measuring the time dependence of the concentration loss of a degraded compound. Usually, this involve dyes, such as MO, Methylene Blue, or environmental pollutants, such as phenol. For this study, MO was used as a model pollutant. Furthermore, the absorbance data of the MO samples were obtained from the optical spectra recorded on a UV-VIS Shimadzu - UV-3101PC, with wavelengths ranging from 200–800 nm. The percentage of adsorption-photodegradation was calculated using the formula in the equation below:-

$$\%A\text{-}P = \frac{C_o - C_t}{Co} \times 100\% \qquad \text{…….. (Equation 3.4)}$$

where:-

%A-P = Percentage of adsorption photodegradation;

C_o = Initial concentration of sample before irradiation under UV-light;

C_t = Concentration of sample after irradiation under UV-light (t, minutes).

CHAPTER 4: RESULTS AND DISCUSSION

4.1 Characterization on $TiO_{2(SY)}$ and $TiO_{2(DP25)}$

4.1.1 As-synthesized sample of TiO_2 nanoparticles using Thermal Gravimetric Analyzer Analysis

The calcination process is a crucial step in the synthesis of nanomaterials for activity-related analysis, which will result in excellent catalytic activities and stabilities (Beranek & Kisch, 2008). In this study, TGA was used to determine the optimal calcination temperature of TiO_2 nanoparticles. Figure 4.1 shows the TGA plots for as-synthesized TiO_2 at RT to 800 °C.

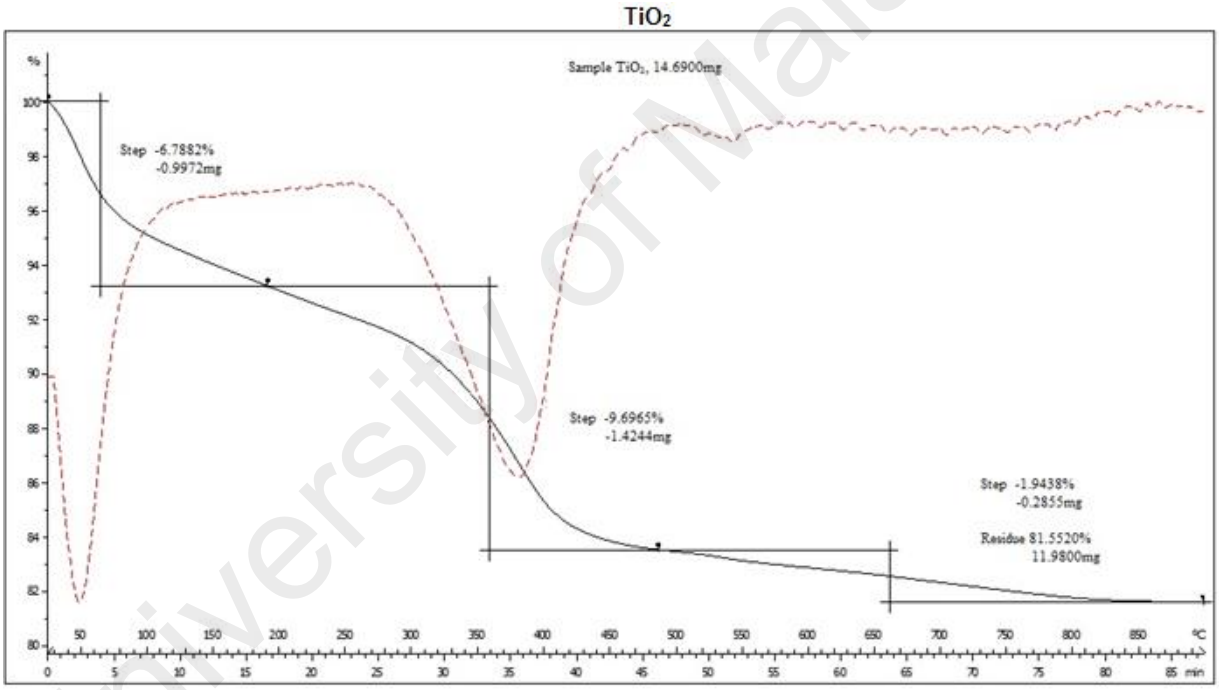

Figure 4.1: The result on TGA (for as-synthesized $TiO_{2(SY)}$ prepared with sol-gel method)

TGA analysis record the mass loss and chemical or physical changes as a function of increasing temperature or time. Based on the TGA plots, a significant loss of mass was evident as the temperature increased from room temperature to 800 °C, which is attributed to the elimination of crystallized water or the dehydration of water.

The removal of water from TiO_2 is required for further elimination of other elements at higher temperatures. As the heating temperature is increased to 400 °C, the loss of mass slowed to 100 ^oC, stopping completely at 370 °C. The first peak at 50 °C indicates an endothermic event, corresponding to the rapid release of moisture/water-H_2O. The second peak at ~450 °C represent the transformation of the precursors into stable TiO_2 nanoparticles. Further calcination at 500 ^oC resulted in pure TiO_2 in powder form. Therefore, it can be concluded that the calcination temperature of as-synthesized TiO_2 for this study is 500 ^oC, which requires 5 hours (X. Pan *et al.*, 2013). According to Ba-Abbad *et al.* (2012), the amorphous precursor was converted to anatase phase as the temperature increases from 425 to 500 ^oC. The relationship of calcination with catalytic activity and stability of TiO_2 is depend on the development of anatase phase (instable phase with higher in catalytic activity) with specific temperature and time during calcination process.

4.1.2 X-Ray Diffraction Analysis

The physical properties of both synthesized and commercialized TiO_2 nanoparticles, including phase transformation and crystallite sizes, are determined using the XRD technique. The XRD patterns of synthesized and commercialized TiO_2 for this study is presented in Figure 4.2. The average crystallite size of TiO_2 was calculated and tabulated in Table 4.1. This is done using the Scherrer equation (the calculation has been done through the PANalytical B.V. X'Pert Highscore Plus V. 3.0.4 software), which utilizes the XRD data which are JCPDS 01-086-1156 and JCPDS 01-086-1157 for $TiO_{2(SY)}$ and $TiO_{2(DP25)}$, respectively.

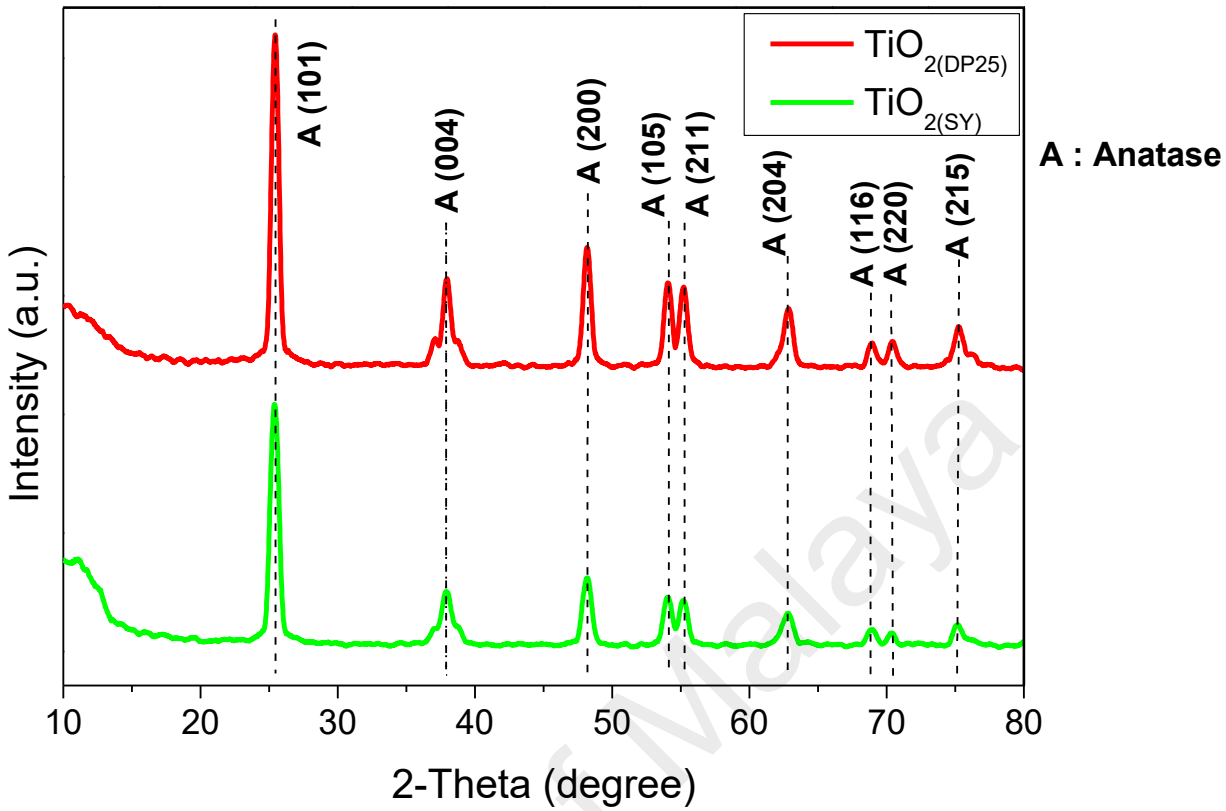

Figure 4.2: The XRD diffraction patterns of $TiO_{2(SY)}$ and $TiO_{2(DP25)}$

Table 4.1: Crystallite size and phase composition of $TiO_{2(SY)}$ and $TiO_{2(DP25)}$ that compare with previous literature, accordingly

	Anatase (%)	**Rutile (%)**	**Brookite (%)**	**Crystallite size (nm)**
Synthesis via sol-gel method				
$TiO_{2(SY)}$	100%	N/A	N/A	21.9
JCPDS 01-086-1156	84.7	1.7	13.6	21.9
Commercial Degussa P25				
$TiO_{2(DP25)}$	99.9%	0.1%	N/A	23.2
JCPDS 01-086-1157	84.7	1.7	13.6	21.5

*N/A = not available

Furthermore, Figure 4.2 also showed the presence of 3 crystallite compositions of TiO_2, which are Anatase, Rutile, and Brookite. The respective percentages of these phases vis-à-vis $TiO_{2(SY)}$ and $TiO_{2(DP25)}$ are also shown in Table 4.1. It was confirmed that the average crystallite size of TiO_2 for this study were 21.9 and 23.2 nm for $TiO_{2(SY)}$ and $TiO_{2(DP25)}$, respectively. The spectra confirms all the related crystallite compositions (phase of TiO_2) and also proved that the introduction of Cs molecules in the form of organic substance did not affect the structure of the photocatalysts much, which is mostly due to the presence of the anatase phase of TiO_2. This can be confirm that the interactions between the TiO_2 surfaces and Cs molecules could be the van der Waals force, which is weaker that of the interactions between the Cs to Cs molecules. This suggests that the dispersion of particle into glass substrate can cause the film to exceed the swelling degree in some extent (Norranattrakul *et al.*, 2013). The TiO_2 particles will attach in the surface of the Cs structure and will make it available to further the photocatalytic process. However, increased intensity of the Cs compounds will be resulted in changes to the crystallinity of TiO_2. This encourages the distribution of organic compounds on TiO_2's surface, and agrees with Yan *et al.* (2013), who highlighted the influence of the synthesis (which has been synthesized using hydrothermal method) process on the formation (contributed by adjusting the surface/bulk defects together with calcination at different temperatures) of the anatase phase within TiO_2 nanoparticles. The anatase phase is crucial towards the application as photocatalysts. The anatase phase acts as a medium that degrades wastewater in a more effective manner via photodegradation. Therefore, anatase TiO_2 was believed to be a more efficient photocatalyst than rutile TiO_2 due to its higher Fermi level and higher degree of hydroxylation (Yan *et al.*, 2013). Other than that, anatase phase of this TiO_2 is more photocatalytic active as compared to brookite and rutile with higher crystalline structure. In the discussion anatase is more photocatalytic active as compared to brookite and rutile with higher crystalline structure. This TiO_2 nanoparticles

are better photocatalysis, due to its large surface area and the abundance of active sites (Mehranpour *et al.*, 2011).

4.1.3 Raman Spectroscopy Analysis

The purity and phase transformation of the TiO_2 was determined using Raman Spectroscopy. The spectra showing the optimal TiO_2 nanoparticles (both $TiO_{2(SY)}$ and $TiO_{2(DP25)}$) are shown in Figure 4.3. The wavenumber of the Raman spectra for both samples are summarized in Table 4.2.

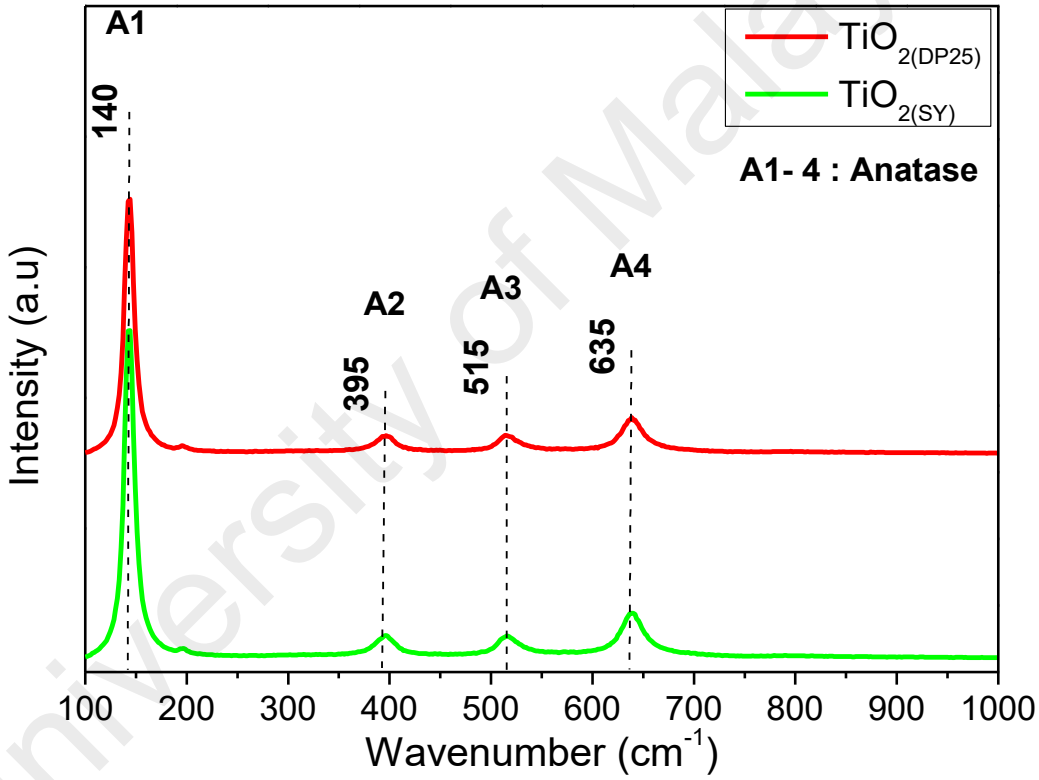

Figure 4.3: The Raman diffraction patterns of $TiO_{2(SY)}$ and $TiO_{2(DP25)}$

Table 4.2: Raman peaks of $TiO_{2(SY)}$ and $TiO_{2(DP25)}$ that compare with previous literature

	Anatase	**Rutile**	**Brookite**
Literature	140, 395, 515, 635	230, 445, 610	N/A
Synthesis via sol-gel method			
$TiO_{2(SY)}$	140, 395, 515, 635	N/A	N/A

Continued on next page

Commercial Degussa P25			
$TiO_{2(DP25)}$	140, 395, 515, 635	N/A	N/A

*N/A = not available

The result shown in Figure 4.3 agreed with the ones presented in the literature regarding wavelengths shift of anatase, rutile, and brookite. The spectra for both samples helped us identify the formation of single anatase nanocrystalline phase by the features, stating that all of the spectra (A1-A4) resulted in similar ones to those reported by Choi *et al.* (2005). The Raman spectra in Figure 4.3 show the presence of the anatase phase in ($TiO_{2(SY)}$ and $TiO_{2(DP25)}$). The Raman spectra has also been compared to the one reported by Choi *et al.* (2005). It was confirmed that the Raman bands shift towards higher wavenumbers from 100 cm^{-1} to 1000 cm^{-1} (shorter chemical bond length of molecules causes to shift higher wavenumber), as shown in Figure 4.3. Consequently, the higher in wavenumber due to increasing force constants. Therefore, the variation in Raman spectra for both TiO_2 nanoparticles is due to the effect of smaller particle size on the force constant (Minh *et al.*, 2008). However, the peak intensity $TiO_{2(SY)}$ (green line) is stronger than $TiO_{2(DP25)}$ (red line) can be attributed to decrease in particle size. As the particle size decreases, peak of green line becomes dominant due to the increase in the surface-to-volume ratio (Choi *et al.*, 2005). These observation is also in good agreement with XRD analysis.

All spectra with specific peaks agree with the ones demonstrated by TiO_2 that is made up of 100% anatase. It is also known that anatase TiO_2 has a higher photocatalytic activity compared to rutile TiO_2, due to its charge carriers being excited deeper in the bulk, thus contributing to the surface reactions in the anatase phase, as opposed to that of rutile (Luttrell *et al.*, 2014). The size of the nanocrystals was estimated to be ~10 nm by projecting the values of the frequency or wavenumber at 140 cm^{-1} of the strongest low

frequency of the A1 peak in the standard correlation plots (Moustakas *et al.*, 2013). This peak presents the blue shift and line broadening relative to that observed in anatase to larger nanocrystals (more than 20 nm), due to the breakdown of the k=0 Raman selection rule induced by phonon confinement (Moustakas *et al.*, 2013).

4.1.4 Fourier Transform Infra-Red Analysis

The functional groups on the surface brought to the active site of TiO_2 was analyzed using FTIR. The FTIR spectrum in Figure 4.4 (in the range of 400–4000 cm^{-1}) demonstrated the spectra of $TiO_{2(SY)}$ and $TiO_{2(DP25)}$. From that plots, the peaks at 400 cm^{-1} to 700 cm^{-1} are for O–Ti–O and Ti–O vibrations of pure TiO_2 nanoparticles, all of which are tabulated in Table 4.3. Figure 4.4 also represents the FTIR spectra of $TiO_{2(SY)}$ that has been calcined at 500 ^oC for 5 hours.

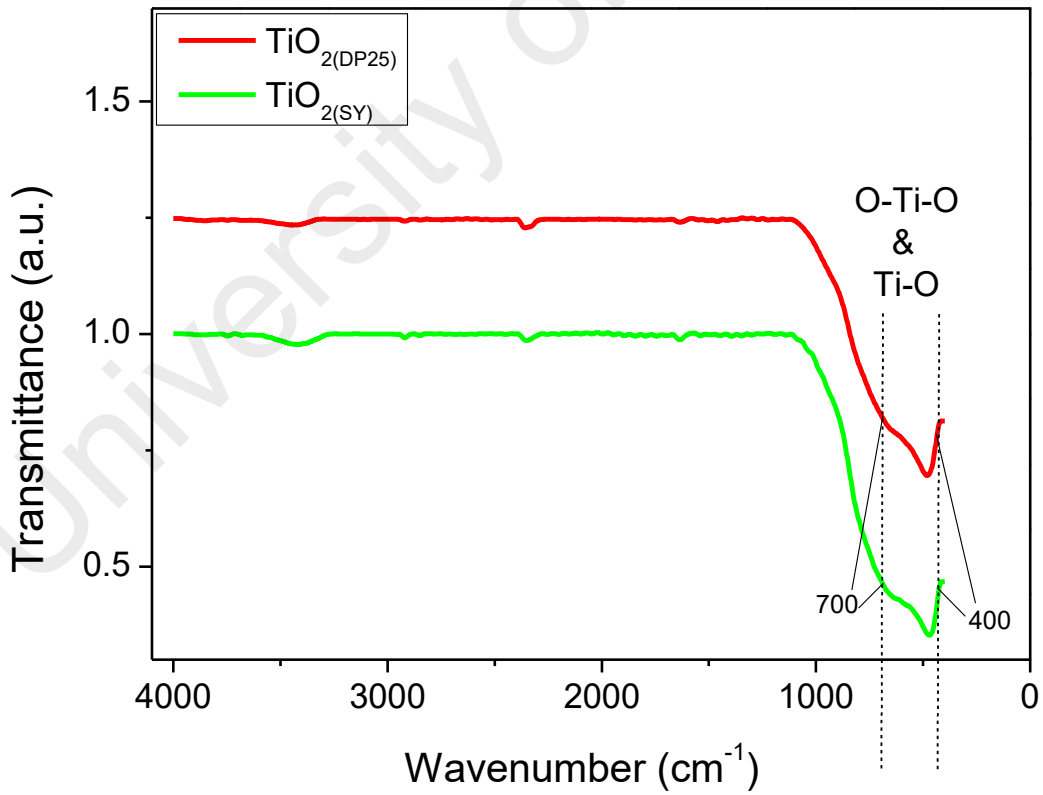

Figure 4.4: FTIR spectra of $TiO_{2(SY)}$ and $TiO_{2(DP25)}$

Table 4.3: FTIR peaks of TiO_2 for both $TiO_{2(SY)}$ and $TiO_{2(DP25)}$ compared with previous literature

	O–Ti–O and Ti–O bands (cm^{-1})
Literature	895 – 770
Synthesis via sol-gel method	
$TiO_{2(SY)}$	400 – 700
Commercial Degussa P25	
$TiO_{2(DP25)}$	400 – 700

The bands centered at 1640 cm^{-1} and 3200 cm^{-1} to 3700 cm^{-1} are characteristics of surface-adsorbed water (H_2O) and hydroxyl groups (-OH), respectively. The broad peaks at 3430 and 2360 cm^{-1} observed in the dried gel sample are indicative of the OH and COOH groups, respectively. A broad peak at 700 cm^{-1} is present due to =C-H bending.

The intensity of the peak at 700 to 400 cm^{-1} has evidently increased due to the stretching vibration of the Ti–O–Ti in anatase phase. The calcination process produces $TiO_{2(SY)}$, resulting in a major peak at 420 cm^{-1} (based on Figure 4.4), which corresponds to Ti-O bond. Another peak at ~3440 cm^{-1} is present, attributed to the adsorbed water and the formation of inter H bonds. There are some minor peaks at 2900 cm^{-1} for plots of TiO_2 vis-à-vis C–H stretching bands. This implies the presence of organic compounds within TiO_2 post-calcinations. It can be concluded that both $TiO_{2(SY)}$ and $TiO_{2(DP25)}$ are hydrophilic and can further enhance the photocatalytic performance. The hydrophilic property of the surface allows water that contain pollutant compound to spread completely across the surface on the photocatalysts which can undergo photodegradation process easily (Guan, 2005).

4.1.5 UV-Vis-Diffusive Reflectance Analysis

The band gap energies of the commercial and prepared TiO_2 were determined using UV-DR analysis. The spectra and the band gap energy of the TiO_2 nanoparticles and data obtained from UV-DR analysis was shown and listed in Figure 4.5 and Table 4.4, respectively.

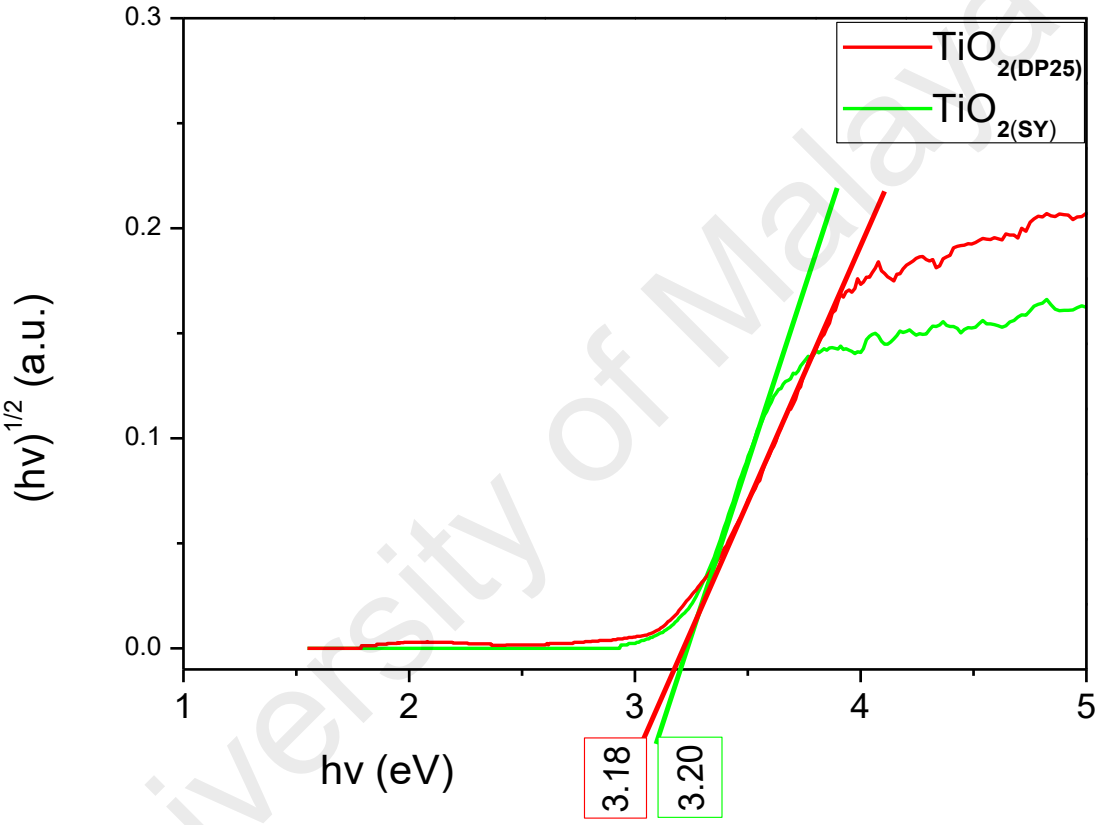

Figure 4.5: UV-DR spectra of TiO_2 nanoparticles which are $TiO_{2(SY)}$ and $TiO_{2(DP25)}$

Table 4.4: Band gap energy (eV) of TiO_2 nanoparticles for both $TiO_{2(SY)}$ and $TiO_{2(DP25)}$ which has been compare between previous literature parameters

	TiO_2 band gap energy (eV)
Theoretical band gap energy	3.20
Synthesis via sol-gel method	
$TiO_{2(SY)}$	3.20
Commercial Degussa P25	
$TiO_{2(DP25)}$	3.18

The band gap energies of a TiO_2 nanoparticles for both $TiO_{2(SY)}$ and $TiO_{2(DP25)}$ were 3.20 eV and 3.18 eV, respectively. Both samples show similar values to the theoretical band gaps energies reported in literature. The TiO_2 photocatalysts for both samples exhibited similar band gap energies, and produced electron-hole pairs for photocatalytic activities. Furthermore, the co-existence of the anatase phase of TiO_2 catalyst post-calcination at 500 °C (refer to the $TiO_{2(SY)}$ photocatalyst) was responsible for the different band gap energies. According to D. Jiang *et al.* (2007), the band gap energy for TiO_2 rutile phase is 0.2 eV lower than the anatase phase. Consequently, the photogenerated electron at the anatase phase might be transferred to the rutile phase during the photodegradation process.

4.1.6 High Resolution-Transmission Electron Microscopy Analysis

For HR-TEM analysis, the interaction of electrons with the specimen provides morphologic and compositional information of nanomaterials. The particle sizes and shape of the nanoparticles sample is determined from the HR-TEM images, and agree

with the values determined by the XRD analysis shown in Figure 4.6. The analysis is conducted based on the results reported in Figure 4.7 and Table 4.5.

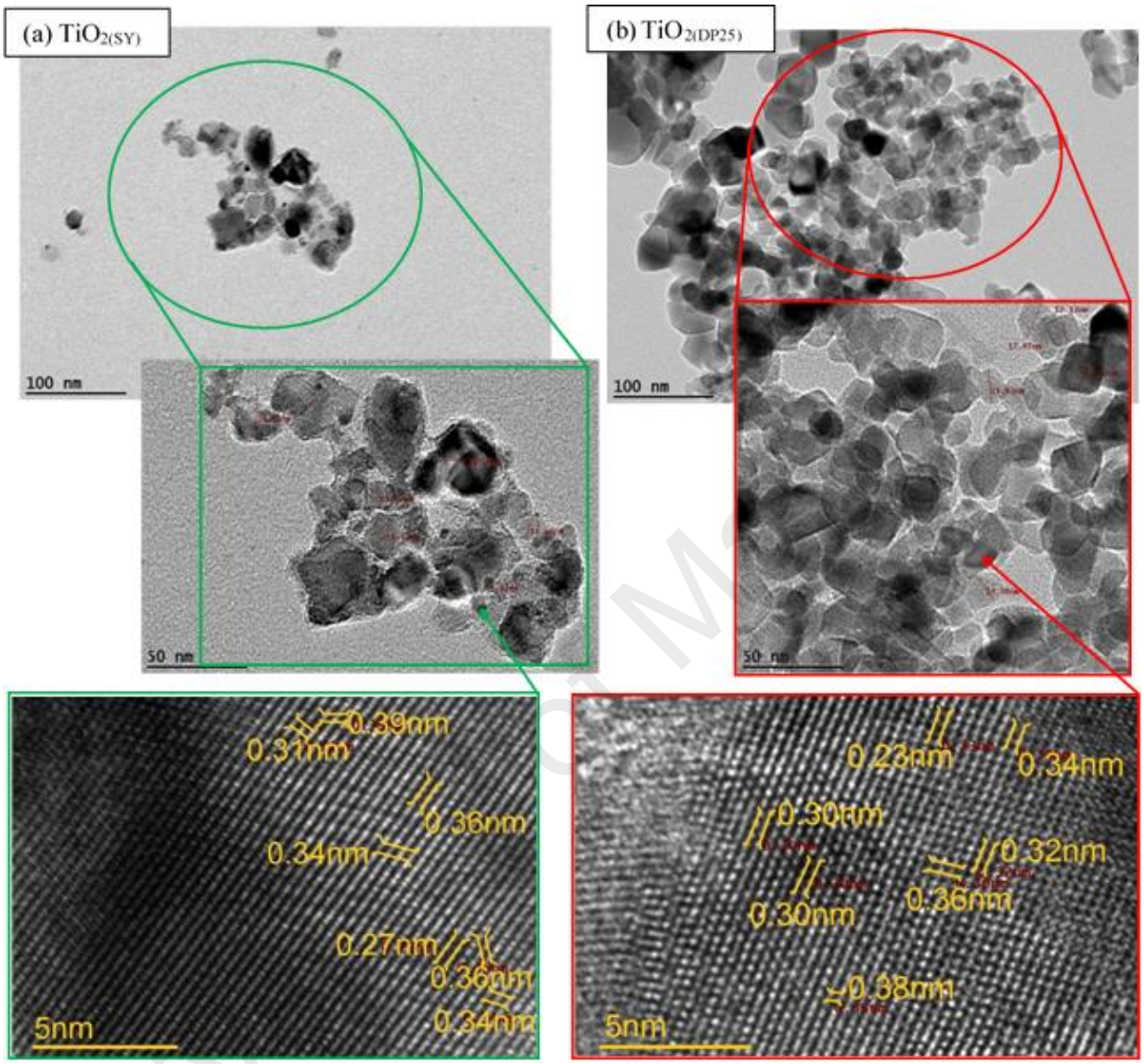

Figure 4.6: HR-TEM micrographs for both TiO_2 of (a) $TiO_{2(SY)}$ and (b) $TiO_{2(DP25))}$ photocatalysts with magnification of 60,000x

Figure 4.6 show the HR-TEM images of the samples obtained after calcination at (a) 500 ^{o}C, and (b) commercial Degussa P25. Generally, a homogenous dispersion and uniform particle features, with particle sizes of 5-30 nm and 10-25 nm for $TiO_{2(SY)}$ and $TiO_{2(DP25)}$, respectively, are shown. It has been demonstrated that almost 90% of the $TiO_{2(SY)}$ are 10-20 nm, while only 75% are $TiO_{2(DP25)}$. Meanwhile, another 10% and 25% of the $TiO_{2(SY)}$ and $TiO_{2(DP25)}$ has been categorized to be less than 5 nm and more than 25 nm, respectively.

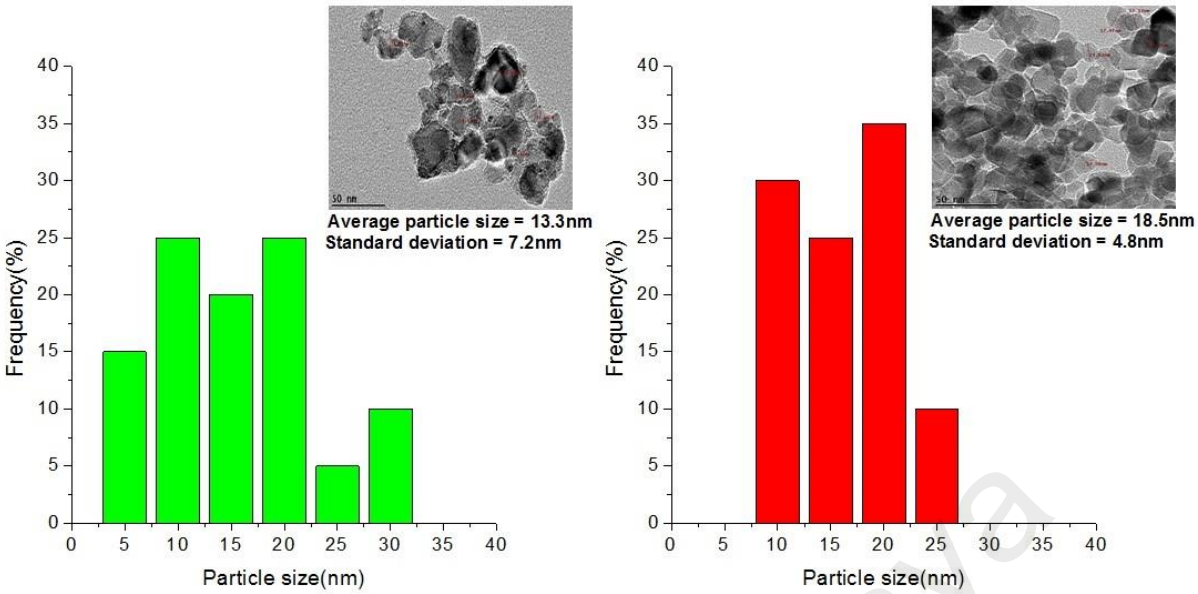

Figure 4.7: PSD of $TiO_{2(SY)}$ (Green) and $TiO_{2(DP25)}$ (Red) with inset at 60,000x magnification

Table 4.5: Particle size and shape of $TiO_{2(SY)}$ and $TiO_{2(DP25)}$

	Size (nm)	**Shape**		
Samples		Cubic	Semi-sphere	Needle
Synthesis via sol-gel method				
$TiO_{2(SY)}$	13.3	A	N/A	N/A
Commercial Degussa P25				
$TiO_{2(DP25)}$	18.5	A	N/A	N/A

*N/A = not available, A = available

Generally, (further analysis based on Figure 4.6), 20 particles of $TiO_{2(SY)}$ had an average particle size of ~13.3 nm at a standard deviation of 7.2 nm, as shown in Figure 4.7 and Table 4.5. XRD and TEM results confirmed this for the TiO_2 was prepared via sol-gel method from the $Ti[OCH(CH_3)_2]_4$ precursor ($TiO_{2(SY)}$) and commercial Degussa P25 ($TiO_{2(DP25)}$), both samples having an anatase phase. This implies that the repartition in size is quite large (14% of extension over the average value). The same method is also

used for $TiO_{2(DP25)}$, resulting in a Gaussian and the average particle size of ~18.5 nm, with a standard deviation of 4.8 nm and an extension of 18%.

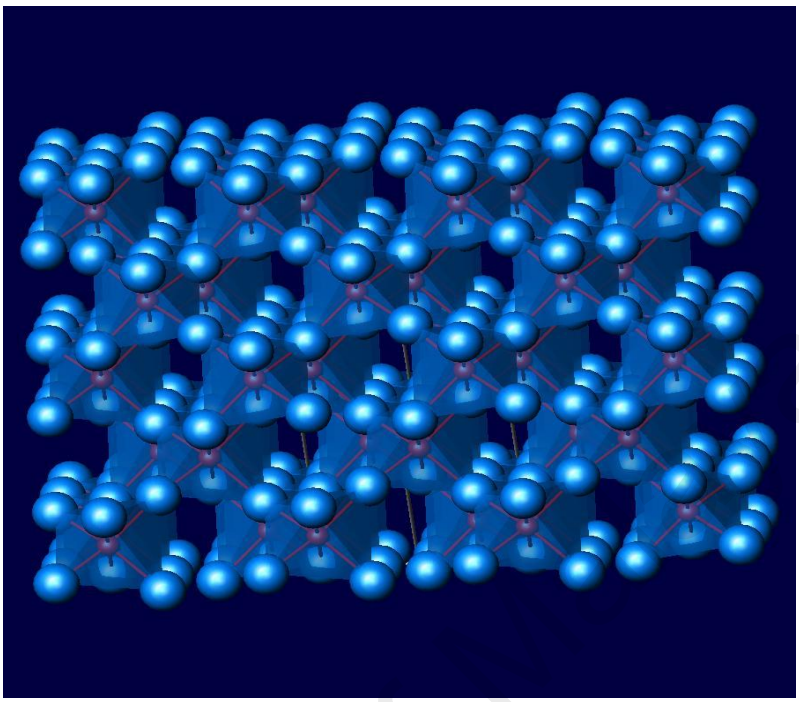

Figure 4.8: The structure of the octahedrally coordinated of anatase TiO_2. Cyan and red spheres are representing Ti and O atoms, respectively.

However, there might be some aggregation due to the nanosized particles. Allen and Smith (2001) posited that the Van der Waals forces are not negligible in this case, and the attraction between particles via their respective polar groups is enough to precipitate agglomeration, as illustrated in Figure 4.8. This makes it difficult to identify the particles, and deviate the real size distribution. The accuracy of the values obtained for the equivalent diameter and from factor is quite considerable. It can therefore be concluded that $TiO_{2(DP25)}$ have a more homogenous and uniform particle size distribution compared to $TiO_{2(SY)}$, due to the agglomeration in $TiO_{2(SY)}$, resulting in inhomogeneity of the particle size and its corresponding distribution. This might be related to the sol-gel synthesis method being applied, where the nucleation of TiO_2 is controlled by increasing the solutions' temperature, precursor used during synthesis (TTIP), and pH (that can excite higher super-saturation), which results in shorter induction time for nucleation and a faster growth rate (Mehranpour *et al.*, 2011). A homogenous and uniform particle size

of photocatalysts is an important factor that contributes to the highly efficient photocatalysis due to the modifications on the surface or bulk ratio of photocatalysts, thus modifying the significance of both volume and surface electron-hole recombination, as well as the optical and electronic properties of photocatalyst.

4.1.7 Field Emission Scanning Electron Microscopy + Energy Dispersive Spectrometer Analysis

The morphology, distribution, dimension, and cross section of the photocatalysts were observed based on Figure 4.9 and Table 4.6, which shows the FESEM micrographs (quite similar with HR-TEM images) and EDS (additional information), respectively. These were done for $TiO_{2(SY)}$ and $TiO_{2(DP25)}$ at a magnification of 60,000 x.

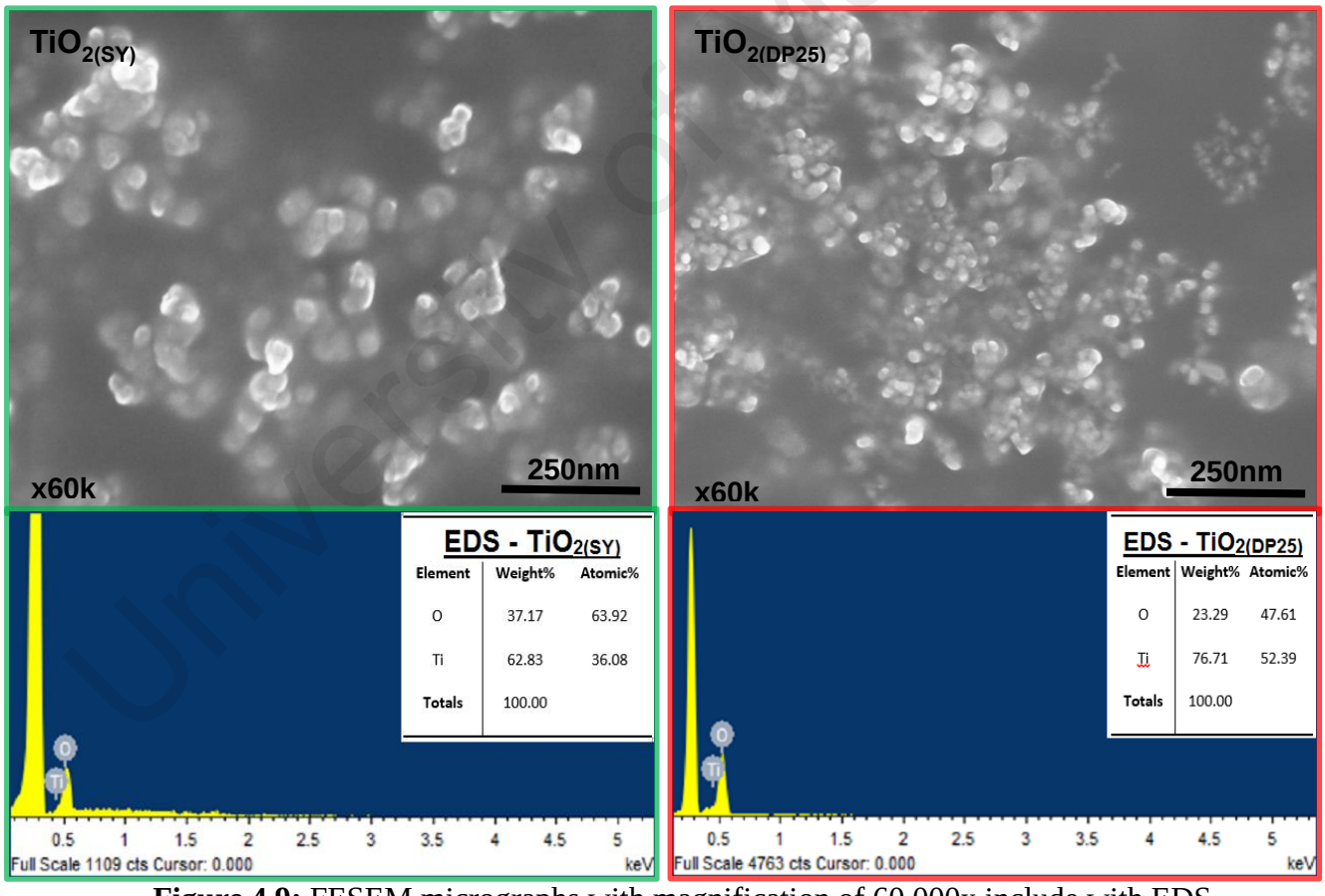

Figure 4.9: FESEM micrographs with magnification of 60,000x include with EDS figures and tables of $TiO_{2(SY)}$ and $TiO_{2(DP25)}$ photocatalysts, respectively

Table 4.6: EDS samples of single photocatalysts that are $TiO_{2(SY)}$ and $TiO_{2(DP25)}$

	Elements weight percentage (%)	
Samples	O	Ti
$TiO_{2(SY)}$	37.17	62.83
$TiO_{2(DP25)}$	23.29	76.71

EDS was used to determine the elemental composition of the samples, and the results are tabulated in Table 4.6. Ti and O elements were taken into account for this analysis. The micrograph shows that $TiO_{2(DP25)}$ consist of regular, homogeneous, and polyhedral particles, while $TiO_{2(SY)}$ are characterized by large particles, due to agglomeration, with straight edges and round corners. Observation from EDS analysis show that both samples are regarded as pure TiO_2. It was also found that $TiO_{2(SY)}$ was almost 10% lower in the Ti element compared to the commercial sample. In contrast, the O_2 element has a much stronger presence in $TiO_{2(SY)}$ rather than $TiO_{2(DP25)}$. The presence of more Ti element is expected, due to the reactivity of the active Ti element on the sample (Folli *et al.*, 2010).

4.2 Result for Cs-$TiO_{2(SY)}$/Glass and Cs-$TiO_{2(DP25)}$/Glass

4.2.1 Fourier Transform Infra-Red Analysis

FTIR spectroscopy analysis provide information regarding active surfaces and functional groups for the prepared photocatalysts. The FTIR spectra for both of Cs-$TiO_{2(SY)}$/Glass and Cs-$TiO_{2(DP25)}$/Glass photocatalysts are presented in this chapter. Initially, photocatalysts with different dip-coated cycles are presented in Figure 4.10, while the FTIR spectrum of photocatalysts with different weight ratios is shown in Figure 4.11.

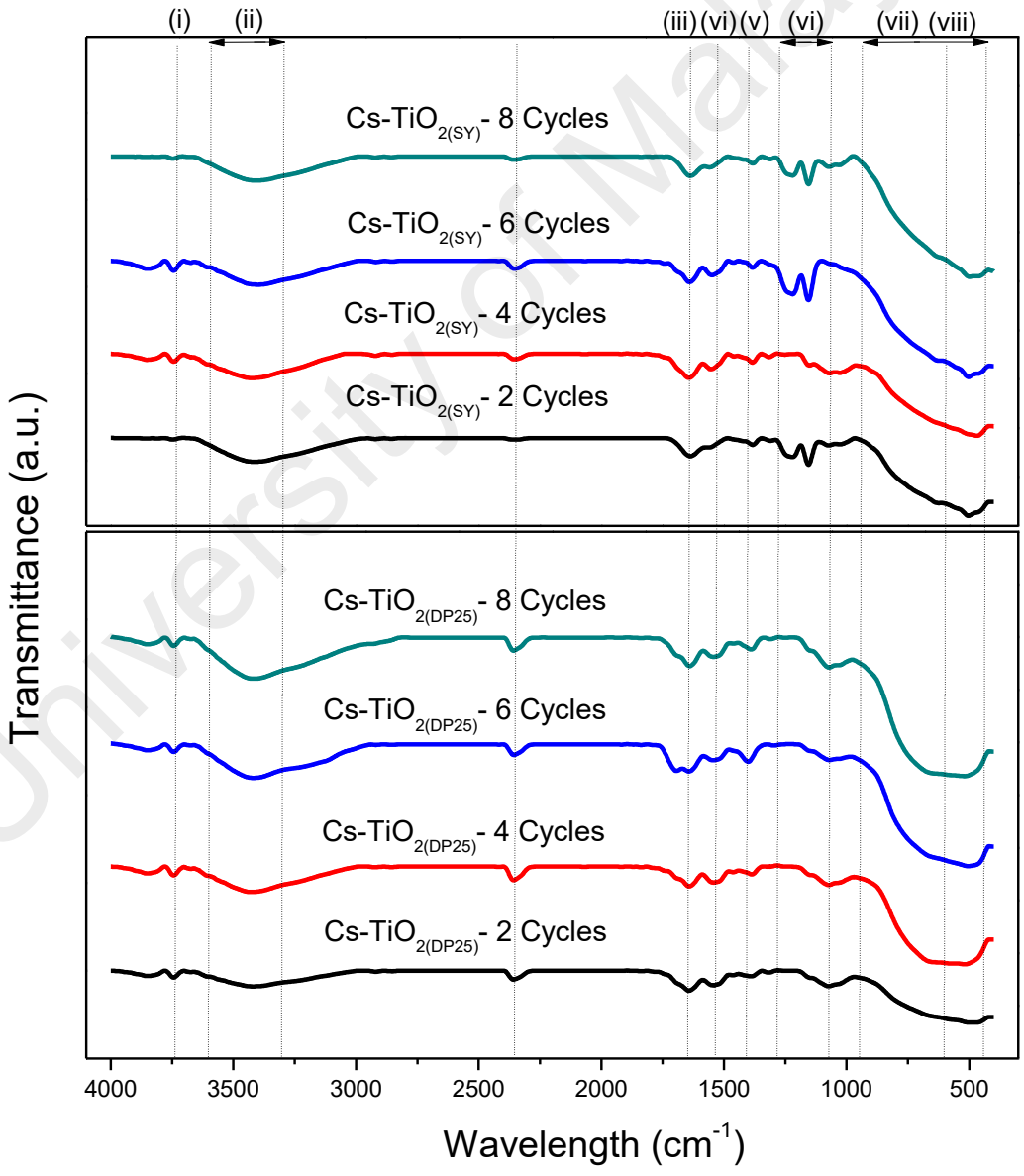

Continued on next page

Symbol	Wavelength (cm^{-1})	Assignment
(i)	3745	–OH bonds
(ii)	3600 to 3300	–OH overlapping together with –NH_2
(iii)	1640	R–NH–R bending
(iv) and (v)	1535 and 1400	–OH deformation
(vi)	1280 to 1070	Bridge of Si-O
(vii)	450 to 950	TiO_2 with shape of cycles formation between Cs-TiO_2 on the glass substrate
(viii)	600	TiO_2 wagging

Figure 4.10: FTIR spectra of different dip-coated cycles for Cs-TiO_2/Glass photocatalyst which are 2, 4, 6 and 8 Cycles by comparing between Cs-$TiO_{2(SY)}$/Glass with Cs-$TiO_{2(DP25)}$/Glass

Absorption bands at 1640 cm^{-1} and 3600 - 3300 cm^{-1} are attributed to amide (R–NH–R) and hydroxyl (–OH), together with amine (–NH_2) functional groups of Cs macromolecules, respectively, for both Cs-$TiO_{2(SY)}$/Glass and Cs-$TiO_{2(DP25)}$/Glass photocatalysts (Figure 4.10). These series of functional groups on Cs chains serve as coordination and reaction sites for the adsorption of transition metals and organic species (Yao *et al.*, 2011). The presence of TiO_2 nanoparticles was confirmed at 400 - 700 cm^{-1} for $TiO_{2(SY)}$ and $TiO_{2(DP25)}$, respectively. However, there is an intriguing anomaly on the adsorption band of FTIR spectrum in the context of Cs-TiO_2 photocatalyst, which is due to the rough absorption spectra at 1400, 1535, 3420, and 3745 cm^{-1} (–OH groups) first, indicate the characteristic of a surface TiO_2–OH functional group. On the other hand, the absorption band at 1280 - 1070 cm^{-1} was attributed to the silicon oxygen bonds (Si-O) functional groups. The appearance of a band at 600 cm^{-1} confirmed the presence of TiO_2 compound. The significant increment on the bands were centered on 450 - 950 cm^{-1}, recorded for both Cs-TiO_2/Glass photocatalysts. The band increment became more significant as the cycle increased from 2 - 8 cycles. It is worth nothing that the FTIR spectra of both the synthesized Cs-TiO_2 catalyst showed more bands with higher intensities compared to the precursor TiO_2 and Cs. It is indicated that the FTIR detection is enhanced when the photocatalysts consisted of both TiO_2 and Cs. Moreover, the apparent existence of NH_2, R-NH, and OH functional groups (enhance adsorption process

of photocatalyst), together with TiO_2 metal oxide (that undergo photodegradation process), should help confirm the effective removal of MO via the adsorption-photodegradation process. It was previously proven that these functional groups act as adsorption sites, and consequently increase the adsorption capacity of photocatalyst systems (Kyzas & Bikiaris, 2015). The band around 2350 cm^{-1} (the line without label) was not characteristic of Cs-TiO_2 photocatalyst, but was due to CO_2, which might affect calculations.

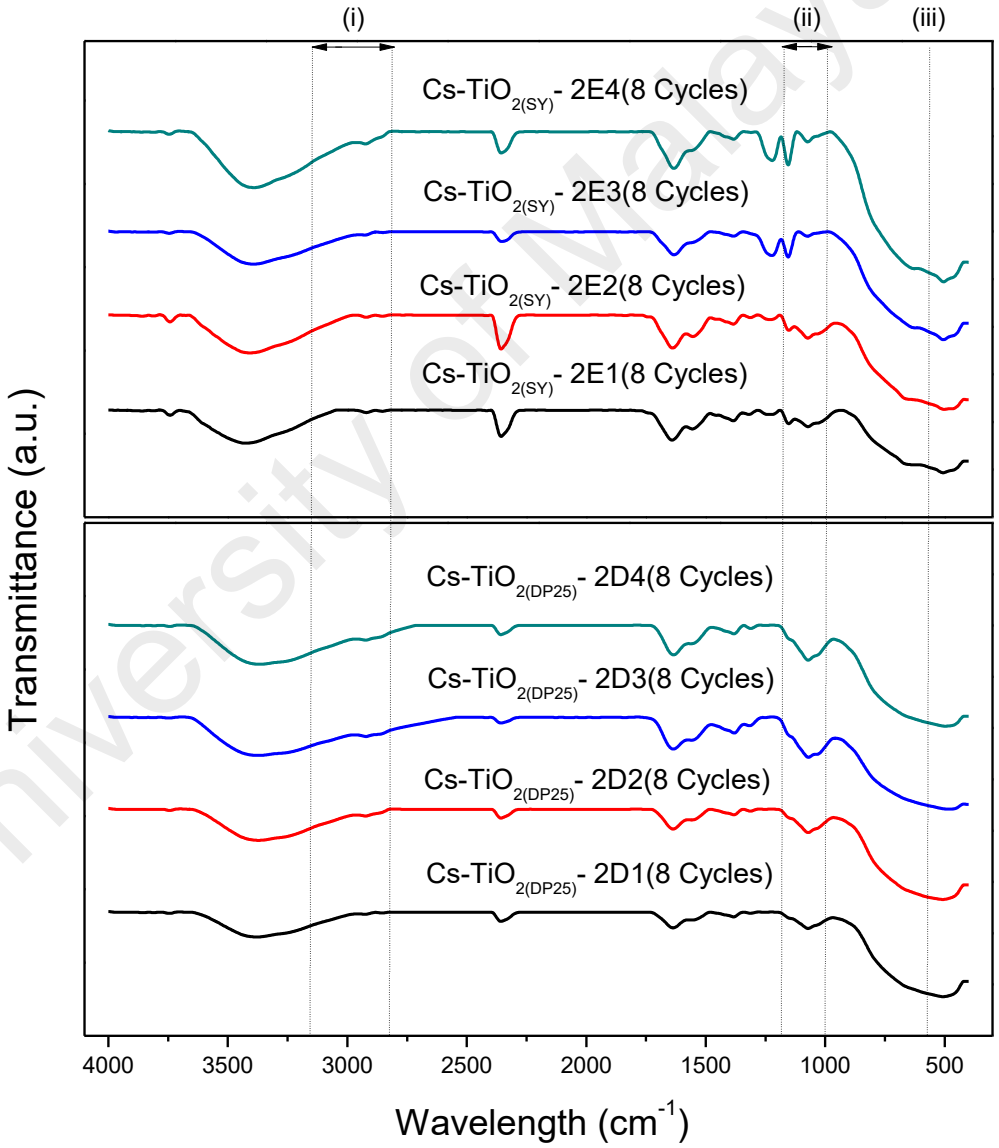

Continued on next page

Symbol	Wavelength (cm^{-1})	Assignment
(i)	2820 to 3160	Shape of weight ratio formation between Cs and TiO_2
(ii)	1000 to 1200	Bridge of Si-O
(iii)	600	TiO_2 wagging

Figure 4.11: FTIR spectra of different weight ratio for Cs-TiO_2/Glass photocatalyst by comparing between Cs-$TiO_{2(SY)}$/Glass with Cs-$TiO_{2(DP25)}$/Glass

Figure 4.11 demonstrated an identical FTIR spectra for 8 cycles with different weight ratios for both Cs-$TiO_{2(SY)}$/glass and Cs-$TiO_{2(DP25)}$/glass photocatalysts. To elucidate the influence of weight ratio, band stretching from 2820 - 3160 cm^{-1} was included in the analysis. It was subsequently proven that band stretching and weight ratio of TiO_2 is directly proportional in the range between 0.125 g - 0.5 g. The amount of TiO_2 was also visualized based on the band at 600 cm^{-1}, which indicates that higher band spectra resulted in a greater amount of TiO_2. Finally, the transmitted band of silicon oxygen bonds (Si-O), in this case a glass substrate, was represented by band stretching within the wavelength region of 1000 - 1200 cm^{-1}. These series of FTIR spectra confirmed the excellent dispersion of TiO_2 nanoparticles and its subsequent bond formation with the Cs matrix, of up to 8 cycles of deposition.

4.2.2 UV-Vis-Diffusive Reflectance Analysis

The UV-DR spectra of Cs-$TiO_{2(DP25)}$/Glass and Cs-$TiO_{2(SY)}$/Glass photocatalysts based on different dip-coated cycles and weight ratios are shown in Figure 4.12 and 4.13, respectively. Consequently, the band gap energies of each photocatalysts' composition is illustrated in Figure 4.14. The glass substrates' band gap energies from different dip-coated cycles and weight ratio for both photocatalysts were also determined by extrapolating the fittings of the onset light absorption to zero.

Generally, there is less than ~10 % difference of the band gap energy between Cs-$TiO_{2(DP25)}$/Glass and Cs-$TiO_{2(SY)}$/Glass photocatalysts. The band gap energy increased with the number of cycles, from 2 to 4. These assumptions are valid for both Cs-$TiO_{2(SY)}$/Glass and Cs-$TiO_{2(DP25)}$/Glass photocatalysts. The band gap decreases gradually from 4 cycles to 8 cycles at up to 0.96 eV and 0.07 eV for Cs-$TiO_{2(SY)}$/Glass and Cs-$TiO_{2(DP25)}$/Glass photocatalysts, respectively. It can be anticipated that the band gap of the 8 cycles photocatalysts for Cs-$TiO_{2(DP25)}$/Glass (3.13 eV) is 0.29 eV higher than that of Cs-$TiO_{2(SY)}$/Glass (2.64 eV). It was also demonstrated that the 8 cycles of Cs-TiO_2/Glass photocatalyst (both photocatalysts) was prepared by successive deposition cycles to guarantee the excellent distribution of TiO_2 nanoparticles. This, in turn, render the Cs-TiO_2/Glass photocatalyst system, with different weight ratio, with the capability of absorbing photonic energy with wavelengths under 391 nm in the reflectance analysis.

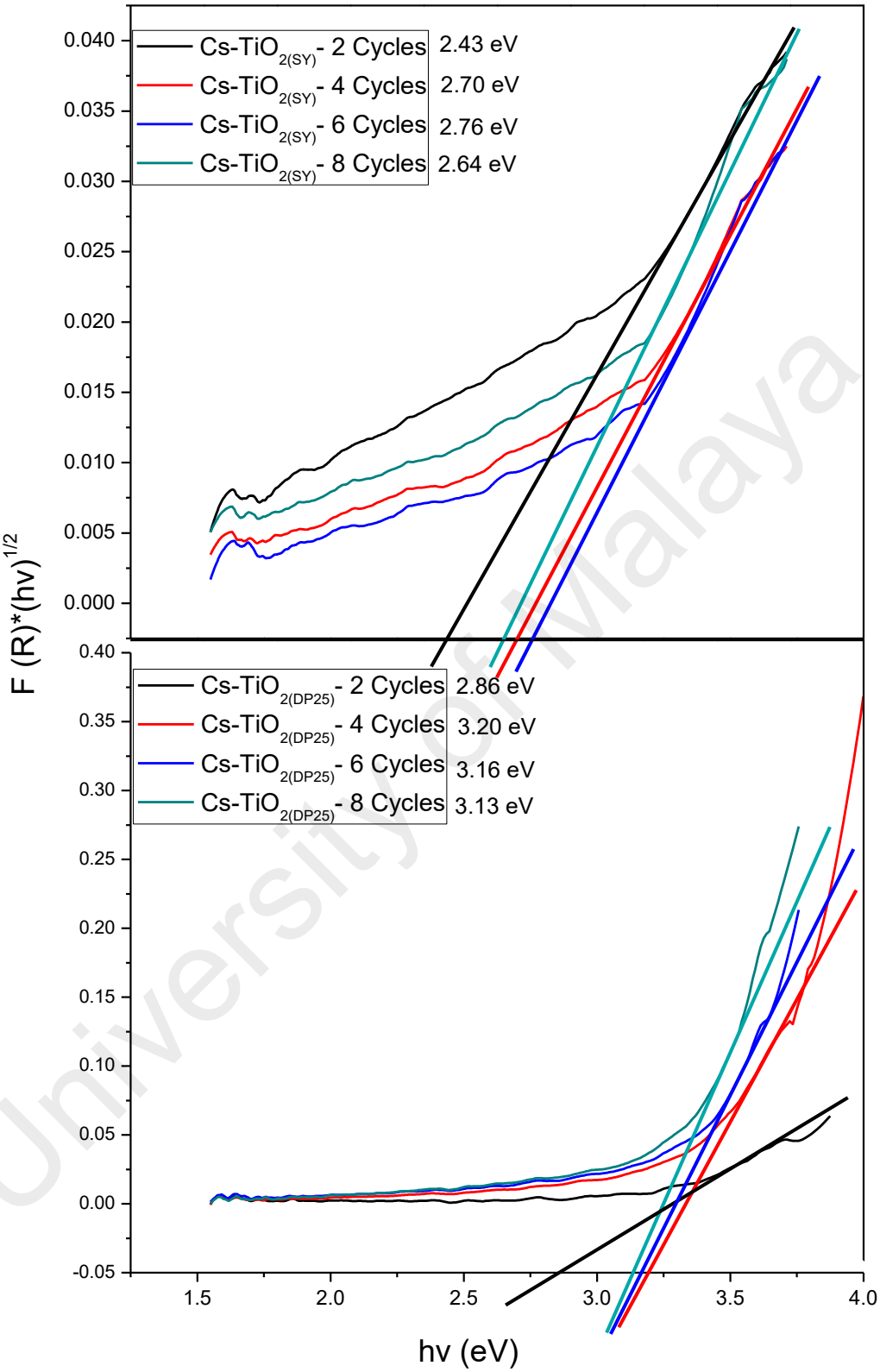

Figure 4.12: UV-DR spectra of different dip-coated cycles for Cs-TiO_2/Glass photocatalyst which are 2, 4, 6 and 8 Cycles by comparing between Cs-$TiO_{2(SY)}$/Glass with Cs-$TiO_{2(DP25)}$/Glass

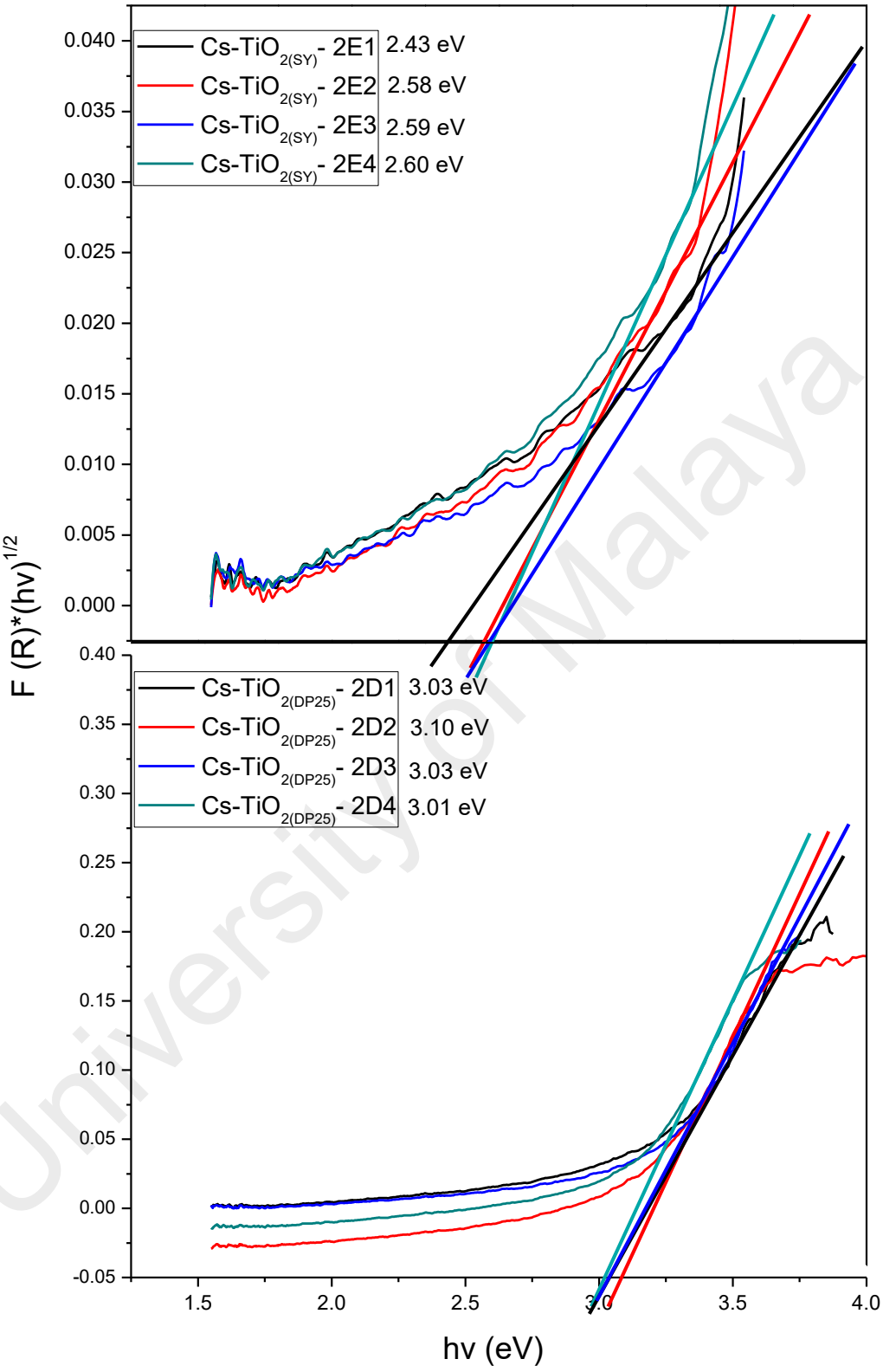

Figure 4.13: UV-DR spectra of different weight ratio for Cs-TiO_2/Glass photocatalyst by comparing between Cs-$TiO_{2(SY)}$/Glass with Cs-$TiO_{2(DP25)}$/Glass

Furthermore, the band gap (first weight ratio) of the 8 cycles photocatalysts for Cs-$TiO_{2(DP25)}$/Glass (3.03 eV) is larger than that of Cs-$TiO_{2(SY)}$/Glass (2.58 eV). Increasing the weight ratio resulted in constant values of the band gap energy for both synthesized and commercial TiO_2 photocatalyst systems. The band gap is inversely related to the amount of TiO_2. It was concluded that using the 8 cycles of Cs-TiO_2/Glass photocatalyst were promote successive deposition cycles and effective photocatalytic activities. The photocatalyst system, with different weight ratios, can absorb the photonic energy from wavelengths under or at 391 nm during the reflectance analysis. This energy can initiate photosensitization, in line with the given band gap of photocatalyst towards the total removal of MO, and further generate photodegradation during photocatalytic activity. According to Lin and Lee (2010), the TiO_2 supported photocatalytic system, with suitable amounts of TiO_2, contribute towards a better photocatalytic system. This is supported by various types of support materials used, such as glass, carbon fibers, woven fiber cloths, or other types of organic or inorganic supports (activated carbon, graphene, Ag, SiO_2, Copper, etc.).

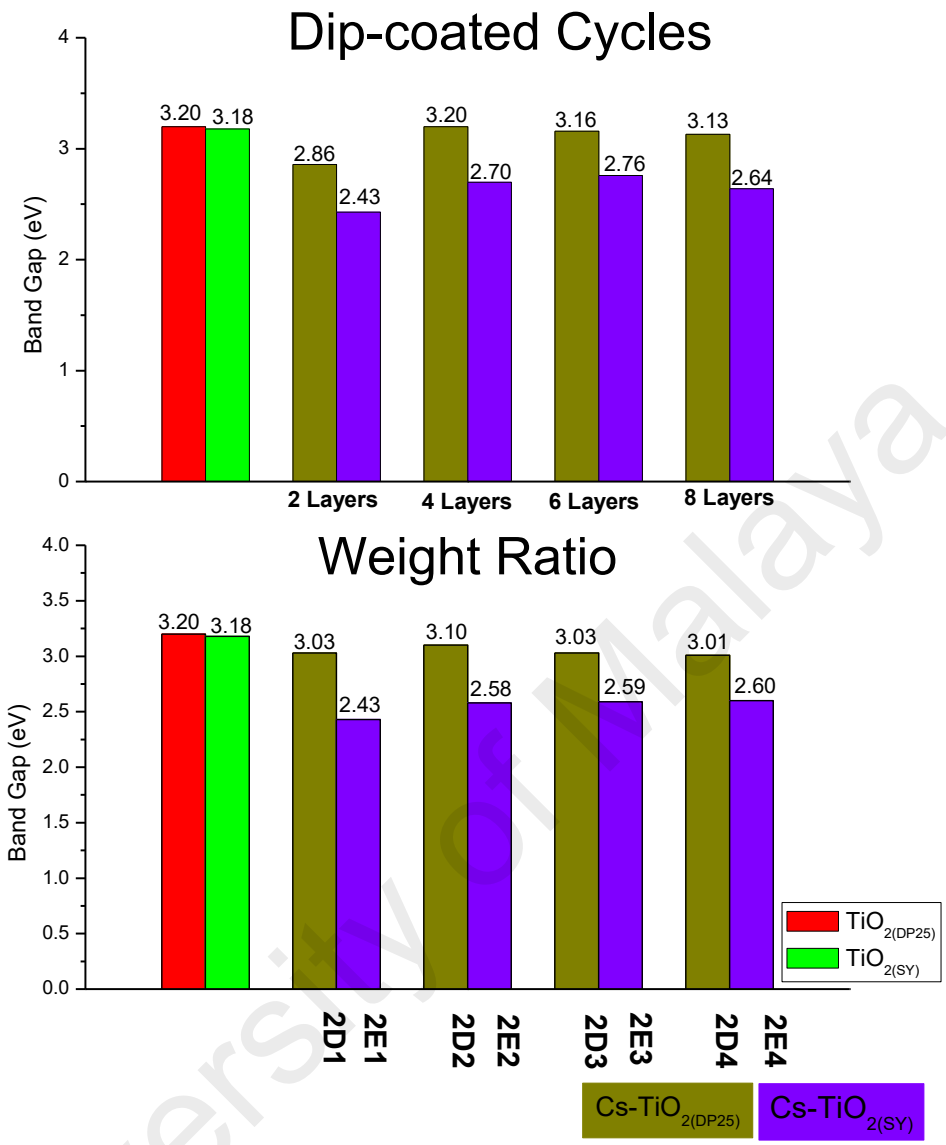

Figure 4.14: List of UV-DR spectra together with different dip-coated cycles and weight ratio for Cs-TiO_2/Glass photocatalyst by comparing between TiO_2 ($TiO_{2(SY)}$ and $TiO_{2(DP25)}$), Cs-$TiO_{2(SY)}$/Glass and Cs-$TiO_{2(DP25)}$/Glass

Based on Figure 4.14, the photocatalyst of Cs-$TiO_{2(DP25)}$/Glass showed higher band gap energies than that of Cs-$TiO_{2(SY)}$/Glass photocatalyst. Moreover, the value is kept constant for single TiO_2 and $TiO_{2(DP25)}$. However, compared to the photocatalysts system from dip-coated cycles and weight ratio, the latter demonstrated lower band gap energies, and due to this, the coupled photocatalysts of Cs-$TiO_{2(DP25)}$/Glass and Cs-$TiO_{2(SY)}$/Glass could potentially result in better adsorption-photodegradation efficiency than a single TiO_2 catalyst in the context of the total removal of MO.

4.2.3 Field Emission Scanning Electron Microscopy and Energy Dispersive Spectrometer Analysis

The distribution, surface structure, and homogeneity of TiO_2 nanoparticles within Cs matrix were analyzed using the FESEM. Figure 4.15(a) and 4.15(b) show the FESEM images for photocatalyst systems for multiple dip-coated cycles. Meanwhile, the micrographs for the photocatalysts system at multiple weight ratios is shown in Figure 4.16(a) and 4.16(b). Furthermore, EDS analysis is used to determine the bonding energies and the elemental percentage in the photocatalysts. Tables 4.7 and 4.8 show the Ti, Si, O, C, and N elements for different dip coating cycles and weight ratios of the photocatalysts, respectively.

The FESEM micrographs of Cs-TiO_2/Glass with similar weight ratio of 2:2 (0.25g of Cs: 0.25g of TiO_2) were shown for $TiO_{2(SY)}$ and $TiO_{2(DP25)}$ in (Figures 4.15(a) and 4.15(b)), respectively. These series of dipping photocatalyst have been prepared for both Cs-$TiO_{2(SY)}$ and Cs-$TiO_{2(DP25)}$ photocatalysts. Generally, all photocatalysts demonstrated a macroreticular structure with a spherical primary TiO_2 nanoparticles and a particle size of 10–30 nm. Figures 4.15(a) and 4.15(b) showed that the photocatalysts of Cs-$TiO_{2(SY)}$/Glass and Cs-$TiO_{2(DP25)}$/Glass are more homogeneous and dispersed uniformly until the number of cycles reached 8.

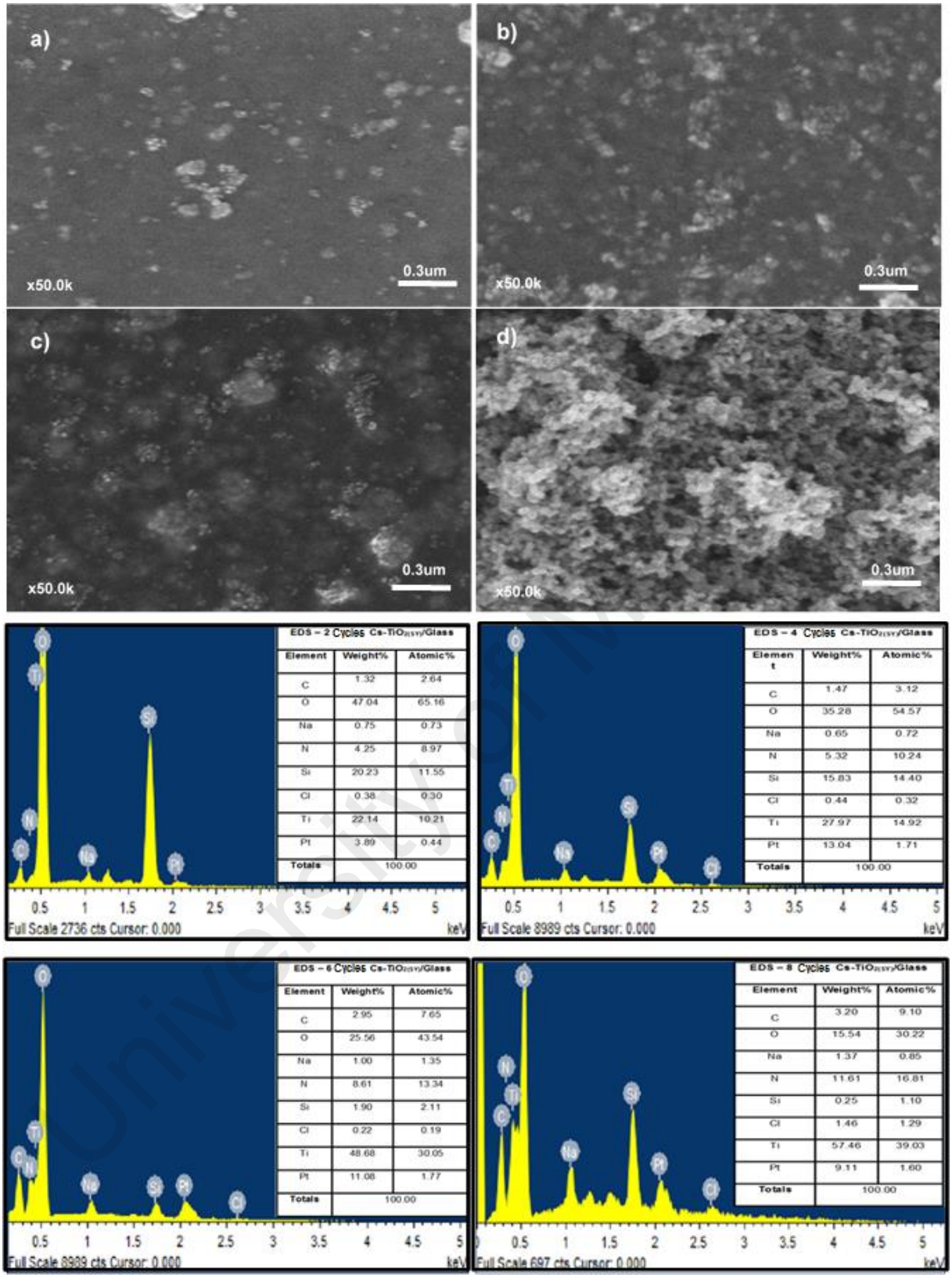

Figure 4.15(a): FESEM micrographs of dip-coated cycles a) 2 cycles b) 4 cycles c) 6 cycles d) 8 cycles for Cs-$TiO_{2(SY)}$/Glass photocatalyst with magnification of 50,000x include with EDS figures and tables

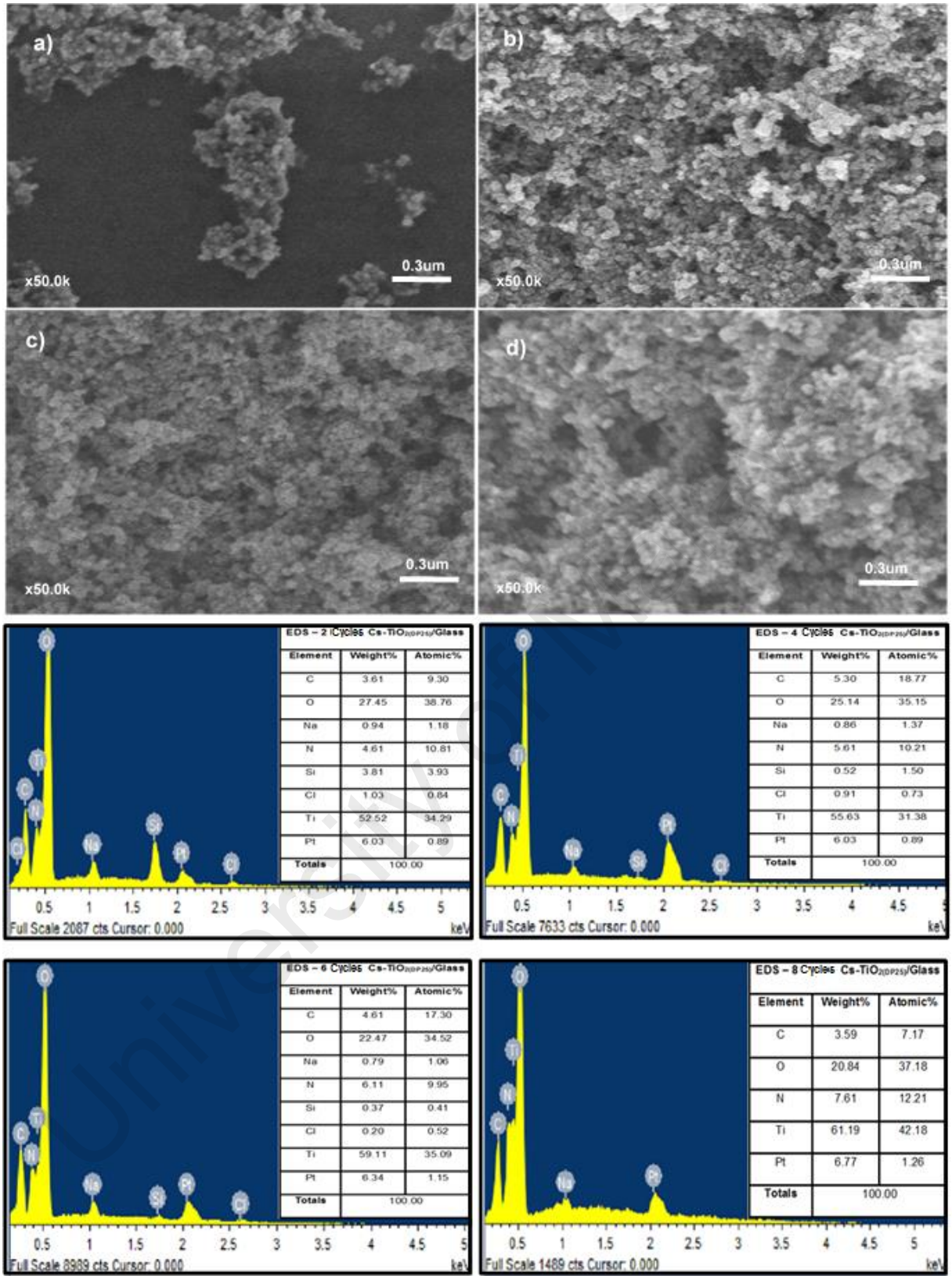

Figure 4.15(b): FESEM micrographs of dip-coated cycles a) 2 cycles b) 4 cycles c) 6 cycles d) 8 cycles for Cs-$TiO_{2(DP25)}$/Glass photocatalyst with magnification of 50,000x include with EDS figures and tables

Table 4.6: EDS photocatalysts of Cs-$TiO_{2(SY)}$/Glass and Cs-$TiO_{2(DP25)}$/Glass that are relatively to cycles formation

Samples		Elements weight percentage (%)				
		C	O	N	Si	Ti
Cs-$TiO_{2(SY)}$/Glass	2 Cycles	1.32	47.04	4.25	20.23	22.14
	4 Cycles	1.47	35.28	5.32	15.83	27.97
	6 Cycles	2.95	25.56	8.61	1.90	48,68
	8 Cycles	3.20	15.54	11.61	0.25	57.46
Cs-$TiO_{2(DP25)}$/Glass	2 Cycles	3.61	27.45	4.61	3.81	52.52
	4 Cycles	5.30	25.14	5.61	0.52	55.63
	6 Cycles	4.61	22.47	6.11	0.37	59.11
	8 Cycles	3.59	20.84	7.61	0	61.19

Overall, the EDS analysis confirms that the TiO_2 particles, with the atomic ratio of Ti to O_2 of calculations for photocatalysts with 2 and 8 dip-coated cycles of Cs-$TiO_{2(SY)}$/Glass and Cs-$TiO_{2(DP25)}$/Glass, were 1:6 and 4:1, respectively. By comparing both photocatalysts, the one with the lesser dip-coated cycles tend to have less amounts of TiO_2 and Cs bonds compared to high dip-coated cycles. Furthermore, the photocatalysts, from 2 to 8 dip-coated cycles of Cs-TiO_2/Glass (both photocatalysts) demonstrated an increment in the amount of O and Ti. In similar cases, there is no Si element observed at the composition of 8 cycles for Cs-$TiO_{2(DP25)}$/Glass photocatalyst. However, that element is reduced for Cs-$TiO_{2(SY)}$/Glass photocatalyst from 2 to 8 dip-coated cycles.

This suggests that TiO_2 was successfully distributed within the Cs matrix via coordinate covalent bonding. Bond formation are possible with Cs via metal ions, such as TiO_2, through the formation between -NH_2 group (obtain from Cs) and Ti^{4+} (obtain

from TiO_2) to produce hydrogels that can be used for attachment to a glass substrate. This would allow the Cs matrix to function as an adsorption medium, while the surface of TiO_2 act as a photoelectron center via promotion and excitation with light illumination of a suitable wavelength (<390 nm or band gap of 3.20 eV and 3.18 eV for catalysts $TiO_{2(SY)}$ and $TiO_{2(DP25)}$, respectively). Moreover, TiO_2 was completely dispersed as the nanoparticles were submerged into the coated cycles (Figures 4.15(a) and 4.15(b)). Further observation leads us to conclude that the surface TiO_2 nanoparticles (both $TiO_{2(SY)}$ and $TiO_{2(DP25)}$) are directly proportional to the number of dip-coated cycles. Hence, this confirmed that the photodegradation process plays a major role in 6 to 8 dip-coated cycles for both photocatalysts of Cs-TiO_2/Glass photocatalyst, due to the abundance of TiO_2, whereas the removal of MO would predominantly be attributed to the adsorption process, with subsequent increase of dip-coating cycles for both photocatalysts of Cs-$TiO_{2(SY)}$/Glass and Cs-$TiO_{2(DP25)}$/Glass.

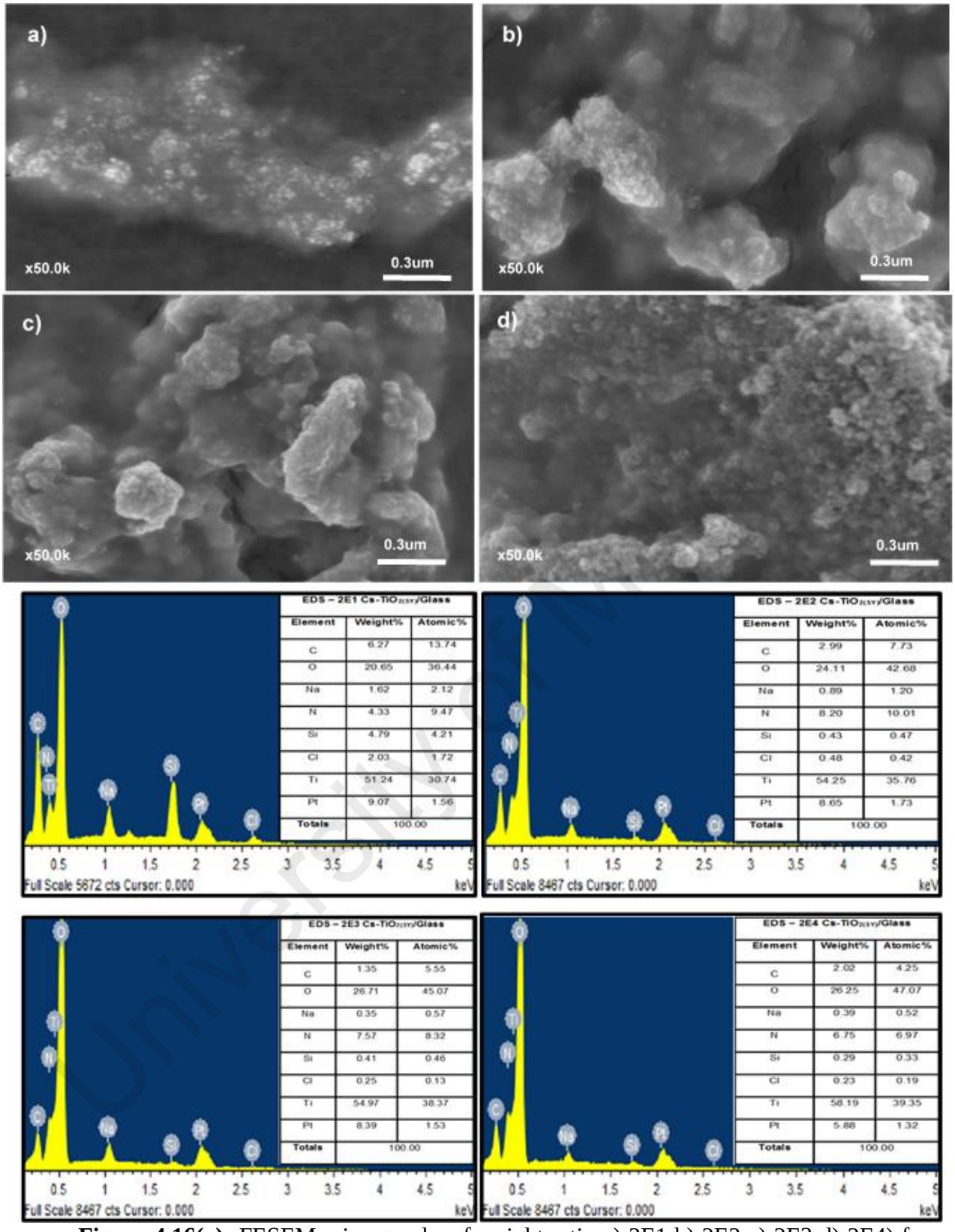

Figure 4.16(a): FESEM micrographs of weight ratio a) 2E1 b) 2E2 c) 2E3 d) 2E4) for Cs-$TiO_{2(SY)}$/Glass photocatalyst with magnification of 50,000x include with EDS figures and tables

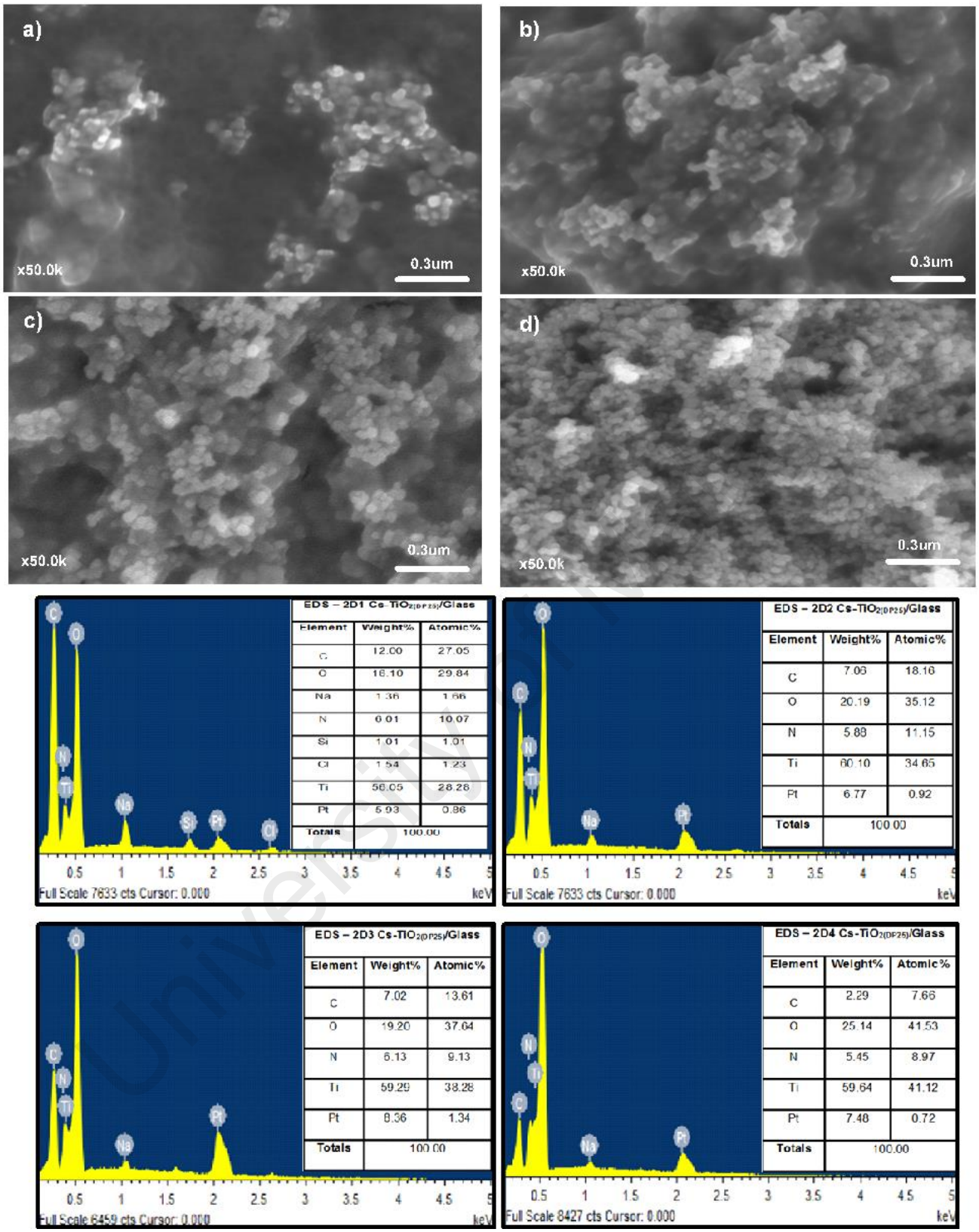

Figure 4.16(b): FESEM micrographs of weight ratio a) 2D1 b) 2D2 c) 2D3 d) 2D4) for Cs-$TiO_{2(DP25)}$/Glass photocatalyst with magnification of 50,000x include with EDS figures and tables

It is expected that the TiO_2 system has physically bounded with other materials at levels that are enough to modify the photocatalytic activities via suitable amounts of Cs and TiO_2 between $TiO_{2(SY)}$ or $TiO_{2(DP25)}$, respectively (from Figures 4.16(a) and 4.16(b)).

Table 4.7: EDS photocatalysts of Cs-$TiO_{2(SY)}$/Glass and Cs-$TiO_{2(DP25)}$/Glass photocatalysts that are relatively to weight ratio formation

		Elements weight percentage (%)				
Samples		C	O	N	Si	Ti
Cs-$TiO_{2(SY)}$/Glass	2E1	6.27	20.65	4.33	4.79	51.24
	2E2	2.99	24.11	8.20	0.43	54.25
	2E3	1.35	26.71	7.57	0.41	54.97
	2E4	2.02	26.25	6.75	0.29	58.19
Cs-$TiO_{2(DP25)}$/Glass	2D1	12.00	16.10	6.01	1.01	56.05
	2D2	7.06	20.19	5.88	0	60.10
	2D3	7.02	19.20	6.13	0	59.29
	2D4	2.29	25.14	5.45	0	59.64

From Table 4.8, the -NH_2 functional groups of Cs could prevent recombination of TiO_2 nanoparticles via the presence of electronic holes. This could be confirmed through the percentage of N element presented from the EDS analysis to justify the presence of both Cs-$TiO_{2(SY)}$/Glass and Cs-$TiO_{2(DP25)}$/Glass photocatalysts. The modification of TiO_2 photocatalyst via the incorporation of Cs with a bulky structure are expected to disrupt the inter-hydrogen bonds of the Cs polymer network, which then reduces the bulk density of the catalyst (Amin, 2012).

4.3 Result for Photocatalytic activity of adsorption-photodegradation MO

4.3.1 MO Calibration

The calibration curve was plotted based on concentrations of 1–20 ppm for the purpose of standardizing the adsorption-photodegradation process of MO (from Figure 4.17).

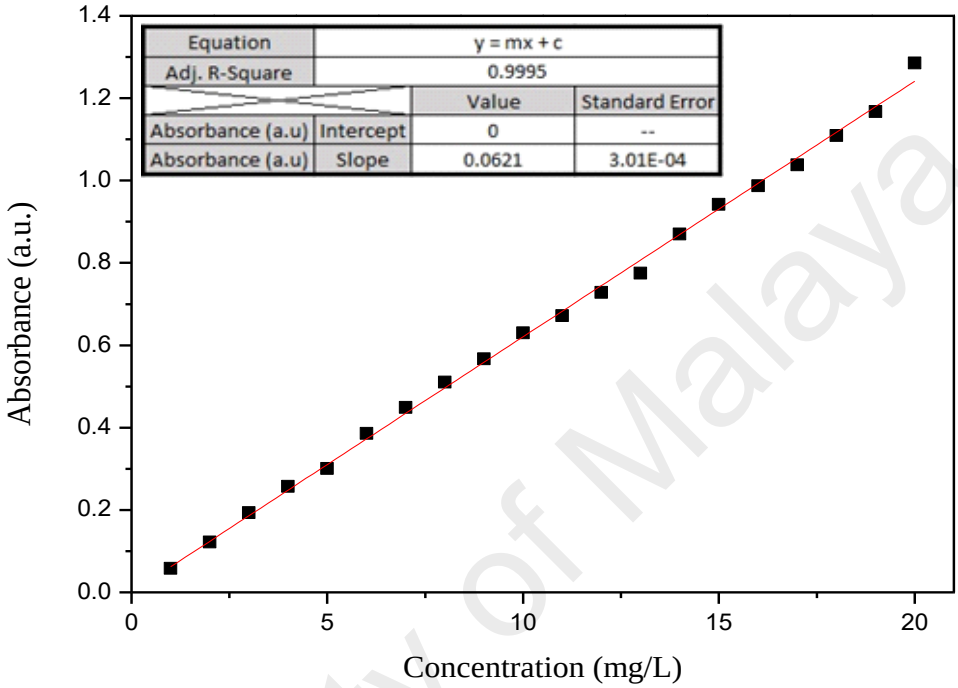

Figure 4.17: Calibration plot of MO with concentration ranging from 1–20 ppm

The linear equation was subsequently determined from this calibration plot, and could be used to further evaluate the photocatalytic degradation efficiency of the photocatalyst toward MO samples (based on concentration, ppm unit). The absorbance of each sample solution was measured to determine the final concentration of the MO once the photodegradation process was completed.

4.3.2 Adsorption and photodegradation analysis

UV-Vis analysis was carried out to quantitatively analyze the adsorption and the photodegradation process of photocatalysis using 2 parameters, which were the number of cycles and weight ratio of Cs-TiO_2/Glass photocatalyst (Cs-$TiO_{2(SY)}$/Glass and Cs-$TiO_{2(DP25)}$/Glass). Furthermore, the photocatalyst sample with the highest adsorption and photocatalytic activities were used to further analyze the effect of pH and initial concentrations of MO.

4.3.2.1 Effect of photocatalyst cycles on glass substrate

The adsorption and photodegradation of Cs-$TiO_{2(SY)}$/Glass and Cs-$TiO_{2(DP25)}$/Glass photocatalysts towards a 10 ppm concentration of MO with of 2, 4, 6 and 8 cycles are shown in Figure 4.18(a). The summary of the adsorption and photodegradation process of Cs-$TiO_{2(DP25)}$/Glass and Cs-$TiO_{2(SY)}$/Glass is further demonstrated in Figure 4.18(b).

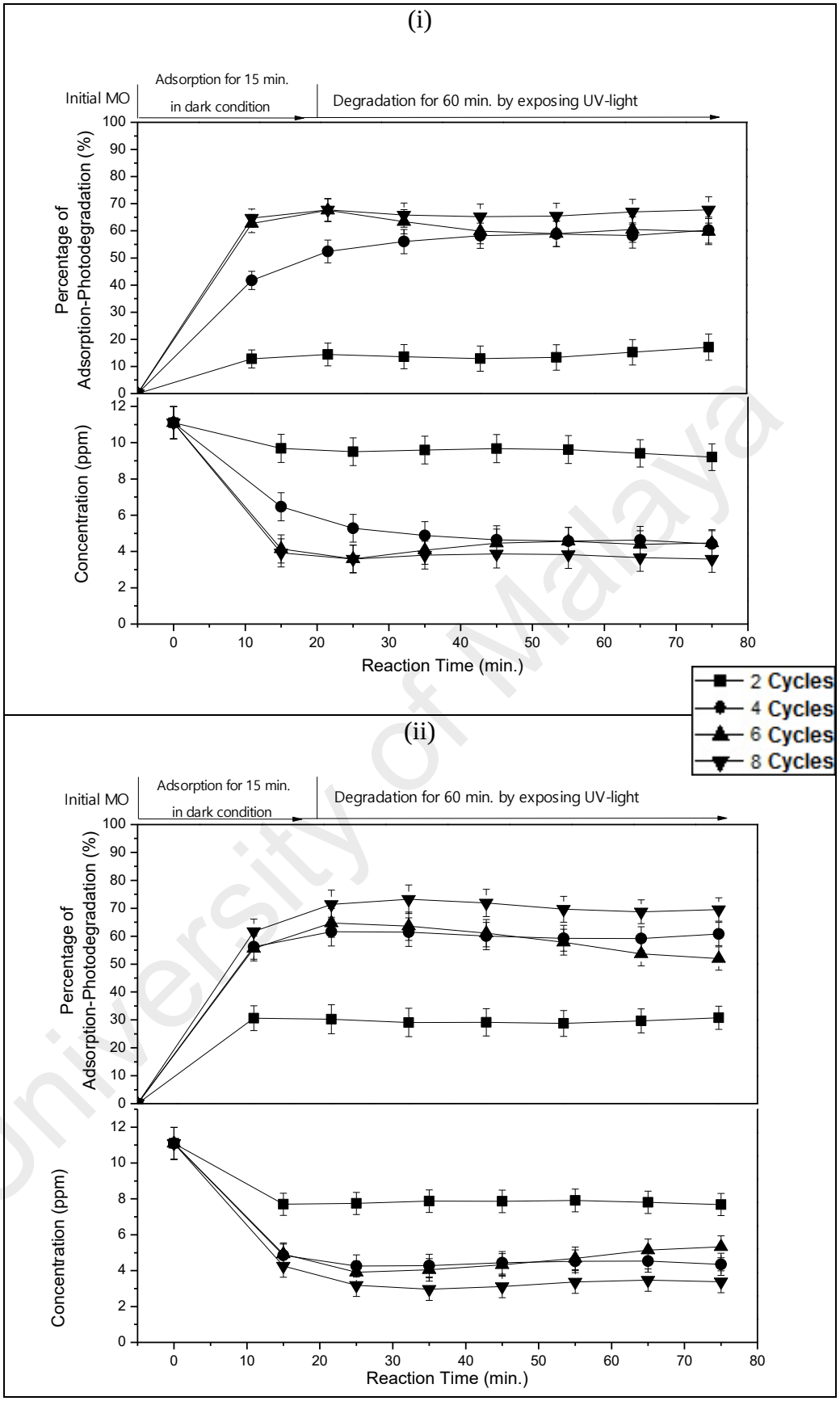

Figure 4.18(a): The adsorption and photodegradation of (i) Cs-$TiO_{2(DP25)}$/Glass and (ii) Cs-$TiO_{2(SY)}$/Glass photocatalysts with different cycles

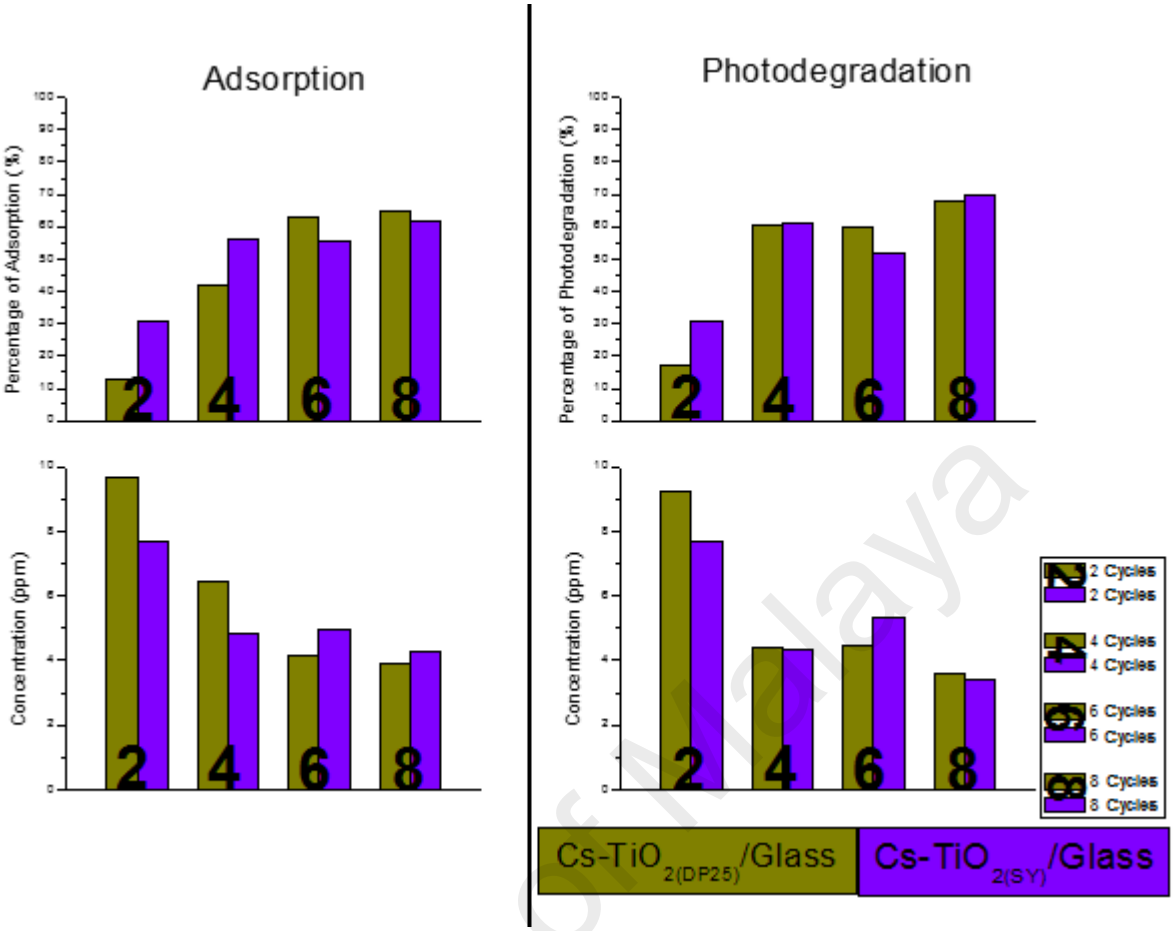

Figure 4.18(b): Summary on adsorption and photodegradation of Cs-TiO_2/Glass photocatalyst at different number of cycles

The photocatalytic activities of Cs-TiO_2/glass photocatalyst was analyzed based on the percentage of adsorption-degradation and final concentrations of MO. Based on Figures 4.18(a) and 4.18(b), photocatalysts with 2 cycles showed the lowest MO adsorption, at 10% (9.0 ppm) and 30% (7.0 ppm) for Cs-$TiO_{2(DP25)}$/Glass and Cs-$TiO_{2(SY)}$/Glass, respectively. With that, the remaining of MO concentration at 10 mins of adsorption process was recorded to be 9.0 ppm and 7.0 ppm for Cs-$TiO_{2(DP25)}$/Glass and Cs-$TiO_{2(SY)}$/Glass photocatalysts, respectively. As far as photodegradation is concerned, 2 cycles of photocatalysts was recorded to be ~20-30%, at 8.5 ppm and 6.4 ppm of MO remaining by Cs-$TiO_{2(SY)}$/Glass and Cs-$TiO_{2(DP25)}$/Glass photocatalysts, respectively. The adsorption and photodegradation process were improved as the number of cycles increased from 4 to 8. For example, photocatalysts with 4 cycles resulted in a ~50% MO adsorption, removing a total of 5.0 ppm. The introduction of UV light resulted in a MO

photodegradation of 60% and 61%, at final concentrations of 4.4 ppm and 4.3 ppm of MO for Cs-$TiO_{2(DP25)}$/Glass and Cs-$TiO_{2(SY)}$/Glass photocatalysts, respectively. The MO adsorption for the photocatalysts sample with 6 cycles was recorded to be 60% and 56%, at MO concentrations of 4.1 ppm and 4.8 ppm for Cs-$TiO_{2(DP25)}$/Glass and Cs-$TiO_{2(SY)}$/Glass photocatalysts, respectively. However, the photodegradation of both photocatalysts did not show much difference in terms of percent of degradation and concentrations of MO.

Furthermore, the 8 cycles of Cs-$TiO_{2(DP25)}$/Glass and Cs-$TiO_{2(SY)}$/Glass photocatalysts demonstrated the highest total removal of the MO. At the adsorption stage, ~62% and 65% of MO removal, with final concentrations of 4.3 ppm and 4.0 ppm for Cs-$TiO_{2(DP25)}$/Glass and Cs-$TiO_{2(SY)}$/Glass photocatalysts, were removed. Then, the photodegradation process was recorded to be 67% to 70% removal for both photocatalysts. Once the photocatalysis process was completed, the concentration of the remaining solution was recorded to be 3.6 ppm and 3.4 ppm, respectively. This can be explained by the fact that samples with more cycles contain higher percentages of Cs as its absorbent and TiO_2 as its center of photodegradation. Based on Figure 4.19, adsorption occurred on the inter H-bonds interaction between the -OH and -NH_2 groups of Cs, with the polar groups of MO.

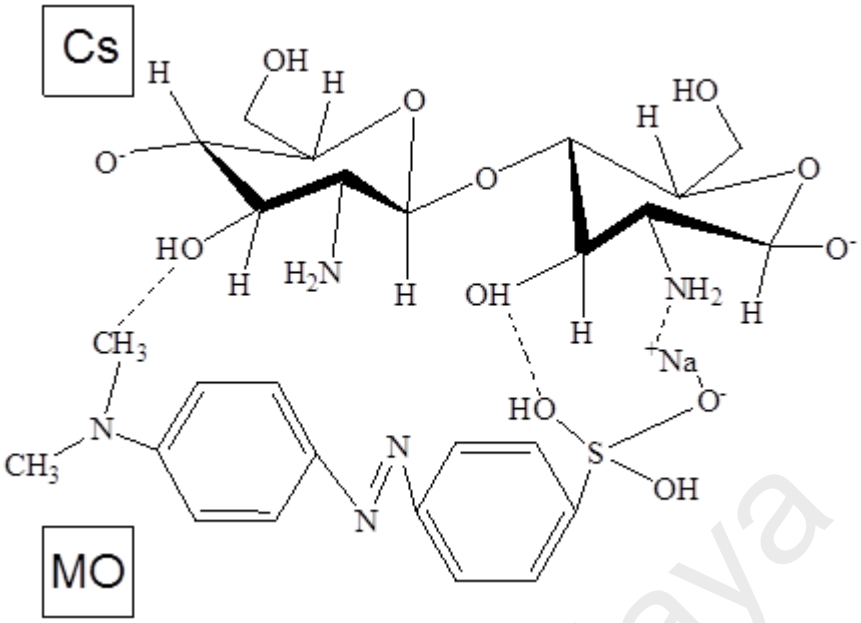

Figure 4.19: Interaction of MO adsorption on Cs

Furthermore, the TiO_2 nanoparticle being the photodegradation center worked based on its natural characteristics, such as its phase, crystallite/particle size and dispersibility. Once the MO molecules were introduced into the photocatalyst system, MO would be removed via continuous adsorption-photodegradation processes. The properties of $TiO_{2(SY)}$ and $TiO_{2(DP25)}$ were significantly different due to their respective physical and morphological properties. It is observed that the $TiO_{2(SY)}$ sample with higher amount of anatase phase has greater tendencies for higher photodegradation of MO as opposed to ones produced by $TiO_{2(DP25)}$. The $TiO_{2(SY)}$ has a band energy that is 0.2 eV higher than $TiO_{2(DP25)}$, which explains the tendency for commercial $TiO_{2(DP25)}$ to form the rutile phase. Additionally, the nanoparticles size of $TiO_{2(SY)}$ was relatively 0.5 - 0.8 nm smaller than $TiO_{2(DP25)}$. With smaller particle sizes, it is expected that the surface area of the nanoparticle is higher, resulting in enhanced photocatalytic performance. Indeed, commercial of $TiO_{2(DP25)}$ exhibited higher levels of dispersion, due to 10% more Ti element, as shown by the EDS analysis. Due to this, the photocatalytic activities is much more predominant in the synthesized TiO_2 compared to commercialized TiO_2.

4.3.2.2 Effect of Photocatalyst (Chitosan to TiO_2) weight ratio

The adsorption and photocatalytic activities of Cs-TiO_2/Glass photocatalyst was further studied via the variation in weight ratio at 2:1 (2D1), 2:2 (2D2), 2:3 (2D3) and 2:4 (2D4) of Cs:TiO2 (from Figure 4.20(a)). The summary on the adsorption and photodegradation was then calculated and illustrated in Figure 4.20(b).

Based on Figure 4.20(a) and 4.20(b), the lowest adsorption and photocatalytic activities were derived from the 2D1 and 2E1 samples. Both samples demonstrated almost 68% and 63% of MO adsorption with MO concentrations of 3.5 ppm and 4.1 ppm. As UV light irradiation was introduced, the photodegradation of MO molecules was recorded to be 64% with a final concentration of 4.0 ppm MO for both Cs-$TiO_{2(DP25)}$/Glass and Cs-$TiO_{2(SY)}$/Glass photocatalysts. The 2D2 and 2E2 photocatalysts was ~70% adsorption of MO molecules. Consequently, the remaining MO concentration becomes 3.2 ppm for both of 2D2 and 2E3 photocatalysts. As far as photodegradation is concerned, the photocatalysts was recorded to be ~72%, corresponding to a removal of 3.0 ppm of MO. The results of the adsorption and photodegradation process began to slowly change as the weight ratio increase to 2:4. The MO adsorption for the photocatalysts of 2D4 and 2E4 was recorded to be 61% and 76%, with final concentrations of 4.3 ppm and 2.6 ppm of MO, respectively. However, photodegradation by both photocatalysts was 66% and 75% with final concentrations of 3.7 ppm and 2.8 ppm of MO, respectively.

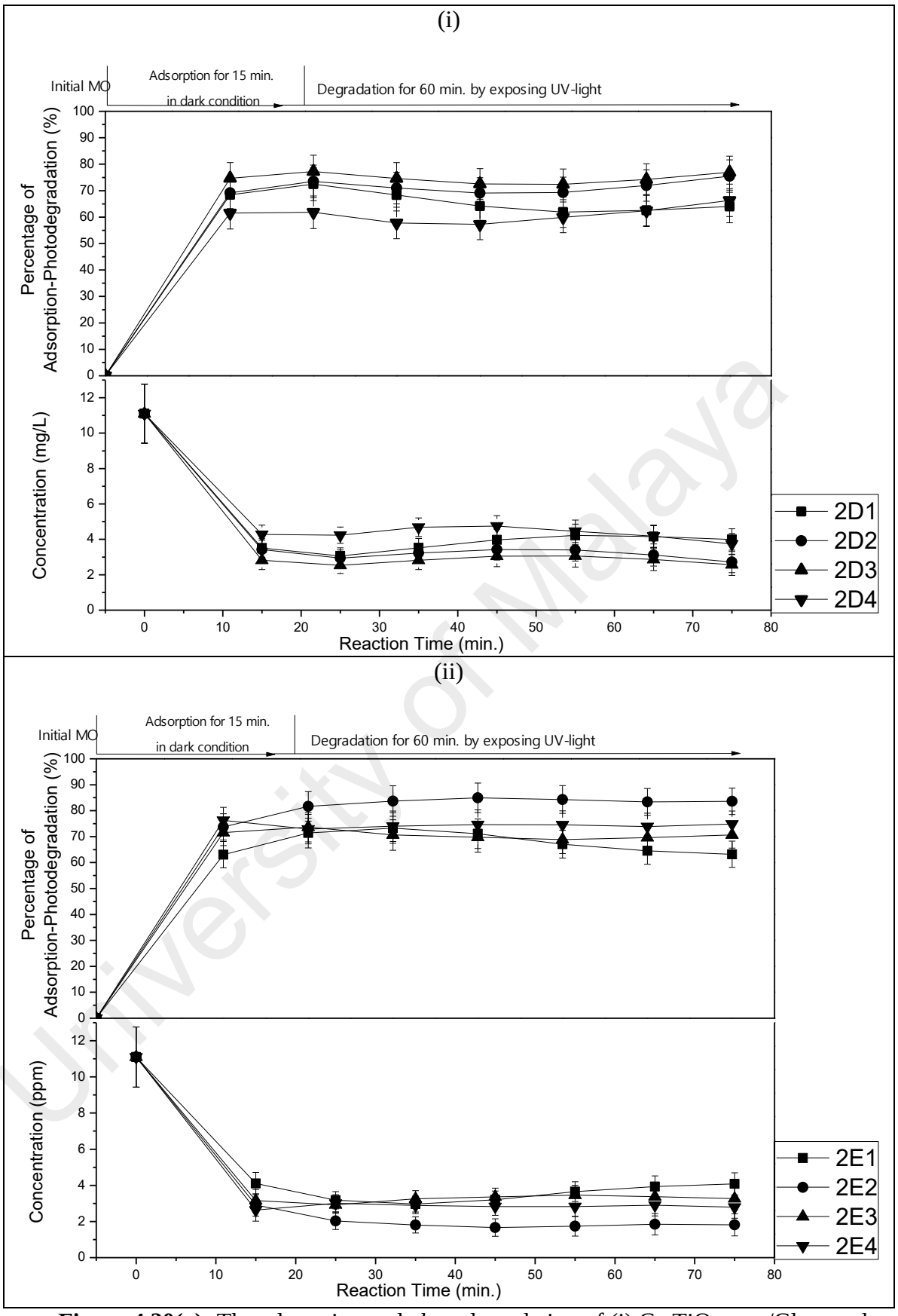

Figure 4.20(a): The adsorption and photodegradation of (i) Cs-$TiO_{2(DP25)}$/Glass and (ii) Cs-$TiO_{2(SY)}$/Glass photocatalysts with different weight ratio

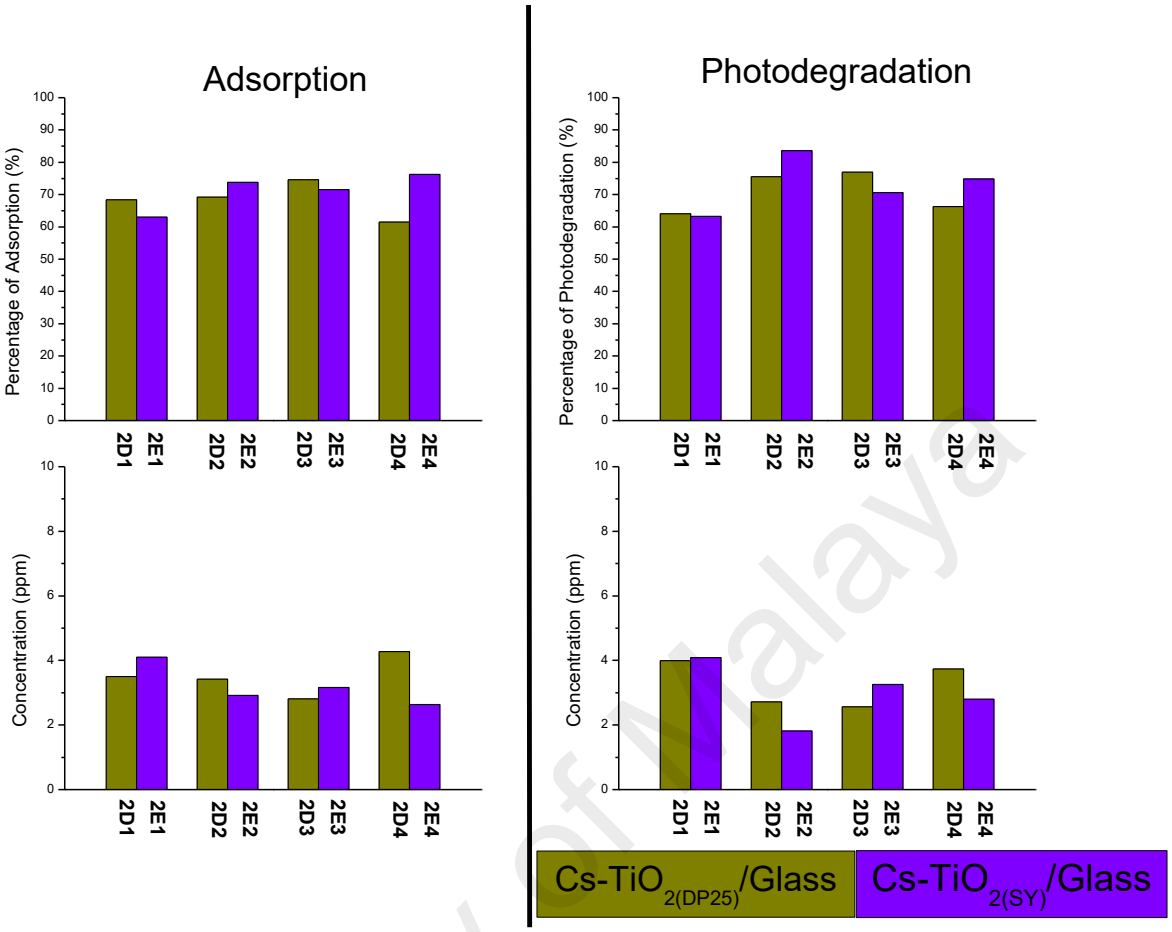

Figure 4.20(b): Summary on adsorption and photodegradation of Cs-TiO_2/Glass photocatalyst at different number of weight ratio

Generally, the 2D3 and 2E2 photocatalysts of both Cs-TiO_2/Glass photocatalyst showed the most significant adsorption and photodegradation of MO. The adsorption of MO were 70% and 75% for the Cs-$TiO_{2(DP25)}$/Glass and Cs-$TiO_{2(SY)}$/Glass photocatalysts, respectively. The concentration of MO was further decreased to 2.6 ppm and 1.8 ppm as UV light was introduced for Cs-$TiO_{2(DP25)}$/Glass and Cs-$TiO_{2(SY)}$/Glass photocatalysts, respectively. Meanwhile, the photodegradation percentages by the 2D3 and 2E2 samples were consistently increased to 77% and 84%, respectively. Furthermore, the concentration of the MO was removed from 10 ppm used after adsorption-photodegradation process was recorded to be 2.6 ppm and 1.8 ppm, respectively.

It is anticipated that photocatalysts with greater amounts of TiO_2 nanoparticles resulted in higher levels of photodegradation. However, it might decrease adsorption, due to the active surface of Cs being coated with larger amounts of TiO_2. This can be further explained by the fact that the increased weight percentage of TiO_2 providing higher degrees of freedom and distribution within the Cs matrix. Finally, the Cs-TiO_2/Glass photocatalyst with better bonding and distribution of the hybrid component resulted in a greater degree of adsorption and photodegradation of photocatalytic activities. This is evident in the FTIR results of photocatalysis, where NH_2, R-NH and OH functional groups on Cs, together with TiO_2 metal oxide, was detected, which confirms the effective removal of MO via the adsorption-photodegradation process.

4.3.2.3 Effect of initial concentration on adsorption and photodegradation activities

Figures 4.21(a) show the adsorption and photodegradation performance of 2D3 (Cs-$TiO_{2(DP25)}$/Glass) and 2E2 (Cs-$TiO_{2(SY)}$/Glass) photocatalysts samples at multiple MO initial concentrations (5, 10, 15, and 20 ppm). The summary of both adsorption and photodegradation are illustrated in Figure 4.21(b).

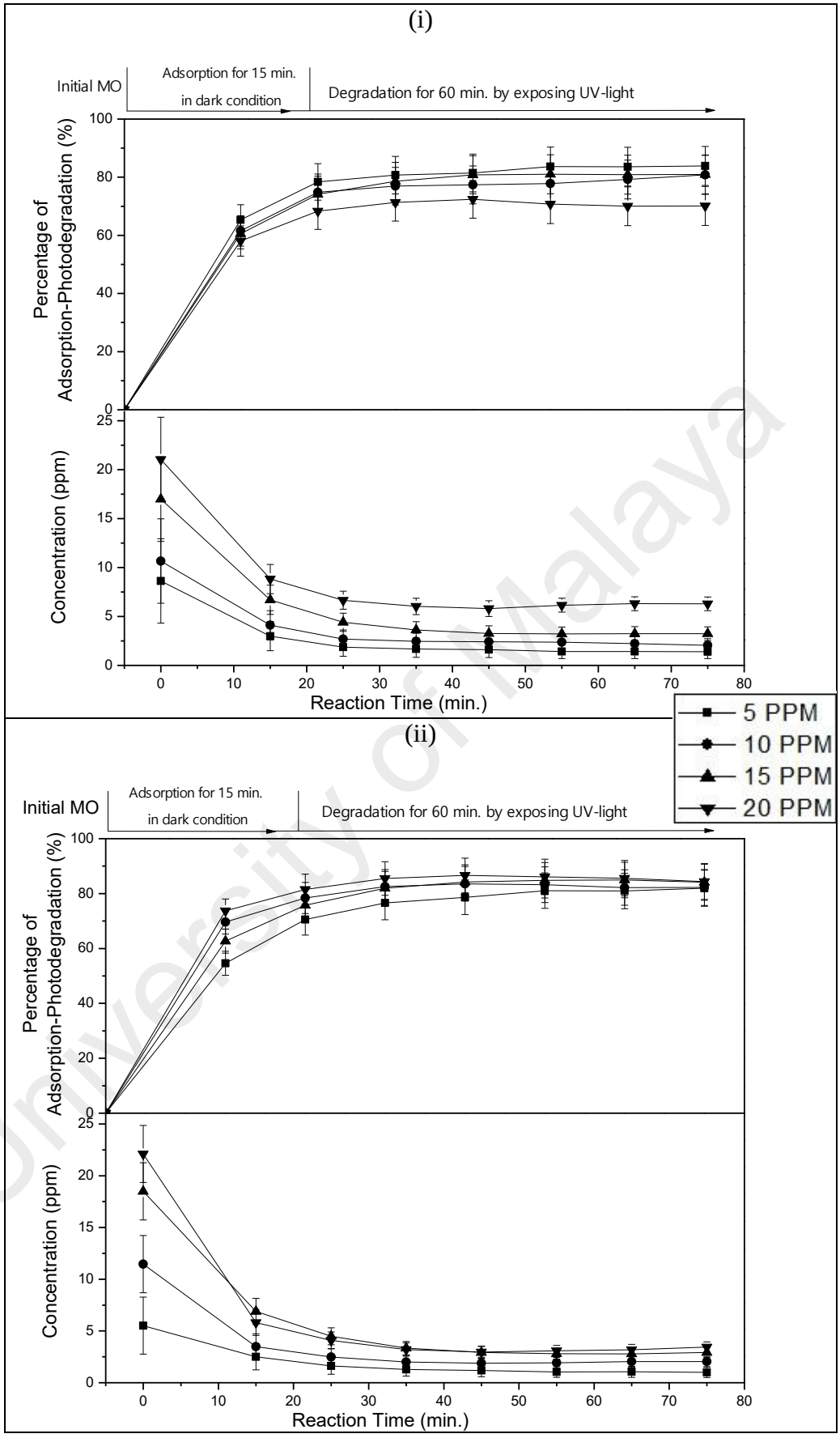

Figure 4.21(a): The adsorption and photodegradation of (i) 2D3-Cs-$TiO_{2(DP25)}$/Glass and (ii) 2E2-Cs-$TiO_{2(SY)}$/Glass photocatalysts with different initial concentration

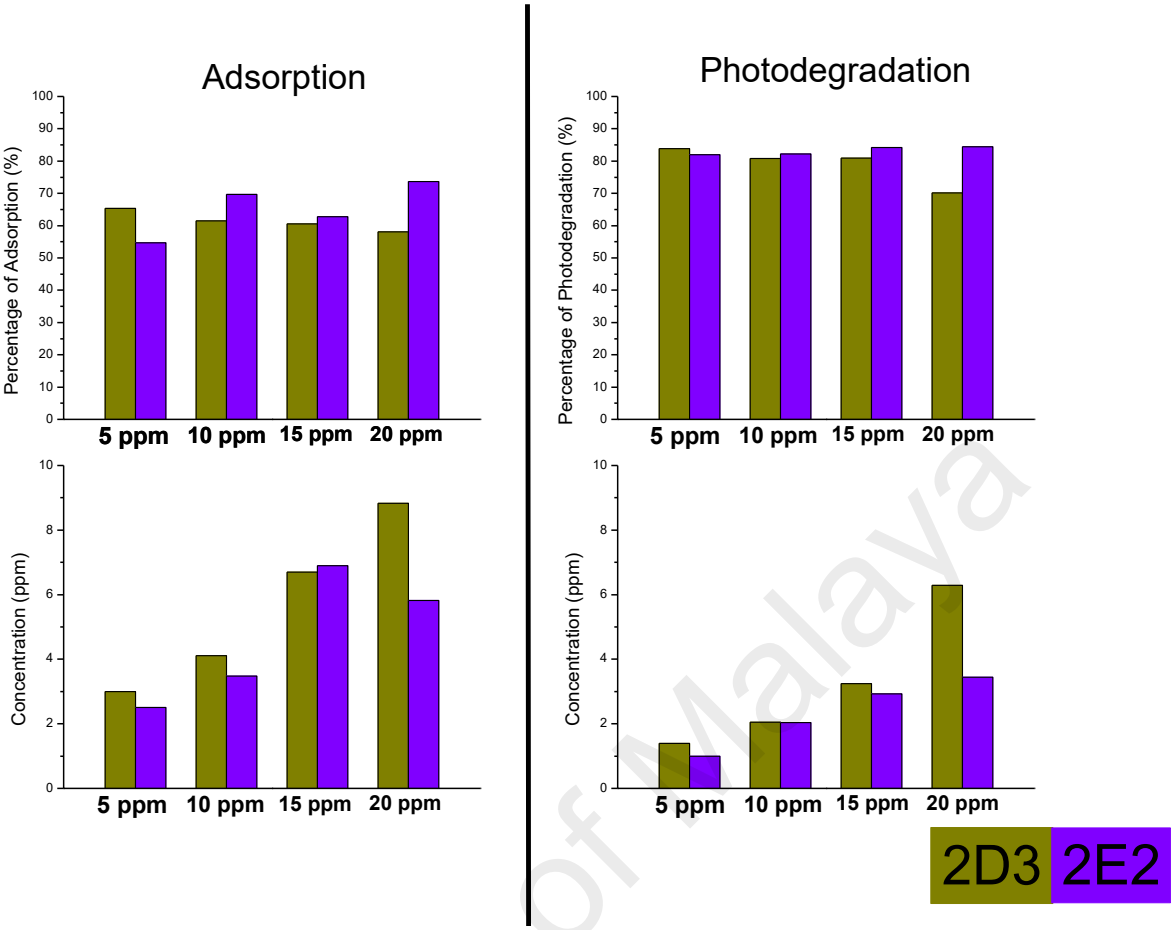

Figure 4.21(b): Summary on adsorption and photodegradation of Cs-TiO_2/Glass photocatalyst at different number of initial concentration

Generally, different initial concentrations of MO insignificantly effected the adsorptions of both photocatalysts. This applies for MO with concentrations of 5 ppm and 10 ppm. Moreover, the adsorption values increased significantly, to 65%, when an MO with a concentration of 15 ppm was used for the pollutant medium. However, the adsorption value was reduced to 60% when the MO concentration reached 20 ppm. It was also observed that the sample derived from Cs-$TiO_{2(DP25)}$/Glass photocatalyst resulted in 10% higher adsorption values (around 65%) compared to the Cs-$TiO_{2(SY)}$/Glass photocatalyst (around 55%). However, at an MO concentration of 10 ppm, the adsorption process was slightly reduced for Cs-$TiO_{2(DP25)}$/Glass photocatalyst to 62%, while it increased to up to 70% for the Cs-$TiO_{2(SY)}$/Glass photocatalyst. At an initial concentration of 15 ppm, both photocatalyst samples demonstrated some reduction of 60% for

adsorption properties. Finally, using an MO with a concentration of 20 ppm as the pollutant medium resulted in adsorption values of 75% and 55% for Cs-$TiO_{2(SY)}$/Glass and Cs-$TiO_{2(DP25)}$/Glass photocatalysts, respectively.

It is expected that at higher concentrations, the ratio of the initial number of the available adsorption sites to the dye molecules was low, thus the number of available adsorption sites becomes lower, which subsequently reduced the rate of removal of dyes. Moreover, as higher concentrations of MO were used, the relationship between MO concentrations of particular obtainable adsorption by the Cs-TiO_2/Glass photocatalyst to the MO pollutant medium is rather minimal. Moreover, the number of obtainable adsorption by the Cs-TiO_2/Glass photocatalyst decreased to the subsequent adsorbed MO (R. Huang *et al.*, 2013). Under UV light irradiation, the Cs-$TiO_{2(DP25)}$/Glass photocatalyst recorded a significant photodegradation of almost 85% when 5 ppm was used as the starting initial concentration. Next, the photodegradation process decreased to 70% as the initial concentration used was increased to 20 ppm. Furthermore, the Cs-$TiO_{2(DP25)}$/Glass photocatalyst was effectively photodegraded until 15 ppm of the initial concentration, with 80% of photodegradation percentage. The process decreased the photodegradation percentage when the initial concentration was 20 ppm. The photocatalytic system become more saturated at higher concentrations of MO, consequently resulting in lesser breakthrough and exhaustion time compared to lower initial concentrations. Furthermore, the photodegradation of Cs-$TiO_{2(SY)}$/Glass photocatalyst fully functioned and retained the percentage from 80% to 85% as the initial concentration of MO was increased from 5 ppm to 20 ppm.

The improvement on adsorption, as well as the photodegradation, was brought about by the saturation of active sites on the catalyst's surface with the MO molecules can be determining using FTIR analysis. Moreover, the MO solution was rendered darker at

higher concentrations (might give darker in color solution), which might block or reduce the penetration of light that helps initiate further reaction with the catalyst for photodegradation (loss of light-energy). Moreover, the following formation of ·OH radical was reduced as well. Indeed, the adsorption ability of the photocatalysts can be related to the characteristics of Cs molecules (the functional groups). The functional groups NH, NH_2, and OH can function as chelation sites, where the MO pollutant medium could be adsorbed. This can be further explained by the fact that the adsorption process of Cs towards MO utilizes electrostatic attraction formed between the Cs and MO solute (Zainal *et al.*, 2009). Furthermore, TiO_2 used in the process initiated the photodegradation process when exposed to UV-light as its source of energy (within the TiO_2 band energy, the excited electron and hole can recombine and release the energy gained from the excitation of the electron as heat), which will help further degrade the MO pollutant medium. The contact between Cs and TiO_2 in the context of this work initiated the highest adsorption process and further improved the degradation capabilities of TiO_2 under UV-irradiation.

4.3.2.4 Effect of initial pH on adsorption and photodegradation activities

The adsorption, as well as the photodegradation of Cs-TiO_2/glass photocatalysis was further analyzed at different pHs (2, 4, 6, 8 and 10) of the MO pollutant medium. (from both Figures 4.22(a) and 4.22(b)).

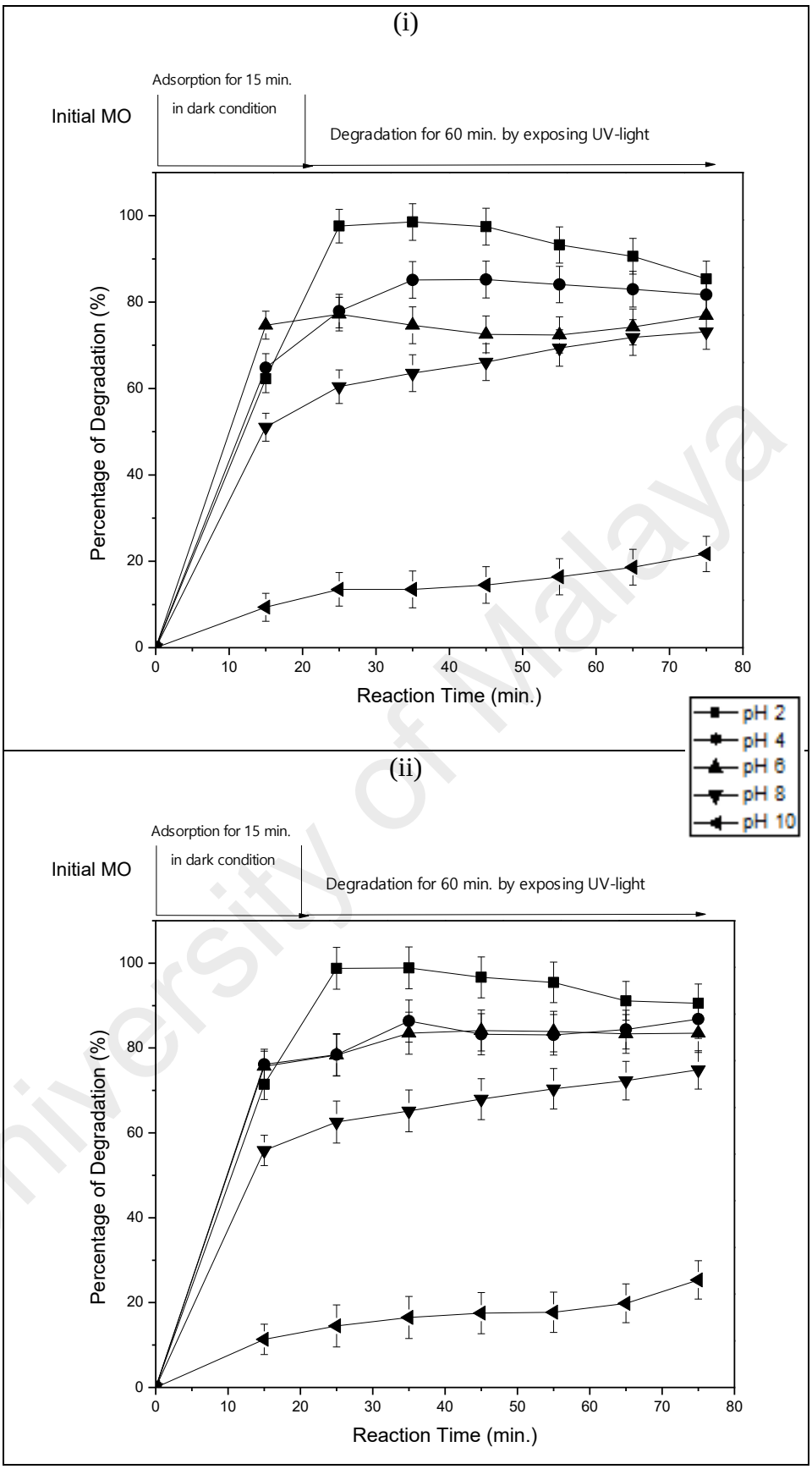

Figure 4.22(a): The adsorption and photodegradation of (i) 2D3-Cs-$TiO_{2(DP25)}$/Glass and (ii) 2E2-Cs-$TiO_{2(SY)}$/Glass photocatalysts with different initial pH

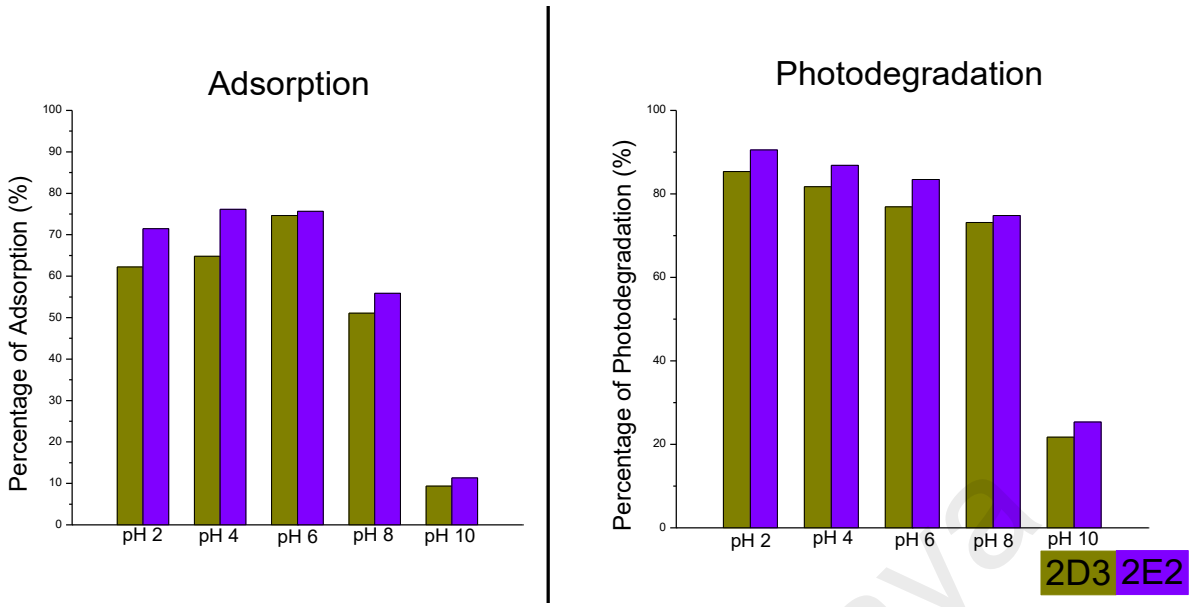

Figure 4.22(b): Summary on adsorption and photodegradation of Cs-TiO_2/Glass photocatalyst at different number of initial pH

At pHs of 2 to 6, the percentage of adsorption increased from 60% to 75% and 70% to 78% for Cs-$TiO_{2(DP25)}$/Glass and Cs-$TiO_{2(SY)}$/Glass photocatalysts, respectively. However, the percentage of adsorption at pHs 6 to 10 slightly decreased from 75% to 10% and 78% to 15% for Cs-$TiO_{2(DP25)}$/Glass and Cs-$TiO_{2(SY)}$/Glass photocatalysts, respectively. Furthermore, the percentage of photodegradation demonstrated improvements once the adsorption process was completed. For the photodegradation process, the percentage of photodegradation demonstrated a reduction tendency when pHs 2 to 10 was used as the pollutant medium. At that rate, the photodegradation was recorded to be 85% to 22% and 91% to 25% for Cs-$TiO_{2(DP25)}$/Glass and Cs-$TiO_{2(SY)}$/Glass photocatalysts, respectively. Generally, the percentage of adsorption activity was determined to be 62% and 72% using Cs-$TiO_{2(DP25)}$/Glass and Cs-$TiO_{2(SY)}$/Glass photocatalysts, respectively which contributed to the highest adsorption process by the MO solution at a pH of 2. Furthermore, the photodegradation of Cs-$TiO_{2(DP25)}$/Glass and Cs-$TiO_{2(SY)}$/Glass photocatalysts could reach 85% and 91%, respectively.

The mechanism between the activity of adsorption-photodegradation by Cs-TiO_2/Glass photocatalyst and initial pH of MO can be explain based on the concentration of H^+ and OH^- ions present in the MO medium. It depends on the nature of the MO being used to adsorb and degrade. Furthermore, most industrial effluents contributing to dye waste will not usually be generated at neutral pH. According to Akpan and Hameed (2009), most study confirmed that the use of catalysts such as TiO_2 is effective for degradation at lower pHs, similar to the ones reported elsewhere, which is attributed to the strong electrostatic field of the Cs-TiO_2/Glass photocatalyst enhancing photocatalytic performance between the surface of TiO_2 catalyst with positive charges, and the charges from solution, which is mostly negative. However, lower pHs could adversely affect the catalyst during the photocatalytic process (Akpan & Hameed, 2009), making it necessary that the adsorption characteristics of MO on the surface of Cs-TiO_2/Glass photocatalyst is investigated prior to the extended photodegradation process. According to R. Huang *et al.* (2013), Cs could be used as an adsorbent at an optimal pH of between 3-6. For the Cs-TiO_2/Glass photocatalyst, high adsorption was obtained at a pH of 2 due to the protonation of the $–NH_3$ groups in Cs prior to adsorption. The process can be explained by the fact that the MO can be contained within an aqueous solution, after which the sulfonate groups ($R–SO_3Na$) of the absorbed MO are dissociated, rendering them anionic for absorption to the MO ions. At this point, the adsorption process is completed, due to the electrostatic attractions between the adsorbent surface, as well as the MO anions. However, the decrease of MO adsorption can be explained by the competition of the abundant presence of $OH^–$ ions in the basic solution for the adsorption sites with MO anions (R. Huang *et al.*, 2013). The recombination of holes and photoelectrons can be avoided when the MO pollutant medium was adsorbed by the photocatalyst media. This can be explained by the fact that the MO molecules can only be degraded near the surface of the Cs-TiO_2/Glass photocatalyst by the ·OH free radical. Furthermore, superoxide free radicals are generated

by irradiating the Cs-TiO_2/Glass photocatalyst. This basically means that higher percentages of MO molecules was adsorbed on the surface of Cs-TiO_2/Glass photocatalyst, which translate into extended degradation time for the MO molecules (Xu *et al.*, 2010).

4.3.2.5 Adsorption analysis

The adsorption and photodegradation of MO molecules have been further analyzed with FTIR analysis. (Figure 4.23) Apparently, the presence on funtional groups of adsorption site could be realize by NH_2, NH, and OH functional groups together with TiO_2 metal oxide. These series of functional groups help to confirm the effective removal of MO through adsorption-photodegradation process. After adsorption-photodegradation process, it has been observed that some changes occured as a result of the interaction between the photocatalysts system toward MO solution. First of all, the presence of TiO_2 molecule recorded with strong absorbance bands at 498 cm^{-1} with shoulder at 680 cm^{-1}. In the peak of 3745 cm^{-1}, the spectral transmittance also appeared as sharper bands for Cs-TiO_2, indicating that –OH groups of Cs has been attached to TiO_2 network (Fajriati *et al.*, 2014). Furthermore, the adsorption bands of Cs were measuring to the peaks of 3420 and 1660 cm^{-1} which is assigned to –OH (mostly adsorption toward TiO_2) and –NH_2 (mostly adsorption toward MO) functional groups, respectively. Furthermore, the mode of the Cs can be also confirmed by peaks of 1535 cm^{-1} which is identified the functional

groups of –C–N and C-N-H. While bands of –NH and C=O has been also observed based on the peak at 1660 cm^{-1} (Kavitha *et al.*, 2013).

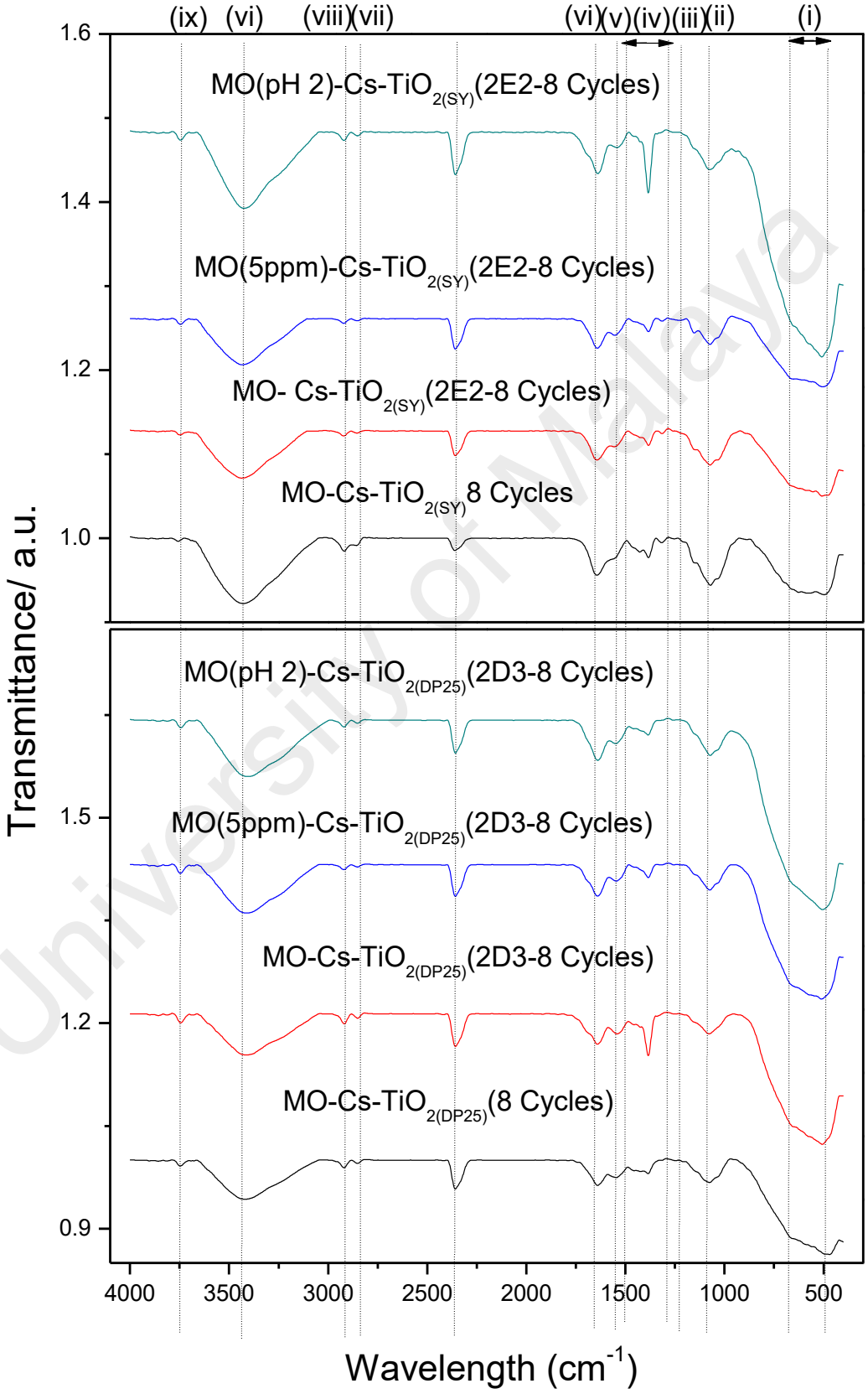

Continued on next page

Symbol	Wavelength (cm^{-1})	Assignment
(i)	498 to 680	TiO_2 with shape of 8 cycles formation with Cs
(ii)	1081	Si=O vibration
(iii)	1315	–C=N stretching of MO
(iv)	1490 to 1280	Stretching bands of $–NH_2$ from Cs to be attached with $–CH_3$ from MO
(v)	1535	C–N and C–N–H mode of Cs
(vi)	1660	N-H bending vibration in $–NH_2$ group of Cs
(vi)	3420	–OH groups of Cs
(vii)	2850	OH bands of surface TiO_2-OH functional groups
(viii)	2920	–C–H stretching
(ix)	3745	Indicating that –OH groups of Cs to be attached with TiO_2 network

Figure 4.23: FTIR spectra of optimize Cs-TiO_2/Glass photocatalyst related with highest MO parameters by comparing between Cs-$TiO_{2(SY)}$/Glass with Cs-$TiO_{2(DP25)}$/Glass

Moreover, the effectiveness of photocatalytic reaction could be explained more on adsorption rather than photodegradation process due to the present amount of MO molecules after photocatalytic reaction. There are some new peaks (MO functional groups) appeared and clearly obvious after analysis. Besides that, MO molecules can be detected after it has been adsorbed by Cs molecules . This peak at 1,660 cm^{-1} distinctly weakened after the photodegradation process and might be suggessted that the involvement of NH_2 groups in the adsorption of MO. Other than that, the range of bending attributed to the –C=N stretching was observed at 1315 cm^{-1} and C=C stretching at 1660 cm^{-1} was observed the binding between Cs and MO. Most of the adsorption funtional groups of Cs has been identified the peaks from 1490 to 1280 cm^{-1} for the attributed to the existence of protonated $–NH_2$ groups in the Cs structure which forms of H-bond toward $–CH_3$ site from MO molecule (Zainal *et al.*, 2009). In the nutshell, most of MO molecules can be obtianed from the adsorption process done by Cs. The interaction of MO molecules with photocatalyst system could be demostrated through the peaks at 1380 cm^{-1} which showed the stretching of C–C and N=N vibrations, respectively. The aromatic –C–H stretching peak at 2920 cm^{-1} indicated the presence of MO molecules within the

photocatalyst system. Furthermore, the spectra was recorded in the form of a strong increase of absorbance below 1081 cm^{-1} represented by the stretching of –S=O functhional groups. Confirmation with the characteristics of MO molecules were exhibited from the peaks at 1081 cm^{-1} –S=O stretching vibrations; 2920 cm^{-1} –CH stretching; 1315 cm^{-1} –C=N stretching were recorded accordingly (Nandini & Vishalakshi, 2012). For confirmation, peak around 2360 cm^{-1} was not a characteristic peaks of Cs-TiO_2 photocatalyst or even MO but was due to CO_2 that may effects through calculating circumstances. Other than that, comparing with single TiO_2 photocatalyst on the glass substrate by studies done by R. F. Chen and Zhang (2008); Ganesh *et al.* (2012); Serpone *et al.* (1986), it may have high surface area and some modification with TiO_2 morphological structure. Furthermore, the photocatalytic activity was highly enhance in performing degradation with dyes pollutant by comparing in using single TiO_2.

CHAPTER 5: CONCLUSION

5.1 Conclusion

TiO_2 nanoparticles have been successfully synthesized via the sol-gel method, with crystalline and particle sizes of 10 and 20 nm, respectively. It can also be confirmed from the XRD and Raman Spectroscopy results the anatase phase for TiO_2 nanoparticle ($TiO_{2(SY)}$) was successfully formed. The morphology analysis of TiO_2 showed agglomerated small and large particles, composed of 63% of the Ti-element. Finally, the band gap energy of TiO_2 was recorded to be 3.20 eV, proving that the nanoparticles are applicable within the UV-light region.

Cs-TiO_2/Glass photocatalyst were formed via the dip coating method. FTIR analysis confirmed that the photocatalysts with 2, 4, 6 and 8 cycles between Cs and TiO_2 on the glass substrate of Cs-$TiO_{2(SY)}$/Glass and Cs-$TiO_{2(DP25)}$/Glass photocatalysts has NH_2, R-NH and OH functional groups, alongside TiO_2. Indeed, a good and homogenous distribution of TiO_2 within the Cs matrix was evident in the FESEM images. Generally, the TiO_2 nanoparticles were spherical and measures between 10-30 nm. EDS analysis revealed that both photocatalysts are equally dominated by TiO_2. The band gap energy of each photocatalysts, determined by UV-DR, proved that the band gap energy was influenced by the change in cycles and weight ratio of the TiO_2 nanoparticles.

Finally, the adsorption and photocatalytic activities were conducted at two different parameters, which are number of cycle and weight ratio. It was determined that the photocatalyst with 8 cycles resulted in the highest adsorption and photocatalytic activities, at 68% and 70% for Cs-$TiO_{2(DP25)}$/Glass and Cs-$TiO_{2(SY)}$/Glass photocatalysts, respectively. It is expected that higher numbers of photocatalysts cycles results in increased adsorption and photodegradation active centers. In terms of weight ratio, it was determined that the sample with weight ratios of 2D3 and 2E2 photocatalysts (most

optimized Cs-TiO_2/Glass) demonstrated ~75% adsorption and 80% of photodegradation. This was due to the fact that the photocatalyst, with certain ratios of Cs and TiO_2, resulted in satisfactory bonding, which consequently enhances adsorption and photodegradation. Furthermore, the highest adsorption and photodegradation was achieved at a concentration of 15 ppm MO. This was so since increased concentration of MO contribute to the reduction of light penetration during photocatalytic activity, slowing the adsorption-photodegradation process. The effect on pH was quite significant, where the adsorption and photodegradation process is significantly more effective at a pH of 2. This was due to the electrostatic field between the photocatalyst and MO being affected.

In a nutshell, combined Cs and TiO_2 results in an advanced and highly efficient adsorption and photodegradation for MO synthetic dye purification. The Cs functions as the host material for the adsorption site of TiO_2, which consequently results in better dispersion and separation of photocatalyst in a pollutant medium. Cs provides the unique components related to the presence of polar groups (OH and NH_2), while TiO_2 could help by further degrading the MO by being supported by the UV-light as its energy source to influence photodegradation. Moreover, Cs, along with TiO_2, would transform their respective chains by being stretched on glass surfaces. Furthermore, it will also straighten itself on the smooth glass surfaces, or form hydrophobic minuscule domains via the dip-coating method. It can also be used on compact glass substrates, which also helps curtail movements.

5.2 Future work

This thesis presented a number of advances for Cs-TiO_2/Glass based photocatalysis system and its application for the adsorption-photodegradation of synthetic dyes in wastewaters. Furthermore, several future directions related to this research were identified, and listed as follows:-

- The efficiency of any Cs-TiO_2/Glass photocatalyst is on par with the standard TiO_2 nanoparticle set, and this study has proven that the adsorption process of the Cs-TiO_2/Glass photocatalyst is much greater than that of TiO_2 nanoparticles. However, 8 cycles of Cs-TiO_2/Glass photocatalyst resulted in high photocatalytic reaction up till 75 minutes. However, the exact time needed to complete the photodegradation process was not accurately determined. This could be addressed by increasing the irradiation time to exceed 75 minutes up till the point where the solution will be fully degraded.
- Other different adsorbent materials, such as activated carbon, cellulose, silica gel, or clay for example, can be combined with the photocatalyst system to increase adsorption and photodegradation activity. Furthermore, the physical, chemical, interfacial, and semiconductive properties of the composite can be further analyzed as well.
- The effect of visible light was not investigated in this work; additional investigative focus on the different irradiation intensity inside the photoreactor include a good evaluation of the impact of irradiation effect for the reactor's performance. Additionally, the alternative light transmitting material could be investigated for the construction of the reaction vessel (e.g. borosilicate glass) cylinders. Solar irradiation could also be investigated using a novel reactor configuration.

- More reaction with different types of pollutants, including metal ions, chemical compounds, herbicides, pesticides, hormones, and others could be degraded using the photocatalysts system. Indeed, many synthetic dyes, such as different azo dyes including Methylene Blue, Malachite Green, Crocein Orange, Methyl Red, or Congo Red can also be the subject or model of pollutant compounds.

REFERENCES

Akpan, U., & Hameed, B. (2009). Parameters affecting the photocatalytic degradation of dyes using TiO 2-based photocatalysts: a review. *Journal of hazardous materials, 170*(2), 520-529.

Allen, E., & Smith, P. (2001). A review of particle agglomeration. *Surfaces, 85*(86), 87.

Amin, K. A. M. (2012). Reinforced materials based on chitosan, TiO2 and Ag composites. *Polymers, 4*(1), 590-599.

Andriantsiferana, C., Mohamed, E. F., & Delmas, H. (2014). Photocatalytic degradation of an azo-dye on TiO2/activated carbon composite material. *Environ Technol, 35*(1-4), 355-363.

Antonio-Cisneros, C. M., Davila-Jimenez, M. M., Elizalde-Gonzalez, M. P., & Garcia-Diaz, E. (2015). TiO2 immobilized on Manihot carbon: optimal preparation and evaluation of its activity in the decomposition of indigo carmine. *Int J Mol Sci, 16*(1), 1590-1612.

Aziz, R. A., & Sopyan, I. (2009). Synthesis of TiO2-SiO2 powder and thin film photocatalysts by sol-gel method. *Indian journal of chemistry. Section A, Inorganic, bio-inorganic, physical, theoretical & analytical chemistry, 48*(7), 951.

Ba-Abbad, M. M., Kadhum, A. A. H., Mohamad, A. B., Takriff, M. S., & Sopian, K. (2012). Synthesis and catalytic activity of TiO2 nanoparticles for photochemical oxidation of concentrated chlorophenols under direct solar radiation. *Int. J. Electrochem. Sci, 7*, 4871-4888.

Bagheri, S., Hir, Z. A. M., Yousefi, A. T., & Hamid, S. B. A. (2015). Progress on mesoporous titanium dioxide: synthesis, modification and applications. *Microporous and Mesoporous Materials, 218*, 206-222.

Bagheri, S., Mohd Hir, Z. A., Termeh Yousefi, A., & Abd Hamid, S. B. (2015). Photocatalytic performance of activated carbon-supported mesoporous titanium dioxide. *Desalination and Water Treatment*, 1-7.

Bagheri, S., Muhd Julkapli, N., & Bee Abd Hamid, S. (2014). Titanium dioxide as a catalyst support in heterogeneous catalysis. *The Scientific World Journal, 2014*.

Bagheri, S., Muhd Julkapli, N., & Bee Abd Hamid, S. (2015). Functionalized activated carbon derived from biomass for photocatalysis applications perspective. *International Journal of Photoenergy, 2015*.

Bagheri, S., Shameli, K., & Abd Hamid, S. B. (2012). Synthesis and characterization of anatase titanium dioxide nanoparticles using egg white solution via Sol-Gel method. *Journal of Chemistry, 2013*.

Benavente, M. (2008). Adsorption of metallic ions onto chitosan: equilibrium and kinetic studies.

Beranek, R., & Kisch, H. (2008). Tuning the optical and photoelectrochemical properties of surface-modified TiO 2. *Photochemical & Photobiological Sciences, 7*(1), 40-48.

Bhalerao, N., Ishita, V. V., Patil, K., & Topare, N. (2013). A review on Parameters Affecting the Photocatalytic Degradation of Dyes using Photocatalysts.

Byranvanda, M. M., Kharata, A. N., Fatholahib, L., & Beiranvandc, Z. M. A Review on Synthesis of Nano-TiO2 via Different Methods.

Castellote, M., & Bengtsson, N. (2011). *Principles of TiO_2 Photocatalysis. In Applications of Titanium Dioxide Photocatalysis to Construction Materials (pp. 5-10)*. Springer Netherlands.

Chang, H., & Seo, M. (2014). Photocatalytic Degradation of Gaseous Formaldehyde and Benzene using TiO2 Particulate Films Prepared by the Flame Aerosol Reactor. *Environmental Engineering Research, 19*(3), 215-221.

Chekin, F., Bagheri, S., & Hamid, S. B. A. (2013). Synthesis of Pt doped TiO 2 nanoparticles: characterization and application for electrocatalytic oxidation of l-methionine. *Sensors and Actuators B: Chemical, 177*, 898-903.

Chen, R. F., & Zhang, C. X. (2008). Preparation and Photocatalytic Activity of TiO2 Films on Silica Glass Substrates by Assembly Technique. *Journal of the Chinese Chemical Society, 55*(5), 1055-1061.

Chen, X., Liu, F., Liu, B., Tian, L., Hu, W., & Xia, Q. (2015). A novel route to graphite-like carbon supporting SnO2 with high electron transfer and photocatalytic activity. *J Hazard Mater, 287*, 126-132.

Cheng, C., Amini, A., Zhu, C., Xu, Z., Song, H., & Wang, N. (2014). Enhanced photocatalytic performance of TiO2-ZnO hybrid nanostructures. *Sci Rep, 4*, 4181.

Chequer, F. M. D., de Oliveira, D. P., Ferraz, E. R. A., de Oliveira, G. A. R., Cardoso, J. C., & Zanoni, M. V. B. (2013). *Textile dyes: dyeing process and environmental impact*: INTECH Open Access Publisher.

Choi, H. C., Jung, Y. M., & Kim, S. B. (2005). Size effects in the Raman spectra of TiO 2 nanoparticles. *Vibrational Spectroscopy, 37*(1), 33-38.

Clara, M., Strenn, B., Gans, O., Martinez, E., Kreuzinger, N., & Kroiss, H. (2005). Removal of selected pharmaceuticals, fragrances and endocrine disrupting compounds in a membrane bioreactor and conventional wastewater treatment plants. *Water Res, 39*(19), 4797-4807.

Daimon, T., & Nosaka, Y. (2007). Formation and behavior of singlet molecular oxygen in TiO2 photocatalysis studied by detection of near-infrared phosphorescence. *The Journal of Physical Chemistry C, 111*(11), 4420-4424.

Danwittayakul, S., Jaisai, M., & Dutta, J. (2015). Efficient solar photocatalytic degradation of textile wastewater using ZnO/ZTO composites. *Applied Catalysis B: Environmental, 163*, 1-8.

Doll, T. E., & Frimmel, F. H. (2004). Development of easy and reproducible immobilization techniques using TiO2 for photocatalytic degradation of aquatic pollutants. *Acta hydrochimica et hydrobiologica, 32*(3), 201-213.

Dutta, P. K., Dutta, J., & Tripathi, V. (2004). Chitin and chitosan: Chemistry, properties and applications. *Journal of Scientific and Industrial Research, 63*(1), 20-31.

Fajriati, I., Mudasir, M., & Wahyuni, E. T. (2014). Photocatalytic Decolorization Study of Methyl Orange by TiO 2–Chitosan Nanocomposites. *Indonesian Journal of Chemistry, 14*(3), 209-218.

Faramarzpour, M., Vossoughi, M., & Borghei, M. (2009). Photocatalytic degradation of furfural by titania nanoparticles in a floating-bed photoreactor. *Chemical Engineering Journal, 146*(1), 79-85.

Farzana, M. H., & Meenakshi, S. (2013a). Enhanced photocatalytic degradation of chromium (VI) under UV light on chitosan/TiO2 composite. *Journal of Chitin and Chitosan Science, 1*(1), 42-49.

Farzana, M. H., & Meenakshi, S. (2013b). Synergistic effect of chitosan and titanium dioxide on the removal of toxic dyes by the photodegradation technique. *Industrial & Engineering Chemistry Research, 53*(1), 55-63.

Folli, A., Pochard, I., Nonat, A., Jakobsen, U. H., Shepherd, A. M., & Macphee, D. E. (2010). Engineering photocatalytic cements: understanding TiO2 surface chemistry to control and modulate photocatalytic performances. *Journal of the American Ceramic Society, 93*(10), 3360-3369.

Fujishima, A. (1972). Electrochemical photolysis of water at a semiconductor electrode. *nature, 238*, 37-38.

Fujishima, A., Zhang, X., & Tryk, D. A. (2007). Heterogeneous photocatalysis: from water photolysis to applications in environmental cleanup. *International journal of hydrogen energy, 32*(14), 2664-2672.

Gan, W., Lee, M., Amal, R., Zhao, H., & Chiang, K. (2008). Photoelectrocatalytic activity of mesoporous TiO2 films prepared using the sol–gel method with tri-block copolymer as structure directing agent. *Journal of Applied Electrochemistry, 38*(5), 703-712.

Ganesh, V. A., Nair, A. S., Raut, H. K., Walsh, T. M., & Ramakrishna, S. (2012). Photocatalytic superhydrophilic TiO 2 coating on glass by electrospinning. *Rsc Advances, 2*(5), 2067-2072.

Gao, B., Yap, P. S., Lim, T. M., & Lim, T.-T. (2011). Adsorption-photocatalytic degradation of Acid Red 88 by supported TiO 2: effect of activated carbon support and aqueous anions. *Chemical Engineering Journal, 171*(3), 1098-1107.

Ghosh, S. N. (2006). *Environmental hydrology and hydraulics: eco-technological practices for sustainable development*: CRC Press.

Gray, N. (2004). Biology of wastewater treatment. Series on environmental science and management: Imperial College Press, London.

Guan, K. (2005). Relationship between photocatalytic activity, hydrophilicity and self-cleaning effect of TiO 2/SiO 2 films. *Surface and Coatings Technology, 191*(2), 155-160.

Guo, Q., Ghadiri, R., Weigel, T., Aumann, A., Gurevich, E. L., Esen, C., . . . Ostendorf, A. (2014). Comparison of in Situ and ex Situ Methods for Synthesis of Two-Photon Polymerization Polymer Nanocomposites. *Polymers, 6*(7), 2037-2050.

Harruddin, N., Othman, N., Lim Ee Sin, A., & Raja Sulaiman, R. N. (2015). Selective removal and recovery of Black B reactive dye from simulated textile wastewater using the supported liquid membrane process. *Environmental technology, 36*(3), 271-280.

Hashimoto, K., Irie, H., & Fujishima, A. (2005). TiO2 photocatalysis: a historical overview and future prospects. *Japanese journal of applied physics, 44*(12R), 8269.

Hosseini, S., Borghei, S., Vossoughi, M., & Taghavinia, N. (2007). Immobilization of TiO 2 on perlite granules for photocatalytic degradation of phenol. *Applied Catalysis B: Environmental, 74*(1), 53-62.

Huang, K.-S., Grumezescu, A. M., Chang, C.-Y., Yang, C.-H., & Wang, C.-Y. (2014). Immobilization and stabilization of TiO2 Nanoparticles in alkaline-solidificated chitosan spheres without cross-linking agent. *International Journal of Latest Research in Science and Technology, 3*(2), 174-178.

Huang, R., Liu, Q., Huo, J., & Yang, B. (2013). Adsorption of methyl orange onto protonated cross-linked chitosan. *Arabian Journal of Chemistry*.

Ibhadon, A. O., & Fitzpatrick, P. (2013). Heterogeneous photocatalysis: recent advances and applications. *Catalysts, 3*(1), 189-218.

Jaafar, N. F., Jalil, A. A., Triwahyono, S., Muhid, M. N. M., Sapawe, N., Satar, M. A. H., & Asaari, H. (2012). Photodecolorization of methyl orange over α-Fe 2 O 3-supported HY catalysts: The effects of catalyst preparation and dealumination. *Chemical Engineering Journal, 191*, 112-122.

Jamal, R., Osman, Y., Rahman, A., Ali, A., Zhang, Y., & Abdiryim, T. (2014). Solid-State Synthesis and Photocatalytic Activity of Polyterthiophene Derivatives/TiO2 Nanocomposites. *Materials, 7*(5), 3786-3801.

Jiang, D., Zhang, S., & Zhao, H. (2007). Photocatalytic degradation characteristics of different organic compounds at TiO2 nanoporous film electrodes with mixed anatase/rutile phases. *Environmental science & technology, 41*(1), 303-308.

Jiang, H.-Y., Liu, G., Li, M., Liu, J., Sun, W., Ye, J., & Lin, J. (2015). Efficient organic degradation under visible light by α-Bi 2 O 3 with a CuO x-assistant electron transfer process. *Applied Catalysis B: Environmental, 163*, 267-276.

Jung, B. S., Boulos, P. F., Wood, D. J., & Bros, C. M. (2009). A Lagrangian wave characteristic method for simulating transient water column separation. *Journal AWWA, 101*(6), 64-73.

Kambur, A., Pozan, G. S., & Boz, I. (2012). Preparation, characterization and photocatalytic activity of TiO 2–ZrO 2 binary oxide nanoparticles. *Applied Catalysis B: Environmental, 115*, 149-158.

Kavitha, K., Sutha, S., Prabhu, M., Rajendran, V., & Jayakumar, T. (2013). In situ synthesized novel biocompatible titania–chitosan nanocomposites with high surface area and antibacterial activity. *Carbohydrate Polymers, 93*(2), 731-739.

Kijima, T. (2010). *Inorganic and Metallic Nanotubular Materials: Recent Technologies and Applications* (Vol. 117): Springer Science & Business Media.

Kim, C., Kim, J. T., Kim, K. S., Jeong, S., Kim, H. Y., & Han, Y. S. (2009). Immobilization of TiO 2 on an ITO substrate to facilitate the photoelectrochemical degradation of an organic dye pollutant. *Electrochimica Acta, 54*(24), 5715-5720.

Kim, C. H., Kim, B.-H., & Yang, K. S. (2012). TiO 2 nanoparticles loaded on graphene/carbon composite nanofibers by electrospinning for increased photocatalysis. *Carbon, 50*(7), 2472-2481.

Klankaw, P., Chawengkijwanich, C., Grisdanurak, N., & Chiarakorn, S. (2012). The hybrid photocatalyst of TiO 2–SiO 2 thin film prepared from rice husk silica. *Superlattices and Microstructures, 51*(3), 343-352.

Kleiman, A., Márquez, A., Vera, M., Meichtry, J., & Litter, M. (2011). Photocatalytic activity of TiO 2 thin films deposited by cathodic arc. *Applied Catalysis B: Environmental, 101*(3), 676-681.

Kumar, J., & Bansal, A. (2013). *Photocatalysis by nanoparticles of titanium dioxide for drinking water purification: a conceptual and state-of-art review.* Paper presented at the Materials Science Forum.

Kumar, S. G., & Devi, L. G. (2011). Review on modified TiO2 photocatalysis under UV/visible light: selected results and related mechanisms on interfacial charge carrier transfer dynamics. *J Phys Chem A, 115*(46), 13211-13241.

Kyzas, G. Z., & Bikiaris, D. N. (2015). Recent modifications of chitosan for adsorption applications: a critical and systematic review. *Mar Drugs, 13*(1), 312-337.

Lazar, M. A., Varghese, S., & Nair, S. S. (2012). Photocatalytic water treatment by titanium dioxide: recent updates. *Catalysts, 2*(4), 572-601.

Leary, R., & Westwood, A. (2011). Carbonaceous nanomaterials for the enhancement of TiO 2 photocatalysis. *Carbon, 49*(3), 741-772.

Lin, Y.-C., & Lee, H.-S. (2010). Effects of TiO 2 coating dosage and operational parameters on a TiO 2/Ag photocatalysis system for decolorizing Procion red MX-5B. *Journal of hazardous materials, 179*(1), 462-470.

Linsebigler, A. L., Lu, G., & Yates Jr, J. T. (1995). Photocatalysis on TiO2 surfaces: principles, mechanisms, and selected results. *Chemical reviews, 95*(3), 735-758.

Liu, G., Zhao, Y., Sun, C., Li, F., Lu, G. Q., & Cheng, H. M. (2008). Synergistic effects of B/N doping on the visible-light photocatalytic activity of mesoporous TiO2. *Angew Chem Int Ed Engl, 47*(24), 4516-4520.

Liu, H., Ramnarayanan, R., & Logan, B. E. (2004). Production of electricity during wastewater treatment using a single chamber microbial fuel cell. *Environmental science & technology, 38*(7), 2281-2285.

Lukes, P., Clupek, M., Sunka, P., Peterka, F., Sano, T., Negishi, N., . . . Takeuchi, K. (2005). Degradation of phenol by underwater pulsed corona discharge in combination with TiO 2 photocatalysis. *Research on Chemical Intermediates, 31*(4), 285-294.

Luttrell, T., Halpegamage, S., Tao, J., Kramer, A., Sutter, E., & Batzill, M. (2014). Why is anatase a better photocatalyst than rutile?-Model studies on epitaxial TiO2 films. *Scientific reports, 4*.

Marković, D., Šaponjić, Z., Radoičić, M., Radetić, T., Vodnik, V., Potkonjak, B., & Radetić, M. (2015). Sonophotocatalytic degradation of dye CI Acid Orange 7 by TiO 2 and Ag nanoparticles immobilized on corona pretreated polypropylene non-woven fabric. *Ultrasonics sonochemistry, 24*, 221-229.

McCullagh, C., Robertson, J. M., Bahnemann, D. W., & Robertson, P. K. (2007). The application of TiO2 photocatalysis for disinfection of water contaminated with pathogenic micro-organisms: a review. *Research on Chemical Intermediates, 33*(3-5), 359-375.

Mehranpour, H., Ghamsari, M. S., & Askari, M. (2011). *Nucleation and Growth of TiO2 Nanoparticles*: INTECH Open Access Publisher.

Meng, H., Hou, W., Xu, X., Xu, J., & Zhang, X. (2014). TiO 2-loaded activated carbon fiber: Hydrothermal synthesis, adsorption properties and photo catalytic activity under visible light irradiation. *Particuology, 14*, 38-43.

Minh, N., Hien, N., Vien, V., Kim, S., Noh, W., Yang, I., . . . Khoi, N. (2008). Nano-Particles of Co Doped TiO~ 2 Anatase: Raman Spectroscopy and Structural Studies. *JOURNAL-KOREAN PHYSICAL SOCIETY, 52*(5), 1629.

Moustakas, N., Kontos, A., Likodimos, V., Katsaros, F., Boukos, N., Tsoutsou, D., . . . Falaras, P. (2013). Inorganic–organic core–shell titania nanoparticles for efficient visible light activated photocatalysis. *Applied Catalysis B: Environmental, 130*, 14-24.

Muhd Julkapli, N., Bagheri, S., & Bee Abd Hamid, S. (2014). Recent advances in heterogeneous photocatalytic decolorization of synthetic dyes. *ScientificWorldJournal, 2014*, 692307.

Murphy, A. (2007). Band-gap determination from diffuse reflectance measurements of semiconductor films, and application to photoelectrochemical water-splitting. *Solar Energy Materials and Solar Cells, 91*(14), 1326-1337.

Nandini, R., & Vishalakshi, B. (2012). A study of interaction of Methyl Orange with some polycations. *Journal of Chemistry, 9*(1), 1-14.

Nawi, M., Jawad, A. H., Sabar, S., & Ngah, W. W. (2011). Immobilized bilayer TiO 2/chitosan system for the removal of phenol under irradiation by a 45watt compact fluorescent lamp. *Desalination, 280*(1), 288-296.

Ngadi, N., Mahmud, M. A., Jusoh, M., Rahman, R. A., & Alias, H. (2014). Removal of ethyl orange dye using hybrid chitosan and zinc oxide. *Jurnal Teknologi, 67*(1).

Norranattrakul, P., Siralertmukul, K., & Nuisin, R. (2013). Fabrication of chitosan/titanium dioxide composites film for the photocatalytic degradation of dye. *Journal of Metals, Materials and Minerals, 23*(2).

Oudenhoven, J., Scheijen, F., & Wollfs, M. (2004). Fundamental of photocatalytic water splitting by visible light. *Chemistry of Catalytic System 2: Photocatalysis*, 1-22.

Pan, C., & Dong, L. (2011). Au/TiO2 Hierarchical Nanofibers Heterostructure: Controllable Synthesis and Enhanced Photocatalytic Performances. *Nanofibers–Production, Properties and Functional Applications*, 449.

Pan, X., Zhao, Y., Wang, S., & Fan, Z. (2013). TiO2/graphene nanocomposite for photocatalytic application *Materials and Processes for Energy: Communicating Current Research and Technological Developments* (pp. 913-920): Formatex.

Pereira, L., & Alves, M. (2012). Dyes—Environmental Impact and Remediation *Environmental protection strategies for sustainable development* (pp. 111-162): Springer.

Popa, M., Diamandescu, L., Vasiliu, F., Teodorescu, C., Cosoveanu, V., Baia, M., . . . Danciu, V. (2009). Synthesis, structural characterization, and photocatalytic properties of iron-doped TiO2 aerogels. *Journal of Materials Science, 44*(2), 358-364.

Pu, Y.-C., Lin, W.-H., & Hsu, Y.-J. (2015). Modulation of charge carrier dynamics of Na x H 2− x Ti 3 O 7-Au-Cu 2 O Z-scheme nanoheterostructures through size effect. *Applied Catalysis B: Environmental, 163*, 343-351.

Schäffer, J. (2012). Immobilization of TiO2: via different routes for photocatalytic reactions in a PDMS based microreactor.

Serpone, N., Borgarello, E., Harris, R., Cahill, P., Borgarello, M., & Pelizzetti, E. (1986). Photocatalysis over TiO2 supported on a glass substrate. *Solar Energy Materials, 14*(2), 121-127.

Shao, X., Lu, W., Zhang, R., & Pan, F. (2013). Enhanced photocatalytic activity of TiO2-C hybrid aerogels for methylene blue degradation. *Scientific reports, 3*.

Sonawane, R., Hegde, S., & Dongare, M. (2003). Preparation of titanium (IV) oxide thin film photocatalyst by sol–gel dip coating. *Materials chemistry and physics, 77*(3), 744-750.

Spagnoli, R. A. (1992). Preparation of differential thickness coatings by dip coating where the substrate is pivoted: Google Patents.

Stovall, H. (2007). Natural Alternatives to Conventional Wastewater Treatment: Jun.

Su, C., Hong, B.-Y., & Tseng, C.-M. (2004). Sol–gel preparation and photocatalysis of titanium dioxide. *Catalysis Today, 96*(3), 119-126.

Subha, P., & Jayaraj, M. (2014). Solar photocatalytic degradation of methyl orange dye using TiO2 nanoparticles synthesised by sol–gel method in neutral medium. *Journal of Experimental Nanoscience*(ahead-of-print), 1-10.

Tachikawa, T., Yamashita, S., & Majima, T. (2011). Evidence for crystal-face-dependent TiO2 photocatalysis from single-molecule imaging and kinetic analysis. *J Am Chem Soc, 133*(18), 7197-7204.

Talebian, N., Nilforoushan, M. R., & Memarnezhad, P. (2013). Photocatalytic activities of multilayered ZnO-based thin films prepared by sol–gel route: effect of SnO2 heterojunction layer. *Journal of sol-gel science and technology, 65*(2), 178-188.

Tseng, T. K., Lin, Y. S., Chen, Y. J., & Chu, H. (2010). A review of photocatalysts prepared by sol-gel method for VOCs removal. *Int J Mol Sci, 11*(6), 2336-2361.

United States Environmental Protection Agency (USEPA), Office of Water, *Development Document for Proposed Effluent Limitations Guidelines and Standards for the Centralized Waste Treatment Industry*, Volume I, Chapter 8-Wastewater Treatment Technologies, 1998.Vaiano, V., Sacco, O., Sannino, D., & Ciambelli, P. (2015). Nanostructured N-doped TiO 2 coated on glass spheres for the photocatalytic removal of organic dyes under UV or visible light irradiation. *Applied Catalysis B: Environmental, 170*, 153-161.

Vaiano, V., Sacco, O., Sannino, D., & Ciambelli, P. (2015). Nanostructured N-doped TiO 2 coated on glass spheres for the photocatalytic removal of organic dyes under UV or visible light irradiation. *Applied Catalysis B: Environmental, 170*, 153-161.

Villa, K., Murcia-López, S., Andreu, T., & Morante, J. R. (2015). Mesoporous WO 3 photocatalyst for the partial oxidation of methane to methanol using electron scavengers. *Applied Catalysis B: Environmental, 163*, 150-155.

WANG, J., HUANG, D., LI, Z., LIU, G., & MIN, Y. (2015). Synthesis of TiO 2 with Cotton as Template and Its Applications as Photocatalysis. *Asian Journal of Chemistry, 27*(1).

Wang, S. (2014). 3 Stress on anti-abrasive performance of sol-gel derived nanocoatings. *Anti-Abrasive Nanocoatings: Current and Future Applications*, 57.

Wang, X., Hu, Z., Chen, Y., Zhao, G., Liu, Y., & Wen, Z. (2009). A novel approach towards high-performance composite photocatalyst of TiO 2 deposited on activated carbon. *Applied Surface Science, 255*(7), 3953-3958.

Wei, X.-X., Cui, H., Guo, S., Zhao, L., & Li, W. (2013). Hybrid BiOBr–TiO 2 nanocomposites with high visible light photocatalytic activity for water treatment. *Journal of hazardous materials, 263*, 650-658.

Wongkupasert, S. (2008). *The effect of salt form and molecular weight of chitosan for efficiency on sirna delivery into cell.* Silpakorn University.

Xiao, J., Chen, W., Wang, F., & Du, J. (2013). Polymer/TiO2 hybrid nanoparticles with highly effective UV-screening but eliminated photocatalytic activity. *Macromolecules, 46*(2), 375-383.

Xu, S., Zhu, Y., Jiang, L., & Dan, Y. (2010). Visible light induced photocatalytic degradation of methyl orange by polythiophene/TiO2 composite particles. *Water, Air, & Soil Pollution, 213*(1-4), 151-159.

Yan, J., Wu, G., Guan, N., Li, L., Li, Z., & Cao, X. (2013). Understanding the effect of surface/bulk defects on the photocatalytic activity of TiO 2: anatase versus rutile. *Physical Chemistry Chemical Physics, 15*(26), 10978-10988.

Yao, K., Li, J., Yao, F., & Yin, Y. (2011). *Chitosan-based hydrogels: functions and applications*: CRC Press.

Yoong, L., Chong, F. K., & Dutta, B. K. (2009). Development of copper-doped TiO 2 photocatalyst for hydrogen production under visible light. *Energy, 34*(10), 1652-1661.

Zainal, Z., Hui, L. K., Hussein, M. Z., & Abdullah, A. H. (2009). Characterization of TiO 2–Chitosan/Glass photocatalyst for the removal of a monoazo dye via photodegradation–adsorption process. *Journal of hazardous materials, 164*(1), 138-145.

Zhang, M., Bando, Y., & Wada, K. (2001). Sol-gel template preparation of TiO2 nanotubes and nanorods. *Journal of materials science letters, 20*(2), 167-170.

Zhang, X., Zhao, X., & Su, H. (2011). Degradation characteristic of TiO2-chitosan adsorbent on Rhodamine B and purification of industrial wastewater. *Korean Journal of Chemical Engineering, 28*(5), 1241-1246.

Zhang, Y., & Li, Q. (2013). Synthesis and characterization of Fe-doped TiO 2 films by electrophoretic method and its photocatalytic activity toward methyl orange. *Solid State Sciences, 16*, 16-20.

Zhu, Y., Chen, Z., Gao, T., Huang, Q., Niu, F., Qin, L., . . . Wang, Y. (2015). Construction of hybrid Z-scheme Pt/CdS–TNTAs with enhanced visible-light photocatalytic performance. *Applied Catalysis B: Environmental, 163*, 16-22.

Zhu, Y., Zhang, L., Gao, C., & Cao, L. (2000). The synthesis of nanosized TiO2 powder using a sol-gel method with TiCl4 as a precursor. *Journal of Materials Science, 35*(16), 4049-4054.

LIST OF PUBLICATIONS AND PAPERS PRESENTED

7.1 Journals publication

7.1.1 Inorganic Review

DE GRUYTER Rev Inorg Chem 2015; aop

Muhammad Nur Iman Amir, Nurhidayatullaili Muhd Julkapli, Samira Bagheri* and Amin Termeh Yousefi

TiO_2 hybrid photocatalytic systems: impact of adsorption and photocatalytic performance

DOI 10.1515/revic-2015-0005
Received May 1, 2015; accepted June 15, 2015

Abstract: For the past 40 years, titanium dioxide (TiO_2) nanomaterials have attracted immense attention because of their potential applications in the photodegradation of organic pollutants, photocatalytic water splitting for H_2 generation, and dye-sensitized solar cells. Despite the fact that the potential applications of TiO_2 nanoparticles are ubiquitous, they are not problem free, examples include a large interfacial area that causes slow charge carrier transport, a wide optical band gap that leads to limited applications using solar light, and single-phase and nanoscales features that induce fast recombination of photo-reduced carriers. Therefore, this review highlights the development associated with the adsorption photocatalysis hybrid system for treating wastewater. The immobilization of TiO_2 photocatalysts in metal oxide, carbon, and ceramic materials to form TiO_2 hybrid systems could prevent the problem of particle recovery, adsorption capacity, and the separation process. Such hybrid systems require significant effort of optimizing the specific surface area-to-volume ratio of the supported photocatalysts with its photocatalytic activities.

Keywords: catalyst support material; hybrid nanomaterials; nanoparticles; photodegradation.

***Corresponding author: Samira Bagheri,** Nanotechnology and Catalysis Research Centre (NANOCAT), IPS Building, University Malaya, 50603 Kuala Lumpur, Malaysia,
e-mail: samira_bagheri@um.edu.my
Muhammad Nur Iman Amir and Nurhidayatullaili Muhd Julkapli: Nanotechnology and Catalysis Research Centre (NANOCAT), IPS Building, University Malaya, 50603 Kuala Lumpur, Malaysia
Amin Termeh Yousefi: ChECA IKohza, Malaysia Japan International Institute of Technology (MJIIT), Department of Environmental and Green Technology (EGT), University Technology Malaysia (UTM), Kuala Lumpur, Malaysia

Introduction

Recently, photocatalysts are attracting increased interest because of its chemical stability, recyclability, low costs, and non-toxic processing routes (Muhd Julkapli et al. 2014, Bagheri et al. 2015a,b). The photocatalysis process is regarded as an eco-friendly approach, mainly because it lacks chemical inputs or outputs, with no sludge residue being generated (Bagheri et al. 2015b). Nanosized photocatalyst are touted for many potential applications in purifying polluted water. The photocatalytic oxidation process is a potential replacement for physical and biological techniques, as it can be carried out under ambient conditions employing atmospheric oxygen as its oxidant, resulting in the total mineralization of the contaminants to CO_2, mineral acids, or water. Indeed, an even more advanced photocatalytic treatment technique provides substantial environmental remediation prospects, including water decontamination and purification, deodorization of air, and others (Bagheri et al. 2013, 2015a). During the photocatalyst process, the semiconductor material absorbs the introduced light and promotes the electron from the valence to the conduction band. Once they reach excitation, the produced electron-hole pair induces the redox reaction, which will photocatalytically degrade organic contaminants (Bagheri et al. 2013, 2015b,c, Muhd Julkapli et al. 2014).

One of the drawbacks of using the photocatalytic procedure is the presence of organic materials within the system (Chen et al. 2015, Pu et al. 2015, Wang et al. 2015). Excessive suspended material loading results in light scattering, which reduces the photocatalytic performance of the process (Muhd Julkapli et al. 2014, Pu et al. 2015). Therefore, the integration of the photocatalysis procedure with a physicochemical treatment process, which includes adsorption and coagulation as its pretreatment stages, is regarded as necessary for an effective industrial process (Jiang et al. 2015). The integration of adsorption and photocatalytic treatment mitigates many problems associated with the wastewater industry. This hybrid process can address the limitations of each method when operated separately, which enhances the total removal efficiency of the entire process (Danwittayakul et al. 2015, Villa et al. 2015, Zhu et al. 2015).

7.1.2 International Journal of Environmental Science and Technology

Int. J. Environ. Sci. Technol.
DOI 10.1007/s13762-015-0914-y

ORIGINAL PAPER

Incorporation of chitosan and glass substrate for improvement in adsorption, separation, and stability of TiO_2 photodegradation

M. N. I. Amir[1] · N. M. Julkapli[1] · S. B. Abd Hamid[1]

Received: 2 September 2015 / Revised: 27 October 2015 / Accepted: 30 November 2015

Abstract It is demonstrated that single titanium dioxide (TiO_2) has high potential for photodegradation of pollutants. However, it is still far from becoming an effective photocatalyst system, due to issues of adsorption process, separation, as well as dissolution. Therefore, this study highlights the high adsorption capacity, simplified separation, and the promising stability of $TiO_{2(SY)}$ (synthesized via sol–gel method) photocatalyst, fabricated using chitosan–$TiO_{2(SY)}$ and supported by glass substrate (Cs–$TiO_{2(SY)}$/glass substrate) photocatalysts. Chitosan (Cs), with abundant –R–NH and NH_2 groups, promotes the adsorption sites of methyl orange (MO) and OH groups for major attachment to $TiO_{2(SY)}$. Meanwhile, the glass substrate increases stability and assists separation of the photocatalysts. Initially, nano-$TiO_{2(SY)}$ has been characterized using high-resolution transmission electron microscope. Cs–$TiO_{2(SY)}$/glass substrate was fabricated via dip-coating. The distribution and interface between the photocatalytic components were characterized by Fourier transform infrared absorption spectroscopy, UV–Vis diffuse reflectance spectroscopy, field emission scanning electron microscopy, and energy-dispersive spectrometer. UV–Vis analysis of the multilayer photocatalyst (2, 4, 6, and 8 layers) was further carried out by the adsorption–photodegradation, with MO as model of pollutant. Seventy percent of the total removal of MO via optimized eight layers of photocatalyst was achieved within 1 h of UV irradiation. The adsorption photocatalyst achieved 50 % with no exposure to UV light for 15 min of irradiation. It is concluded that suitable photocatalytic conditions and sample parameters possessing the multilayer photocatalyst of Cs–$TiO_{2(SY)}$ are beneficial toward the adsorption–photodegradation process in wastewater treatment.

Keywords Adsorption–photodegradation · Methyl orange · Titanium dioxide · Chitosan · Glass substrate

Introduction

One of the major sources of water contamination is the textile industry, due to its heavy usage of various synthetic and organic dyes (Liu et al. 2004; Pereira and Alves 2012). Various methods have been used to treat synthetic dyes, such as adsorption by various adsorbents, reverse osmosis, and flocculation. These methods are commonly used in wastewater treatment facilities, and among them, photocatalysis stands out due to its environmental-friendly nature, cost-effectiveness, and the lack of the production of secondary pollutants after the degradation of dyes.

Titanium dioxide (TiO_2) nanoparticles, or nano-TiO_2 with one-dimensional structure, is a well-known semiconductor used as a photocatalyst, due to its chemical structure, biocompatibility, physical properties, catalytic activity, high surface area, non-toxicity, and promising electroconductivity (Fujishima 1972; Kijima 2010). However, nano-TiO_2 is still far from becoming a potential candidate for photocatalyst systems. Bundling phenomenon and weak adherence due to the multiphase nature of TiO_2 substrate remain a great challenge. Moreover, poor visible light absorption and rapid recombination of charge carriers limit the widespread use of TiO_2. Therefore, the

✉ N. M. Julkapli
nurhidayatullaili@um.edu.my

[1] Nanotechnology and Catalysis Research Centre (NANOCAT), 3rd Floor, Block A, Institute of Postgraduate Studies (IPS), University of Malaya, 50603 Kuala Lumpur, Malaysia

Published online: 04 January 2016

7.2 Proceeding Papers

7.2.1 18 Malaysian International Chemical Congress

Location: PWTC, Kuala Lumpur

Date: Nov 2014

Effects Of Layers and Ratio Of Chitosan_TiO_2/Glass Photocatalyst Towards The Removal of Methylene Orange via Adsorption-Photodegradation Process

Muhammad Nur Iman Amir, Nurhidayatullaili Muhd Julkapli* and Sharifah Bee Abd Hamid

Nanotechnology & Catalysis Research Centre (NANOCAT),
3rd Floor, Block A, Institute of Postgraduate Studies (IPS),
University of Malaya, 50603 Kuala Lumpur,
MALAYSIA.

*Corresponding author: nurhidayatullaili@um.edu.my

Abstract

The objective of this study is to prepare the Cs–TiO_2 films by using glass substrate with synthesized TiO_2 and to study the photocatalytic activity of Cs–TiO_2 in the removal of methyl orange (MO) under the optimum conditions. First, TiO_2 nanoparticles was synthesized via sol gel methods and its chemical, physical and photocatalytic properties were characterized accordingly. This was divided into two parts which involved the as-synthesized sample (before calcination) - undergoing Thermo-gravimetric analysis (TGA) and then the same synthesized sample underwent Fourier Transform Infrared Spectroscopy (FTIR), X-ray Diffraction (XRD) and Raman Spectroscopy analyses after it was calcined. Then, TiO_2 was incorporated with Cs solution in acidic medium before immobilized on glass plates. UV-Vis analysis was done to study the adsorption–photodegradation analysis of MO. It demonstrated that, the combination effects on adsorption–photodegradation process for the removal of MO occur promisingly when eight layers at 3:2 weight ratio (TiO_2:Cs) of Cs–TiO_2/Glass photocatalyst was used for MO photodegradation. Approximately, 70% to 85% of total MO degradation by photocatalyst analysis was achieved. Therefore, a suitable photocatalytic conditions and sample parameters, possessing the Cs–TiO_2 gave the benefits of adsorption–photodegradation practice in the abatement of wastewater contaminants.

Keywords: Adsorption–Photodegradation, Methylene Orange, Titanium Dioxide Nanoparticles, Chitosan, Glass Plate

7.2.2 4th International Scientific Conference on Applied Sciences and Engineering

Location: Langkawi Lagoon Resort, Malaysia

Date: Oct 2015

International Journal of Natural Sciences Research, 2016, 4(1): 6-14

International Journal of Natural Sciences Research
ISSN(e): 2311-4746/ISSN(p): 2311-7435

URL: www.pakinsight.com

INCORPORATION OF CHITOSAN AND GLASS SUBSTRATE FOR IMPROVEMENT ON ADSORPTION, SEPARATION AND STABILITY OF TIO_2 PHOTOCATALYSIS

Muhammad Nur Iman Amir[1†] --- Nurhidayatullaili Muhd Julkapli[2] --- Sharifah Bee Abd Hamid[3]
[1,2,3]*NANOCAT Research Center, Universiti Malaya, Malaysia*

ABSTRACT

It has been demonstrated that the single TiO_2 has high capabilites for photodegradation process for all types pollutants. However, TiO_2 are still far from becoming a potential candidate for photocatalytic system due to weakness for the adsorbtion process, separation as well as dissolution during the treatment. Therefore, this study highlights on the highly adsorption, easy separation and promising stability of $TiO_{2(SY)}$ photocatalyst by fabrication of Chitosan-$TiO_{2(SY)}$ supported glass substrate (Cs-$TiO_{2(SY)}$/Glass substrate) photocatalysts. Cs with abundant R-NH and NH2 groups promotes adsorption sites of synthetic dyes. Meanwhile, present of glass substrate support increase the stability and easy separation of the potocatalysts. The fabrication process Cs- $TiO_{2(SY)}$/Glass substrate has been done through dip-coating methods. Further analyzed by the adsorption photodegradation with Methyl Orange (MO) as a model of synthetic dyes compound. Approximately, 70% of total removal of MO by optimize 8 layers of photocatalyst analysis has been achieved within 1 hour of UV irradiation. Besides that, the adsorption photocatalyst has been achieved about 50% when no exposure of light for 15 minutes irradiation. It concluded that, a suitable photocatalytic conditions and sample parameters, possessing the Cs-$TiO_{2(SY)}$ gave the benefits of adsorption-photodegradation practice in the abatement of wastewater contaminants.

Keywords: Photodegradation, Waste water, Treatment, Aromatic compounds, Photocatalyst, Nanomaterials, Semiconductor, Chitosan, Synthetic dyes

1. INTRODUCTION

It has been verified that many aromatic compounds derived from synthetic dyes could be successfully degraded and effectively mineralization to end products, which are CO_2, H_2O, and nutrient acids [1, 2]. Various environmental applications to remove synthetic dyes in water and air have been utilized using the photocatalytic properties of Titanium Dioxide (TiO_2) nanoparticles, which is a very well-known semiconductor, used as a photocatalyst, due to the stability of its

† Corresponding author
DOI: 10.18488/journal.63/2016.4.1/63.1.6.14
ISSN(e): 2311-4746/ISSN(p): 2311-7435